AUXETIC BEHAVIOR IN SOME FIBER NETWORK STRUCTURES

A dissertation
Presented to
The Academic Faculty

by

Prateek Verma

In partial fulfillment
of the Requirements for the Degree
Doctor of Philosophy in the
School of Materials Science and Engineering

Georgia Institute of Technology
December, 2015

AUXETIC BEHAVIOR IN SOME FIBER NETWORK STRUCTURES

Approved by:

Dr. Anselm C. Griffin, co-advisor
School of Materials Science and Engineering
Georgia Institute of Technology

Dr. David G. Bucknall
School of Materials Science and Engineering
Georgia Institute of Technology

Dr. Meisha L. Shofner, co-advisor
School of Materials Science and Engineering
Georgia Institute of Technology

Dr. Preet Singh
School of Materials Science and Engineering
Georgia Institute of Technology

Dr. Naresh Thadhani
School of Materials Science and Engineering
Georgia Institute of Technology

Dr. Angus P. Wilkinson
School of Chemistry and Biochemistry
Georgia Institute of Technology

Date Approved: June 1, 2015

To humanity:

with the hope that the research presented here
helps future scientists and contributes to
real-world applications

ACKNOWLEDGEMENTS

I would like to express my deepest gratitude and sincere thanks to my research advisors, Dr. Griffin and Dr. Shofner, for their continuous and prompt support, guidance and encouragement all along my Doctoral research. I learned from them how to think scientifically and critically. Their trust and suggestions helped me to improve and expand my problem solving skills. I hope that I could be half as smart and patient as them one day. I would like to thank my committee members – Dr. Singh, Dr. Wilkinson, Dr. Thadhani and Dr. Bucknall for their continual guidance and immensely useful insights that gave direction and helped shape this research.

At the outset, it is my duty to acknowledge with gratitude the consummate facilities and generous help that I have received from the School of Material Science and Engineering at Georgia Tech. I am indebted to the fellowship award from Renewable Bioproducts Institute at Georgia Tech that supported my PhD work. I would like to thank Dr. Kamath for helping me understand nonwovens better, Dr. Realff for letting me use her microscope, Dr. Guldberg for letting me use his micro-CT facility, Dr. Parachuru for frequent help with Instron and with understanding textiles, and last but not the least Dr. Marsolan for letting me use the facilities at RBI, Georgia Tech, for valuable discussions, and for letting me be a part of the wonderful paper science community.

This research could not have been accomplished without the splendid support, input and cooperation from Angela Lin, who helped me in every phase of the complex micro-CT scanning work and Matthew Priddy, for helping me with Abaqus and building and running finite element analysis on my networks. My special thanks goes out to Dr.

Rallming Yang, Dr. Dongho Kim and my friends and colleagues, Sudhir Sharma and Sandeep Mora, for providing me with materials and helping me mastering the art of papermaking. This thesis could not have been completed without the invaluable research work done by my dear undergraduate students and researchers – C. J. Layer, Tony Shu and Karla Wagner. I would like to thank them for their time, their dedication, their input, and the interest they showed in this research. I would also like to thank Yolande Berta (MSE, Georgia Tech) and Brooke Barta (GTRI, Georgia Tech) for their help with SEM and the entire MSE staff at Georgia Tech – Hope, Susan, Angie, Teresa, Rusty, Rod, Linda, Sherry, Jamar and Jasmine for their beautiful smiles and willingness to help in all situations.

I acknowledge my deep gratitude to Mike Allen and Keith Hubbard of TenCate Protective Fabrics, for their valuable time, for helpful and insightful discussions and for providing us with the nonwoven samples. It was also my immense pleasure to participate in and give a talk at the International Auxetic Conference held in Poznan, Poland in Sep 2014. I would like to thank Dr. Wojciechowski, Dr. Alderson, Dr. Scarpa and Dr. Grima – the experts in the auxetic world – for their precious inputs, advice and comments.

Lastly, I thank my friends – Abhishek, Abhishek, Danish, Nakul, Hari, Charmaine, Cait, Nabankur, Emily and Abhiram for their constant and unconditional support, sometimes even from far across the world. I am thankful to Neha, for her sweetness, care and wonderful advices. And I am indebted to my family – my parents and my sisters for their sacrifices and love.

TABLE OF CONTENTS

LIST OF TABLES

LIST OF FIGURES

LIST OF SYMBOLS

ε_i	Strain along direction '*i*'
v	Poisson's ratio
v_{xy}	Poisson's ratio measured in direction '*x*' corresponding to a strain in direction '*y*'
G	Shear modulus
B	Bulk modulus
l	Length of a solid material (cuboid)
w	Width of a solid material (cuboid)
t	Thickness of a solid material (cuboid)
T_g	Glass transition temperature
x_0	Paper model: half of spacing between two fiber contacts
l	Paper model: length of fiber between two fiber contacts
d	Paper model: smaller diameter (minor axis) of a fiber
θ	Paper model: Angle made by second layer fiber with the sheet plane
S1	Outermost secondary cell wall in wood fiber
S2	Secondary cell wall sandwiched between S1 and S2
S3	Innermost secondary cell wall in wood fiber

LIST OF ABBREVIATIONS

MD	Machine direction
CD	Cross direction
PE	poly(ethylene)
PP	poly(propylene)
PET	poly(ethylene terephthalate)
PTFE	poly(tetra fluoro ethylene)
SEM	Scanning electron micrograph
µCT	Micro computed tomography
CSF	Canadian standard freeness
FEA	Finite element analysis
TAPPI	Technical Association of the Pulp and Paper Industry

SUMMARY

Auxetic materials are a rare class of materials that exhibit negative Poisson's ratio. While most substances (like a rubber band) become thinner in lateral direction when stretched, auxetic materials grow thicker. The broad objective of this research is to study the origins of auxetic behavior in fibrous networks and to develop predictive processing-structure-property relations for these materials systems. We start by examining out-of-plane Poisson's ratio in paper by investigating a range of carefully chosen commercial paper samples. Laboratory handsheets were also produced and examined for their out-of-plane auxetic response. A geometrical model was devised and a finite element analysis on the model was performed to understand the origin of and underlying mechanism responsible for this auxetic response. Additionally, we were able to create a similar auxetic response in needle-punched nonwoven fiber networks by a heat-compression treatment. Thickness direction strain with respect to uniaxial in-plane strain was measured for these materials and a series of microscopic and tomographic characterization was performed. From results on paper and nonwovens, it is evident that the fiber network structure itself plays an important role in defining the Poisson's ratio behavior. The type of network stabilization (hydrogen bonding in paper and needle-punching in nonwovens) and the choice of subsequent processing conditions have a significant influence on the out-of-plane Poisson's ratio in these materials. Ultimately, a fundamental understanding of the origins of deformation behavior in these fiber networks should lead to the prospect of rational design of new auxetics and, in turn, to new product development opportunities for fiber-network materials.

CHAPTER 1

INTRODUCTION

The term ‘auxetic’ refers to materials that exhibit a negative Poisson's ratio. These materials grow fatter when stretched and are very rare in nature. The objective of this research was to examine the presence of auxetic behavior and possibility of inducing such behavior in fiber network structures. A few extant reports of negative out-of-plane Poisson's ratio in commercially produced paper were revisited and confirmed by examining a broader set of samples – both commercial and laboratory made. Further, the origin and underlying mechanism responsible for this phenomenon was proposed using a simplified geometrical network model. Finite element analysis was performed to support the hypothesis for the mechanism. Auxetic behavior was also discovered in laboratory made handsheets produced from unrefined and refined hardwood and softwood pulps. Making handsheets in lab provided more control over various parameters involved in the complex process of papermaking.

In addition to studying auxetic behavior in papers, it was intended to examine the possibility of producing this response in other nonwoven fiber networks. As-produced, nonwoven materials are not known to be auxetic in any direction. It was found that certain processing can potentially convert otherwise ordinary nonwovens (having positive Poisson's ratio) into auxetic materials. We concentrated our research on needle-punched nonwoven fabrics, which showed a lot of promise to be converted into an out-of-plane auxetic material, primarily due to the presence of fiber-columns in their network

structure. A heat-compression processing protocol was developed to successfully induce out-of-plane auxetic behavior in polyester fiber based needle-punched nonwovens.

A series of experiments was performed to examine the thickness change with uniaxial (in-plane) strain in these sheet-like materials – both paper and nonwovens. A universal testing machine (Instron®) was used for straining the sample and a digital micrometer was used for measuring thicknesses. Out-of-plane Poisson's ratio was calculated from plots of thickness direction strain versus axial strain and was found to be negative for many papers and processed nonwoven samples.

Further, microscopic and tomographic characterization was performed to assist with the understanding of the mechanism for this increase in thickness. SEM images of commercial and laboratory made paper showed the network structure, the bonding between fibers, fiber size and spacing between network contact points. Similarly, the technique of μCT was extremely helpful in looking into the microstructure of nonwovens. Fiber orientation, network density and fiber bundles present in needle-punched nonwovens were observed. From the experimental and microscopic analysis, it was found that in addition to the network structure, the processing conditions during (in case of paper) and after (in case of nonwovens) production plays an important role in determining the nature and extent of out-of-plane auxetic response.

Results also indicated that auxetic response in paper is related to the cellulose fiber network and inter-fiber hydrogen bonding. Bent network fibers push the transverse fibers that are in contact with them outwards when strained along their lengths, causing an increase in thickness. In case of needle-punched nonwovens, a thermal-compression treatment made the fabric auxetic. Image analysis indicated that the presence of columnar

fiber bundles (along thickness direction) is mainly responsible for thickness recovery on stretch. These columns get tilted or buckled during compression and can rotate back to their original state when the fabric is stretched, causing an increase in thickness.

In summary, two novel designs, one inspired from paper and one from needle-punched nonwovens, of creating an auxetic response in materials were found. These design solutions are scale and material independent, pending processing and production challenges. The fundamental understanding resulting from this research should lead to the establishment of predictive structure-property relations for auxetic materials as well as to new product development opportunities for fiber-network materials. The next chapter gives a background of the field of auxetic materials and describes our motivation for this research. CHAPTER 3 and CHAPTER 4 introduce and describe the work on paper and needle-punched nonwovens respectively.

[†] Parts of this thesis have been taken / adapted from author's publications – [30] and [61]

CHAPTER 2

BACKGROUND

2.1 What are auxetic materials?

Auxetic materials are a rare class of materials that exhibit negative Poisson's ratio. The term 'auxetic' (from Greek *auxetos*: "that may be increased") was given to materials exhibiting negative Poisson's ratio by Evans et al. [1] in 1991. While most substances (like a rubber band) become thinner in the lateral direction when stretched, auxetic materials grow thicker. During compression too, most substances expand laterally but auxetic materials contract. Evans and Alderson [2] describe this with an example of a stopper and a test tube. It is difficult to push a rubber stopper (a material having a positive Poisson's ratio) into the test tube because it expands in diameter when compressed but it is easier to pull it out of the tube because then it contracts in diameter. However, if the stopper is made of an auxetic material it becomes very difficult to pull it out. This helps to understand then, as to why, bottle stoppers are usually made out of cork, which has a Poisson's ratio of approximately zero.

Poisson's ratio (ν) is formally defined as the negative value of the ratio of lateral strain to longitudinal strain, when the direction of applied strain is longitudinal. For a film-like material, a stress along its length causes dimensional changes in both the width and the thickness directions. Therefore, two separate Poisson's ratios can be defined for a film – one along the width and one along the thickness direction, each with respect to a strain along its length. Similarly for a cylindrical material, a strain along its axis will lead to dimensional changes along the radial directions. In this case, there is only one

Poisson's ratio – along the radial direction with respect to strain along the axial direction. Therefore for a cuboidal or a cylindrical solid, the Poisson's ratio is better expressed using the index notation shown in Equation (1). The second index denotes the direction of applied strain (ε_x) and the first index denotes the direction of observed lateral strain (ε_y). Because most materials contract laterally when strained longitudinally, the negative sign in the definition makes the Poisson's ratio positive for these common materials.

It is important to note here that an increase in either of the lateral dimensions leads to a negative Poisson's ratio in that direction. For a cuboidal solid (a solid with six rectangular faces orthogonal to each other), therefore, two types of auxetic responses can be defined. Corresponding to a positive strain in length direction, if an increase in width is observed, the material is said to exhibit an in-plane auxetic behavior; and if an increase in thickness is observed, then the material is said to exhibit an out-of-plane auxetic behavior. If Poisson's ratio in one direction is negative while in the other direction it is positive, then the material is called 'partially auxetic' [3]. Materials exhibiting negative Poisson's ratio in both directions are called 'fully auxetic' or simply 'auxetic' [3]. In Cartesian coordinates, the length (*x*-axis) and the width (*y*-axis) directions are said to make the plane of the cuboidal (assume it is more like a sheet or film) material while the thickness direction (*z*-axis) is called the out-of-plane direction (Figure 1). The two kinds of auxetic responses can be identified by the index-notation for Poisson's ratio as shown below (Equations 1 and 2), where index '*x*' denotes the direction of applied stress and index '*y*' and '*z*' denote the direction of corresponding dimensional changes along the width and the thickness directions respectively.

$$\nu_{yx} = -\left(\frac{\varepsilon_y}{\varepsilon_x}\right) \quad \text{in-plane Poisson's ratio} \quad (1)$$

$$\nu_{zx} = -\left(\frac{\varepsilon_z}{\varepsilon_x}\right) \quad \text{out-of-plane Poisson's ratio} \quad (2)$$

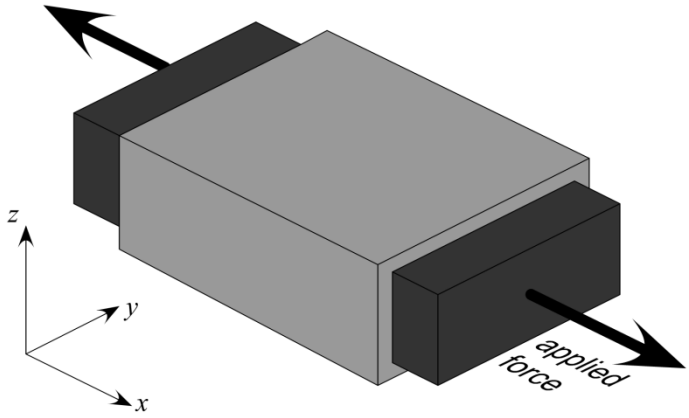

Figure 1: Cartesian coordinates for a cuboidal solid and effect of strain on a material exhibiting a positive Poisson's ratio. Light grey shows the original dimensions and dark grey shows the dimensions upon strain.

Figure 1 shows a material with light grey area showing the initial state (at zero strain). The material is then strained along the *x*-axis which results in the reduction of its width as well as its thickness. The final state is shown in dark grey. This material thus exhibits a positive Poisson's ratio along both the thickness and the width directions. Consider now, that the original sample dimensions are l_0 (length), w_0 (width) and t_0 (thickness). Assume that the sample is now stretched in the length direction at a constant rate and all three dimensions are measured at small intervals of strain (say at every 1% length strain). At any i^{th} strain level, let the measured dimensions be l_i, w_i and t_i. Now the i^{th} strain along length direction can be calculated by subtracting the original length from

the current length ($l_i - l_0$) (called engineering strain) or it can be calculated by subtracting the one previous length value from the current length ($l_i - l_{i-1}$) (called true strain). The same two kinds of strains, engineering strain or true strain, can be calculated for the width and thickness directions as well. These two ways of reporting strains give rise to two important ways (among several others [4]) in which Poisson's ratio can be reported –

Instantaneous Poisson's ratio (IPR) – When true strain values are used for both the direction of applied stress and for the direction of measured changes. The way to calculate an instantaneous out-of-plane Poisson's ratio is shown below

$$\nu_i = -\frac{(t_i - t_{i-1})/t_{i-1}}{(l_i - l_{i-1})/l_{i-1}} \tag{3}$$

Effective Poisson's ratio (EPR) – When engineering strain values are used for both the direction of applied stress and for the direction of measured changes. The way to calculate an effective out-of-plane Poisson's ratio is shown below

$$\nu_i^{eng} = -\frac{(t_i - t_0)/t_0}{(l_i - l_0)/l_0} \tag{4}$$

For consistency, strain along the sample length will be called '**axial strain**' and the strain along thickness direction will be called '**thickness strain**'. To denote a strain perpendicular to the axial direction, i.e. strain in either the width or the thickness direction, the term '**transverse strain**' will be used.

Poisson's ratio is one of the fundamental elastic constants along with Young's modulus (E), shear modulus (G) and bulk modulus (B) [2, 5]. It is a dimensionless quantity. These constants are related to each other as shown in Equation 5. According to the classical elasticity theory [5], if the Poisson's ratio is less than 0.5, a material increases in volume upon strain (such that its density decreases). Perfect volume

conservation for an isotropic elastic material makes its Poisson's ratio to be 0.5 [6], as in ideal rubber and in liquids. If an increase in volume is not accompanied with any change in lateral dimensions (that is the cross-sectional area is conserved), then its Poisson's ratio is *zero* (like cork) [7]. However, if it causes a lateral dimension to increase then the Poisson's ratio becomes negative. At a Poisson's ratio of –1.0, the aspect ratio of the material stands conserved for the two involved directions. For an isotropic material strained within elastic limits, the value of Poisson's ratio can lie between –1.0 and +0.5 [8]. There are however, no limits on the values of Poisson's ratio if the strain is beyond elastic limits or if the material is anisotropic [8, 9].

$$\nu = \frac{3B - 2G}{6B + 2G} \tag{5}$$

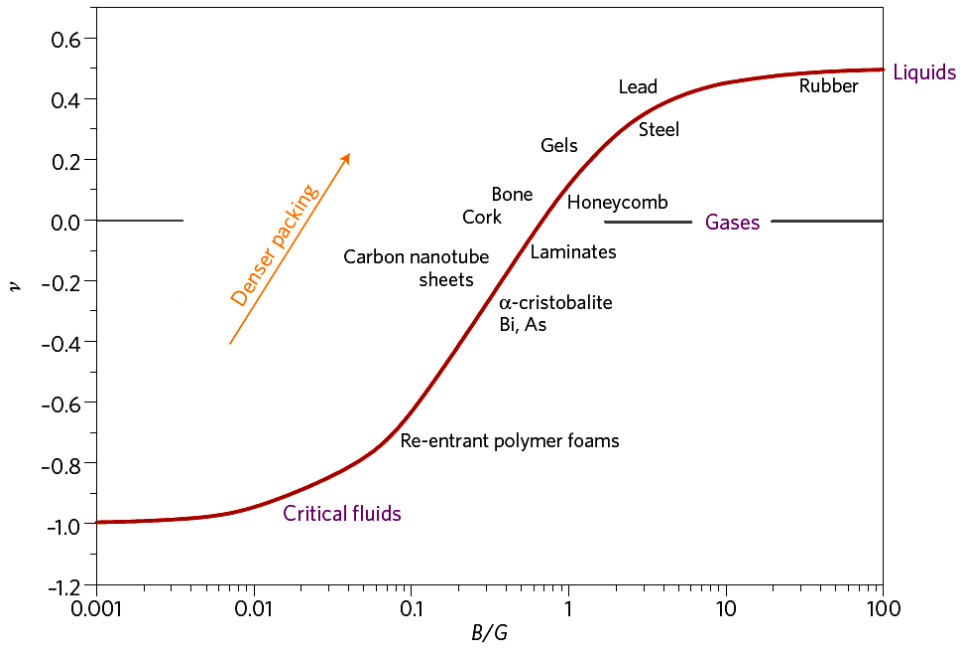

Figure 2: Relationship of Poisson's ratio as a function of ratio of bulk to shear moduli for a range of isotropic materials (*adapted from* [10])

Figure 2 shows the variation of Poisson's ratio with the ratio of bulk modulus (B) to shear modulus (G). The following relationships can be established from the fundamental equation of elasticity shown in Equation 5. For $B/G >> 1$, the material is quite incompressible and its Poisson's ratio approaches 0.5 (like that in rubbers) and when $B/G << 1$, the material is highly compressible and its Poisson's ratio approaches –1.0 (like in auxetic foams [11]). Terms like 'anti-rubber' and 'dilational' were used to describe materials with a negative Poisson's ratio [12] until the term auxetic was coined. When B = G, Poisson's ratio takes the value of *zero*. The physical properties of most commonly used materials lie between that of cork and rubbers – including the stiff metals and relatively very compliant plastics, both of which exhibit Poisson's ratio values around +0.3.

It is interesting to note that there are no commonly used materials showing a Poisson's ratio value below zero despite being within the range allowed by the theory of elasticity; although certain examples of materials from Section 2.2 and Section 2.4 can be thought of being common in certain industries. The examples shown in Figure 2 are rare instances found in nature or of materials recently manufactured. Cork retains its cross-sectional area because of the presence of stiff ribs of honeycomb pores normal to the loading direction [10, 13]. Figure 3 shows these ribs as seen from the radial cross-section and tangential cross-section. Such rib-like structures, hinged at acute angles to each other, can open up during loading leading to a negative Poisson's ratio in most (if not all) examples of auxetic materials.

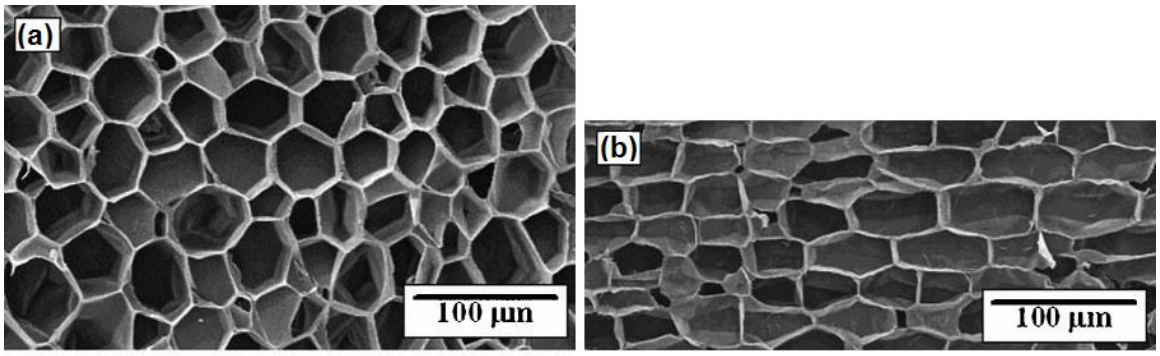

Figure 3: SEM images of cork in cross-section (a) normal (radial direction) to the direction of cell growth and (b) parallel to the direction of cell growth (tangential direction) [13]

2.2 Naturally occurring auxetic materials

Only a few naturally-occurring substances [2] are known to show auxetic behavior. Iron pyrite [5, 14], some crystals of arsenic, antimony, bismuth [15] and cadmium [16], some cubic metals [17] and some face-centered-cubic crystals [18] along specific directions, the α-cristobalite form of silica crystal [19], cat skin [20], cow teat skin [21] and certain types of bones [22] are known examples of such materials. Baughman et al. have predicted that 69% of all cubic elemental metals will show auxetic response when strained along the (110) direction (being partially auxetic) [17]. As shown in Figure 4, the solid tries to minimize a decrease in density during deformation along the direction (110) (joining spheres 2 and 4), by maintaining the inter-sphere (inter-atomic) contact – spheres 1 and 3 move in while spheres 5 and 6 move out. Simple geometrical calculations [17] showed that the Poisson's ratio for (110, 001) is +2 and for (110, 110) is –1. Twisting and bending of iron-pyrite monocrystal mineral rods produced a Poisson's ratio of about –1/7 [5, 23]. This result, reported in 1882, was probably the first discovery

of an auxetic material. Gunton and Saunders [15] calculated Poisson's ratios from experimentally known values of elastic compliance constants for arsenic, antimony and bismuth and found them to be negative along certain directions. Using similar calculations Li found auxetic behavior in hexagonal Cadmium crystals [16]. Milstein and Huang [18] concluded through theoretical calculations that the Poisson's ratios for many face-centered-cubic solid crystals are of opposite signs in the two principal crystal directions normal to the (110) uniaxial load.

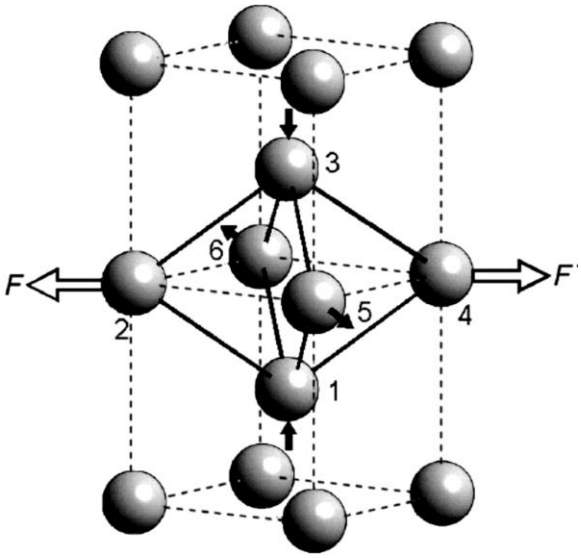

Figure 4: Origin of negative Poisson's ratio (due to displacement of spheres 5 and 6) and a large positive Poisson's ratio (due to displacement of spheres 1 and 3) in a body-centered-cubic solid crystal [17]

Yeganeh-Haeri et al. in 1992 [19] were the first to experimentally establish auxetic behavior in the α-cristobalite polymorph of silica. They found using laser Brillouin spectroscopy that α-cristobalite contracted laterally when compressed and expanded laterally when stretched showing Poisson's ratio values of as low as –0.5 in

certain directions and an aggregate average value of –0.16. In the same year, Chelikowsky et al. reproduced the negative Poisson's ratio in α-cristobalite through *ab initio* calculations [24, 25] (Figure 5). Kimizuka [26] studied the auxetic response in cristobalites over the temperature range of 300 – 1800 K (including alpha to beta transitions) using molecular dynamics simulations and found differing mechanisms operating in the two phases. Later Grima et al. [27] attributed the auxetic response in α-cristobalite to the presence of two dimensional rigid rotating rectangles in its molecular structure.

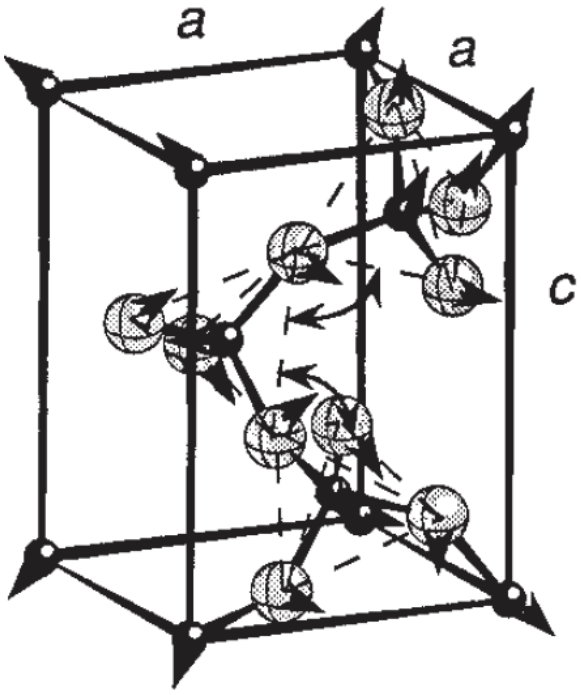

Figure 5: Motion of atoms – dark (Si) and light (O) – in α-cristobalite when it is subjected to uniaxial tension shows an expansion of the unit cell and thus an auxetic response. '*a*' and '*c*' are lattice parameters [25]

The occurrence of a negative Poisson's ratio at this (atomic/molecular) small scale has only been observed in natural materials as shown by the above mentioned examples. We will discuss later that synthesis of auxetic materials on a molecular scale has not been achieved yet.

Among biological systems, Veronda and Westmann performed uniaxial tests on cat skin and observed (among other interesting properties) an initial thickness increase due to "straightening, translating and rotating of the dermal fibers" [20]. Lees et al. found structural analogies between cow teat skin and knitted fabrics which causes them to show a negative Poisson's ratio at small strains [21]. Uniaxial experiments and finite element analysis on cancellous bone cubes from the human tibia also showed negative Poisson's ratio (about –0.07) along one direction and positive Poisson's ratio (about 0.52) in the other [22].

Continued investigation of minerals, crystal structures and biological systems may change the perception of auxetic behavior being a rare phenomenon in future. Natural auxetic structural features serve as an inspiration to scientists in investigating auxetic response in synthetic materials.

2.3 Common mechanisms of auxetic response

Known mechanisms of auxetic response usually stem from the structural geometry of materials and/or their deformation characteristics [2]. In most cases it is either opening up of acute angles between rigid struts/ribs/columns and structural hinges [27, 28] or a fibrillar network deformation (like in auxetic tissue) [20, 29, 30]. Many geometrical structures are inherently auxetic. Figure 6 below shows some of these 2D and

3D structures, which, upon visual observation, strongly hint of an auxetic deformation. In case of 2D structures, the deformation too is assumed to be strictly in the 2D plane. Such design elements have the potential to be incorporated into a material's structure to induce auxetic response. The scale of the design structure can vary greatly; in fact Poisson's ratio and other classical elastic properties have no length scale restriction [11], excluding quantum and galactic length scales of course. Figure 6 (a) illustrates a honeycomb structure (showing positive Poisson's ratio) and an inverted honeycomb structure (also called a reentrant or a 'bow-tie' structure) that shows a negative Poisson's ratio. The opening up of angles between the ribs of the reentrant hexagon causes the structure to expand in a direction perpendicular to the strain [31].

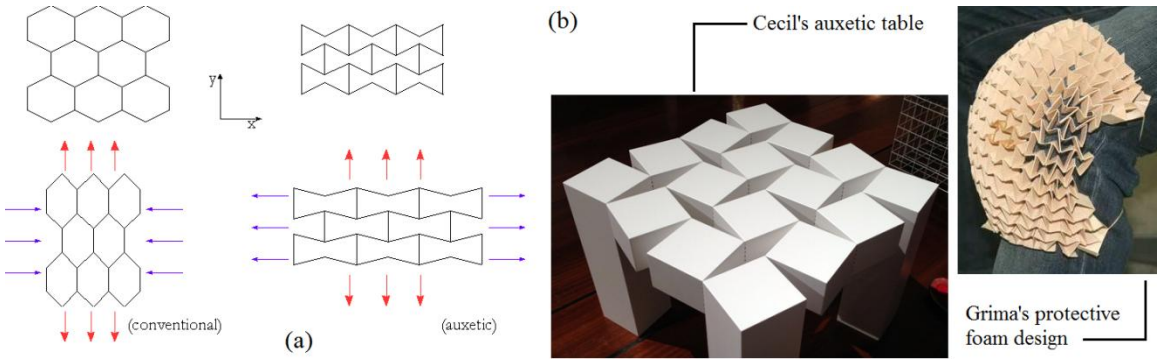

Figure 6: Geometrical auxetic structures (a) Honeycomb structure on left and inverted honeycomb structure on right (b) examples of some 3D structures that are auxetic [32]

Grima and Evans [33, 34] demonstrate the use of hinged rotating squares and rotating triangles as a structural unit in producing auxetic materials. Figure 7(a) shows an interconnected network of triangles hinged at points in a way such that a hexagonal cavity is created. In the most compact state, the edges of the triangle touch each other

(angle, θ = 0°). When pulled along a planar axis, the rigid triangles rotate such that the angle between the edges increases continuously to 30°, 60°, 90° and further up to a maximum of 120°. This results in an increase of dimension perpendicular to the pull [34]. The model of rotating squares works similarly (see Figure 7b) [33].

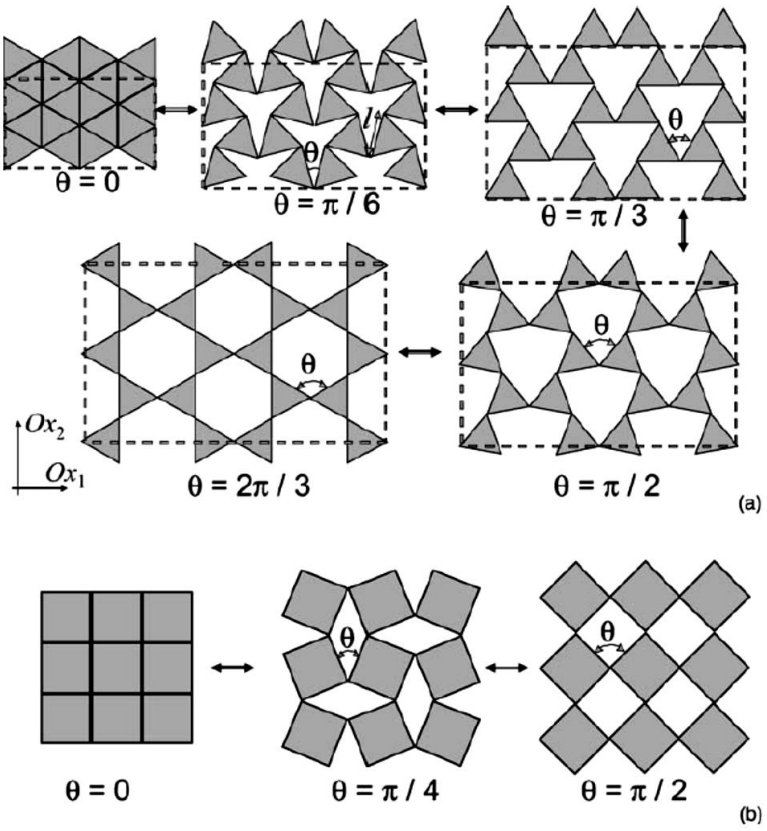

Figure 7: Mechanism of auxetic response in hinged rotating triangles (a) and rotating squares (b) [33, 34]

Grima's rotating squares and rotating equilateral triangles exhibit a Poisson's ratio of –1.0 irrespective of direction of loading and irrespective of the size of units. Grima also suggested that this mechanism should be discoverable in real crystal systems. Figure

6 (b) shows some 3D auxetic structures consisting of volume units enclosed by hinged and rotating squares, cubes or bowtie walls. Many other 3D auxetic structures are also possible and are occasionally derived from analogous 2D auxetic geometries. Wojciechowski et al. have found negative Poisson's ratio at high packing density in hexagonal molecules on a triangular lattice [35], in atomic cyclic trimers [36, 37] and in hard cyclic pentamers and heptamers [38]. Similarly, Neville et al. very recently used kirigami techniques to produce and characterize PEEK honeycombs that exhibited a Poisson's ratio of zero [39].

2.4 Synthetic auxetic materials

The development of synthetic auxetic materials started with the invention of Lakes's auxetic foams [11] in 1987 (see Figure 8a). A polyester foam of density 0.03 g cm^{-3}, cell size 1.2 mm and Poisson's ratio of 0.4 was heat-compressed triaxially in a mold at about 170 °C (temperature slightly above the softening point of the foam) and then cooled to room temperature while still under compression before taking it out of the mold. The resulting foams, with permanent volume compression by a factor of 1.4 to 4, were found to exhibit a negative Poisson's ratio. In one case, a Poisson's ratio of –0.7 was observed for one of these foams whose volume had been halved during compression. The cell structure had also changed from one having obtuse angles between cell walls to one having acute angles (reentrant structure) between them. This change in cell structure can be seen in Figure 8a, top and bottom. Subsequent to Lakes's treatment of conventional open-cell polymeric foams to produce a negative Poisson's ratio, other process modification of linear polymers such as PE and PTFE was successful in achieving

auxetic response. In 1989, Evans and Caddock found large negative Poisson's ratios as low as –12 in expanded-PTFE [40]. Expanded-PTFE is produced by rapid heating and drawing of sintered PTFE resulting in a porous microstructure consisting of oblong nodules interconnected by fibrils (Figure 8c). They reasoned that when strained, the tension in fibrils causes first the displacement of nodes and then further rotation to cause lateral displacement (and hence material expansion) of nodes (see Figure 8b).

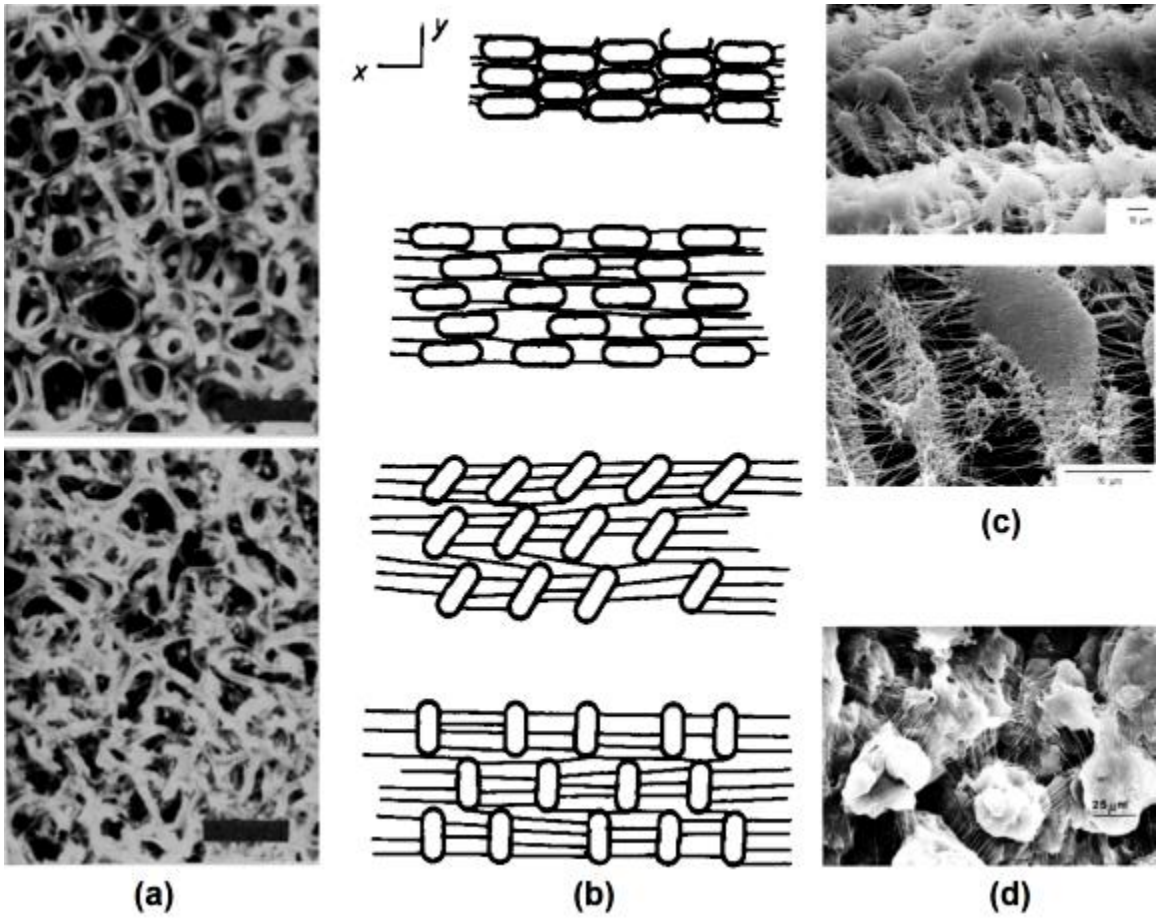

Figure 8: Examples of synthetic auxetic materials (a) Lakes's foams, (b) mechanism of lateral expansion in expanded-PTFE (c) SEM micrograph of expanded-PTFE and (d) SEM micrograph of ultra-high molecular weight PE [11, 40, 41]

Thereafter, Alderson and Evans developed a processing route to produce a microporous form of ultra-high-molecular-weight polyethylene exhibiting Poisson's ratio as low as –1.2 [41]. Alderson's auxetic PE was prepared by compaction of PE powder at 110 °C followed by sintering and extrusion at 100 – 190 °C which, again, resulted in a microstructure composed of nodules (more spherical in this case) and fibrils similar to Evans's expanded PTFE (Figure 8d). It is noteworthy in these examples that the polymers themselves were not inherently auxetic by virtue of their molecular/chemical structure, but instead a processing method was devised to produce a macroscopically auxetic structure.

In addition to approaches to induce auxetic response via clever tailoring of processing conditions using conventional polymers as described above, there have been extensive efforts in synthetic macromolecular approaches to produce a nanoscale material with intrinsic auxetic properties. Recently, modeling attempts (not experimental) were made to introduce auxetic character in the polymeric chains themselves by trying to introduce reentrant geometries into molecular networks. Evans [1], Grima [42–45] and Baughman et al. [46] have modeled and simulated various polymer networks that should exhibit negative Poisson's ratio. Evans suggested a reentrant honeycomb structured compound of (1,4)-reflexyne as a potential candidate to exhibit auxetic behavior on a molecular level [1]. Similarly, Grima prescribed polyphenlyacetylene and polycalix-4-arene based structures (Figure 9 a, b) as auxetic possibilities. Both structures are based on geometrical models, which have been theoretically predicted to exhibit auxetic behavior. The deformation mechanism in Grima's molecular structures is rather complex and out of the scope of this thesis, so it is not discussed further. Baughman showed that some

hypothetical phases of carbon such as hinged polyacetylenes should show this behavior [46]. However, synthesis of such polymers has been a daunting task for over more than a decade of research primarily because of molecular complexity and the huge energy barrier involved in changing (increasing) the chemical bond angles during straining of the molecular models. Chemical bond angles would not change under normal mechanical stress levels, thus not allowing the opening up of acute angles prescribed in the models. Following the idea on polymer chain designs, Griffin et al. [47–50] proposed that certain liquid crystalline polymers with transverse rigid rods in the main chain should show an increase in inter-chain separation upon straining (Figure 9c). In 1998, Griffin et al. showed through X-ray diffraction studies that the inter-chain separation increased under stress on incorporation of laterally attached rods in a main chain liquid crystal polymer [47]. Different kinds of lateral rods – terphenyls [47, 49], quaterphenyls [47, 48] and pentaphenyl [47, 49, 50] – were later synthesized to control the maximum attainable angle of rods to the main chain (Figure 9d). Despite X-ray diffraction evidence of increased chain separation, macroscopic expansion (and hence macroscopic auxetic behavior) of the liquid crystal material (films) has not be observed experimentally. Grima et al. also showed auxetic behavior in idealized zeolite structures using force-field-based molecular simulations [51].

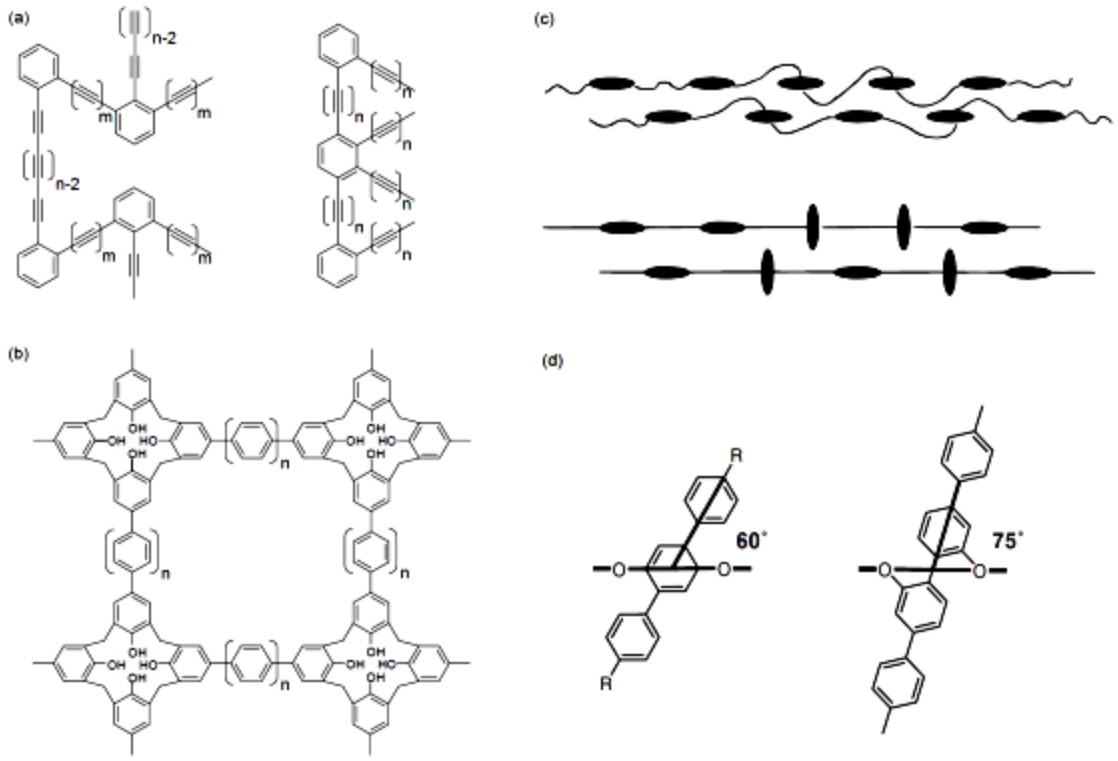

Figure 9: Molecular design approaches to create auxetic materials (a, b) Grima's designs based on phenylacetylenes and calixarenes, (c, d) Griffin's idea of using transverse rods in liquid crystal polymers [43, 45, 47, 48]

Some fiber-based auxetic structures have also been produced. In-plane auxetic behavior was observed in Baughman's buckypapers [52], whose Poisson's ratio changed from positive to negative by increasing the ratio of multi-walled carbon nanotubes to single-walled carbon nanotubes. Egg-rack type models (see Figure 10) were built to interpret the Poisson's ratio and predict other properties for these buckypapers [53]. Although the study is quite complex, it can be seen from simplified model in Figure 10 that an in-plane (*xy*-plane) uniaxial force causes the contact point between the red and the pink model fibers to move downward along the z-direction – resulting in a decrease in thickness and hence large positive *out-of-plane* Poisson's ratio value. However, this also

results in expansion of the structure in the planar direction, thus showing a negative *in-plane* Poisson's ratio. These buckypapers were prepared by a process similar to making paper from wood fibers. In-plane auxetic behavior has also been inferred from Raman band-shift data very recently for bacterial and microfibrillated cellulose networks [54]. On a larger scale of fiber networks, paper (made from cellulose fibers) [30, 55–58] and some textile materials [59–63] also exhibit auxetic behavior (more discussion in subsequent chapters).

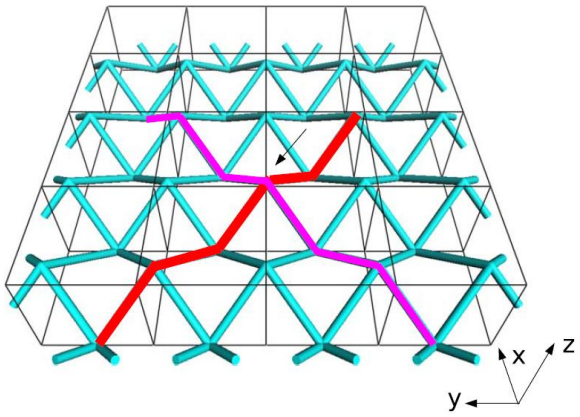

Figure 10: Egg-rack type model explaining the in-plane auxetic behavior in Baughman's buckypapers. The arrow indicates the position where the two model fibers (pink and the red) contact each other [53]

Composite materials, based on fiber networks too, were first theoretically predicted by Berhan et al. [64] to exhibit negative Poisson's ratio and later were synthesized [65] validating their hypothesis. Berhan [64, 66] also modeled networks of fused fibers that should show auxetic behavior. These auxetic fiber-mat networks made of steel were embedded in an ordinary (positive Poisson's ratio) polymer matrix, and it

was shown that the resulting composite was auxetic [65]. The negative values of Poisson's ratio associated with these fiber mats and composites were as large as –18 and –9, respectively. Alderson et al. reviewed various methods by which composites containing auxetic fibers could be produced and found better resistance to indentation and to fiber pullout in certain composites [67]. Many angled-ply laminates and composites have both been theoretically predicted and also experimentally produced to show auxetic behavior [68, 69]. Bezazi et al. studied auxetic carbon/epoxy laminate composites and found that the stiffness and maximum failure load decreased with fiber orientation angle in the laminates [70].

In terms of recent advances in the field, Grima et al. have described a novel solvent based process for inducing auxetic behavior in conventional open cell foams [71]. By using a solvent, Grima eliminated the need of thermal treatment in the heat-compression protocol he commonly used. In his experiments, the foam was wetted and compressed triaxially until the solvent dried to produce a reentrant structure. Another benefit of this method was that the reentrant foams could be converted back into conventional foams by wetting them again in an organic solvent [71].

Theoretical studies of model molecular systems [37] and examination of auxetics as smart metamaterials [72] has added much to our understanding of this phenomenon. At the macroscale there are ingeniously designed structures such as chiral honeycombs [28, 39] that show negative Poisson's ratio upon extension. Also, fiber-based composites [67, 69, 70] can be suitably assembled to produce a structure having a negative Poisson's ratio. Specially designed textile structures can also exhibit auxetic response [60, 62, 63,

73]. The background on some of these fiber based auxetic structures will be discussed in Sections 3.1.4 and 4.1.5 in more detail.

The possibility of employing a post-manufacture processing protocol to produce a structural feature(s) that confers auxetic response in a ubiquitous, commodity polymeric material, as described above, has given rise to much recent research and development effort and continues to be a desirable goal. In the following sub-section, some unique properties of auxetic materials and how these properties help in satisfying the application needs have been described.

2.5 Properties and applications of auxetic materials

Auxetic materials are rare and their properties, often the inverse of those of typical materials, are also rare: densification upon impact, becoming fatter when stretched, and exhibiting synclastic double curvature (described below), as examples [12, 74]. The combination of theoretical interest and practical applications has led to significant research and development activity on these unique materials.

Auxetic materials grow fatter when stretched. This means that a nail made up of an auxetic material is very difficult to pull out. For the same reason, auxetic materials are thought to make excellent fillers in composites [65, 67, 75]. When these composites are strained, the auxetic filler (in the form of fibers or discs) inside grows in lateral dimensions enhancing matrix-filler interfacial adhesion and thus improves load transfer through a mechanical interlocking mechanism.

Arterial prosthesis is expected to benefit from auxetic behavior [29] too. The pulse of blood causes these arteries to stretch but also thicken at the same time (Figure

11), thus preventing thinning and rupture of the arterial wall, which could happen if they were made of an ordinary material with positive Poisson's ratio.

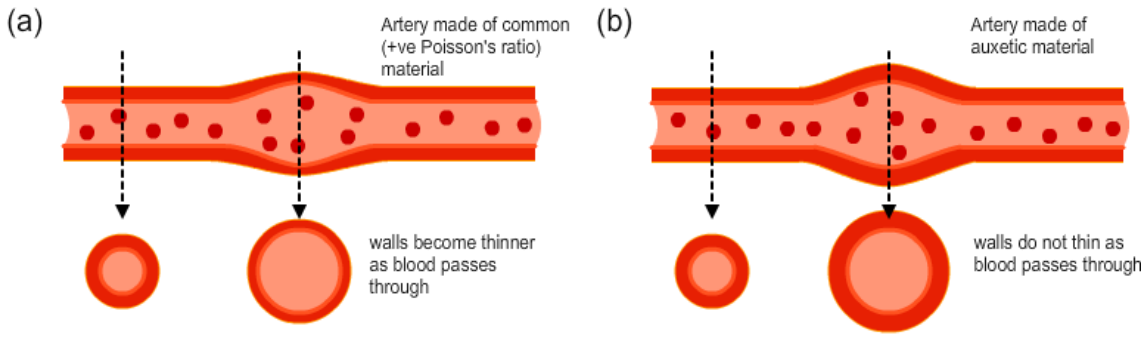

Figure 11: Flow of blood causes artificial artery walls made out of common materials to stretch and thin out (a) but causes a wall made of auxetic material to thicken (b) [2]

Auxetic materials also contract and densify when compressed – a behavior directly opposite to ordinary materials. This property can enhance the indentation resistance, impact strength [76] and hardness of auxetic materials [2] depending upon the direction of auxetic response. Research emphasis has recently turned to constructing bullet-proof vests and impact-curtains out of auxetic knitted structures and composites [31, 62, 77].

In-plane auxetic materials also exhibit synclastic curvature [2] (see Figure 12). This property allows them to be bent into a doubly-curved surface like that of a sphere or a dome without creasing (and without loss of uniformity in stress). Ordinary materials are easy to fold into a cone or cylinder but develop creases or fracture if tried to be put into a spherical shape. Dome shaped structures are usually constructed by joining together ordinary material parts which makes them susceptible to failure at joints. Similarly,

cushions and mattresses made from auxetic foams offer better conformability and more uniform support to our bodies [78].

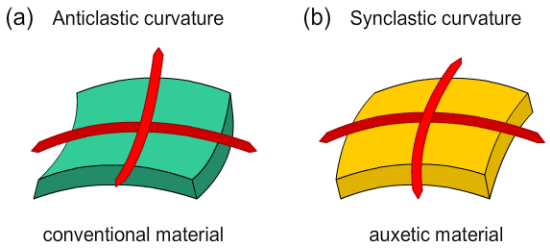

Figure 12: Anticlastic curvature in common materials with positive Poisson's ratio (a) and synclastic curvature in auxetic materials (b) (*adapted from* [2])

The average pore size in auxetic networks (regular or random size pores) increases when they are stretched and contracts when compressed. This is a direct result of an increase in volume when stretched. This property has a potential for application in 'defouling' of filtration membranes [79]. Pores of filtration membranes are susceptible to frequent clogging. Flexible membranes with positive Poisson's ratio cannot be compressed on the sides to open up the pores. However, if they are made from auxetic networks, they can rather be stretched to open the pores up and clean by flushing the dirt out with water. We believe that this property can also be utilized in producing tunable molecular sieves or microscopic scale filtration in the future.

Auxetic metal crystals may be used as electrodes that can amplify response of piezoelectric sensors [17]. Recently, Grima et al. have devised stimulus based (electric, solvent, magnetic) usage of auxetic smart metamaterials that should find application [72]. Due to their porous nature, their ability to be formed from common and inert polymers

(such as PTFE) and other unique properties such as synclastic curvature; auxetic materials have promising potential in medical applications.

2.6 Motivation

Study of dimensional changes as a response to stress, especially auxetic responses, in fiber based network structures has been an area that has largely remained under-explored. Two such fiber based materials, paper and nonwoven fabrics, are ubiquitous commodity materials used all over the world for over tens of centuries. The wide use of these materials and easy availability of raw materials for their production, coupled with the unique properties and applications of auxetic materials, makes the study of auxetic behavior in fiber networks an exciting and a fruitful prospect.

There have been a few reports that paper shows an increase in thickness (out-of-plane auxetic response) when strained uniaxially in a planar direction and that the auxetic response is large [55–58]. However, these reports examined only a small set of commercial papers and have not received much notice by the auxetic community. There have been no reports (in our knowledge) of auxetic behavior in nonwoven fabrics, despite their wide use and availability. Producing an auxetic response in other kinds of fiber systems (carbon nanotubes, steel nanowires, knitted fabrics) as described above, however, has been an area of emerging and active research. Paper, nonwovens and other fiber network systems have not been fully researched for the mechanistic origin of auxetic behavior and its possible applications. Furthermore, the potential application of these materials in textiles, construction and composites increases the importance of such studies many folds.

Existing but very reports on out-of-plane auxetic response in paper have inspired us to investigate and better understand the occurrence of this behavior in various types of paper. Similarly, inducing the same behavior in other kinds of nonwovens presents a processing challenge but greatly extends our ability to produce new and inexpensive auxetic materials. It is desired to discover novel operating mechanisms for auxetic response in both paper and needle-punched nonwovens which can ultimately help researchers in the fabrication of many types of polymer networks providing ample design space for meeting a spectrum of application requirements. It is also anticipated to establish some fundamental relationships between out-of-plane Poisson's ratio and network/processing parameters to help better predict structure-property relations in newer systems.

There has been relatively more amount of research done on in-plane auxetic behavior than out-of-plane auxetic behavior. However, as also noted by Evans et al. [2], the difference in the way these two kinds of auxetic responses affect material properties (shear resistance, compressibility, strength etc.) is not yet fully understood. Out-of-plane auxetic materials exhibit unique properties of indentation, impact resistance, blast and burst resistance and also wave dampening. The protocols developed during this research too, for the accurate measurement of out-of-plane Poisson's ratio and for the processing of nonwovens should assist other researchers working on similar systems.

CHAPTER 3

AUXETIC BEHAVIOR IN PAPER

3.1 Background

Papermaking is an ancient science that has evolved with time and technology to improve the properties of paper products depending upon their end use. Fibers used for making paper are mostly derived from wood – which in scientific terms is the secondary xylem tissue of seed-bearing plants. Wood fibers are mainly composed of cellulose, hemicellulose and lignin. Cellulose is the crystalline component accounting for most of the fiber strength while hemicellulose and lignin, required mainly for other biological functions, are amorphous, and surround the crystalline regions of cellulose. It is important to understand the morphology of wood to understand the structure of fibers and the process of papermaking altogether.

3.1.1 Anatomy of wood

A tree's trunk is protected by a non-living bark on the outside (Figure 13). The remaining and the majority of trunk is composed of 'vascular cambium' tissue containing phloem cells on the outside and xylem cells on the inside [80]. The xylem portion of the cambium is commonly referred to as 'wood'. Wood is composed of highly ordered axial and radial cells. Fibers used to make paper are mostly derived from these vertically bundled axial cells [81]. Axial cells perform many transport functions along the height of the tree, and are responsible for its structural strength (Figure 14).

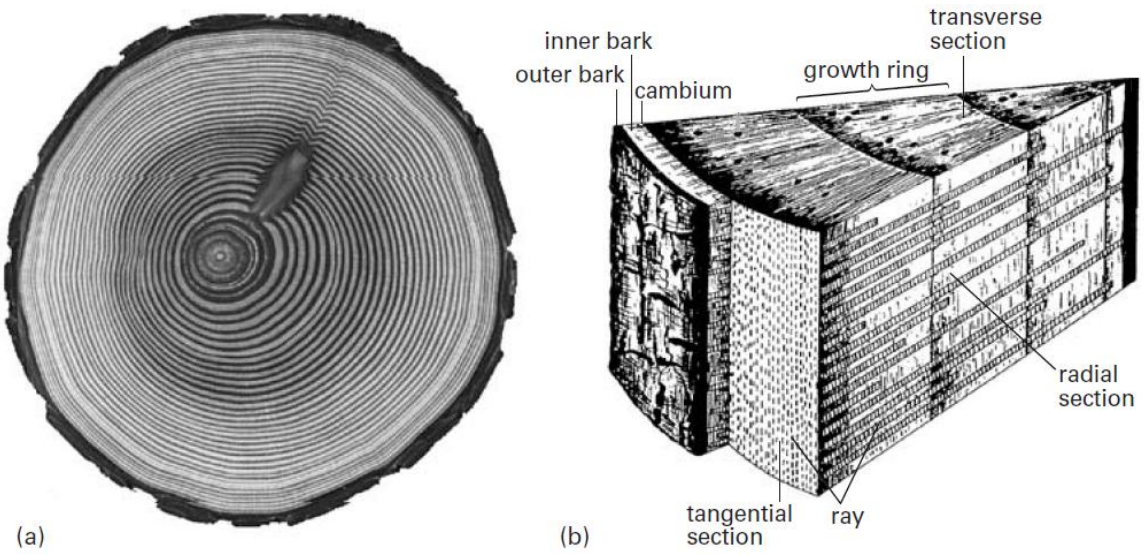

Figure 13: Morphology of a woody tree trunk (a) a tree cross-section showing the bark on the outside, pith at the center and annual growth rings and (b) a pie-cross-section showing the arrangement of xylem and phloem tissues and the radial and axial cells (*adapted from* [80])

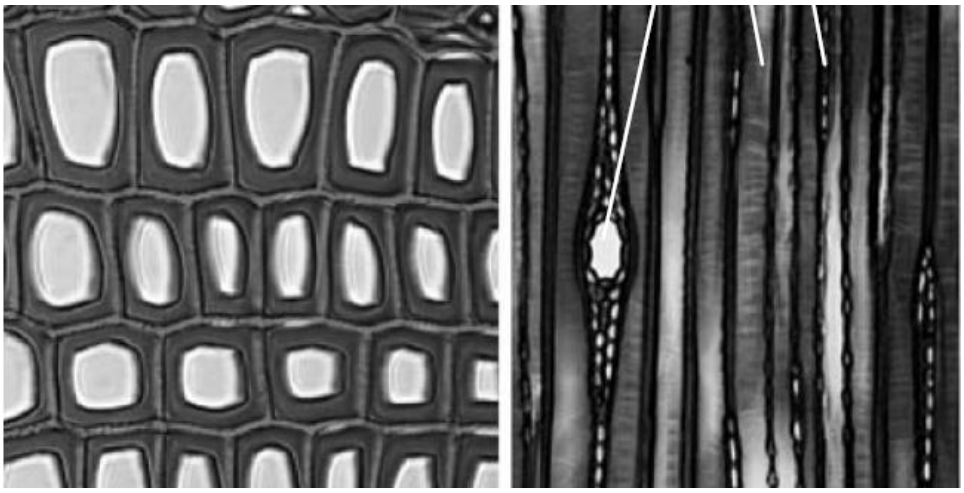

Figure 14: SEM of transverse section (a – left) and axial section (b – right) of xylem cells (tracheids or wood fibers) of a spruce tree [80]

Wood can be broadly classified into softwood, which is produced by coniferous trees (Gymnosperms) and hardwood, which is produced by broad-leafed deciduous trees (Angiosperms) [80]. Wood fibers, tracheids, or wood cells (all synonymous terms for this thesis), from which paper is made, are hollow tubules with a square or rectangular cross-section and aspect ratio (length to diameter ratio) of roughly about 100 (Figure 14b) [80]. The hollow portion of the fiber is called the 'lumen' and is responsible for fluid transport in the plant. These are shown as bright regions and the fiber walls are shown as dark regions in Figure 14a. These walls (cell walls) – composed mainly of cellulose, hemicellulose and lignin – provide structural support to the plant and perform some other important biological functions.

A crude approximation of the average tracheid length (and hence the fiber length) for softwoods is about 3 mm and for hardwoods is about 1 mm. Its width is about 30 μm in softwoods and about 20 μm in hardwoods [80, 82]. Fiber walls and the lumen undergo immense structural and chemical changes during the process of papermaking [83], all of which directly affect the physical properties of the resulting paper.

Plant cell/fiber walls are mainly composed of cellulose, hemicellulose and lignin [84]. Cellulose is a linear polymer of cellobiose units, which in turn is a $\beta\ (1\rightarrow4)$ dimer of glucose. Figure 15 shows the cellulose molecular structure, its assembly into crystalline cellulose chains and further to form microfibrils which then form the cell wall. Hemicelluloses are a class of hetero polysaccharides such as xylan, glucomannan etc. that have a random or amorphous structure [85]. Lignins are complex polymer molecules that are amorphous and hydrophobic and covalently bond to hydrophilic hemicelluloses and cellulose [80, 84]. Lignin thus holds cellulose/hemicellulose together between adjacent

cell walls and makes it waterproof (see Figure 16). Plant cell/fiber wall is thus composed of cellulose-hemicellulose microfibrils and most of the lignin is present between two fiber walls, gluing them together [80]. Figure 15 and Figure 16 show the distribution of cellulose, lignin and hemicellulose in a plant cell wall.

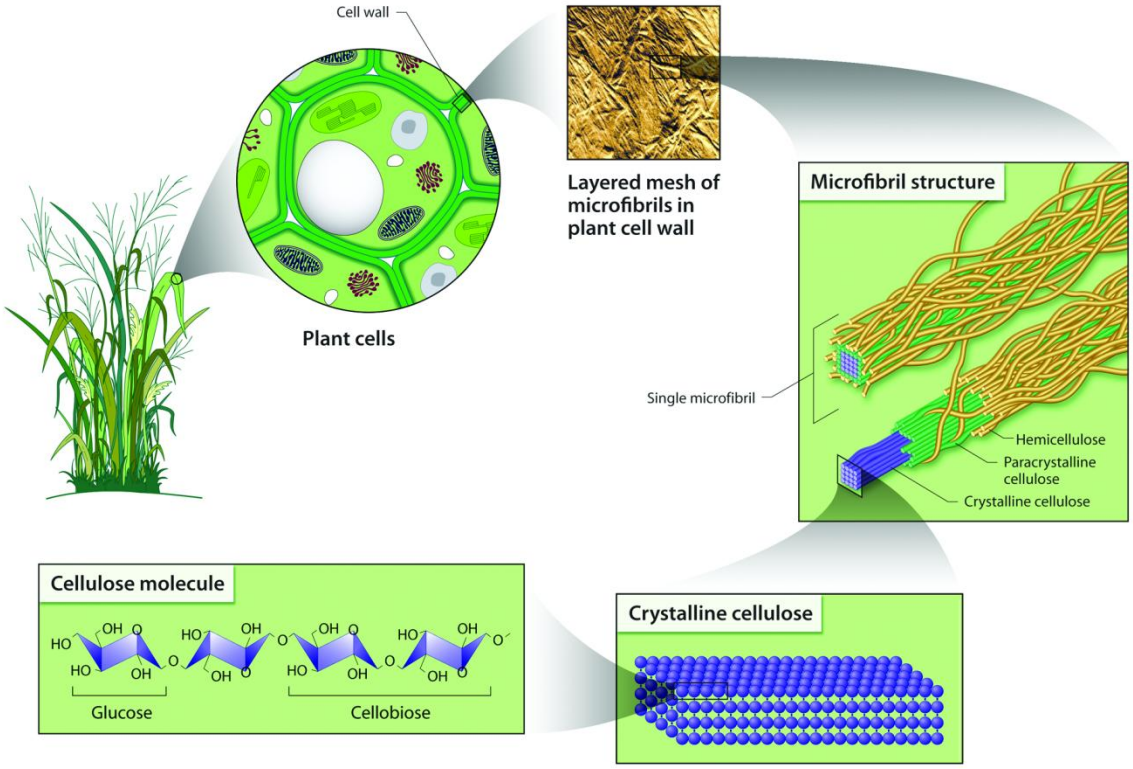

Figure 15: Organization of glucose units, cellulose chains, microfibrils and fibers in a plant cell wall (Source: https://public.ornl.gov/)

When the fibers are seen along the radial direction, they are organized into distinct concentric layers as shown in Figure 17. The lignin-rich layer gluing adjacent fibers together is called the ‘compound middle lamella’. Next to the middle lamella is the outermost layer of the fiber/cell called the primary wall that is made from randomly

oriented cellulose microfibrils. Inside the primary wall is 'secondary wall' which is further divided into concentric S1 (outermost), S2 and S3 (innermost) sublayers [80, 86]. Each of these three layers is distinct from each other due to the different direction of cellulose microfibrils within them. S2 sublayer also contributes most to the volume of the entire cell wall in majority of trees and is therefore the major contributor of cellulose and hemicellulose.

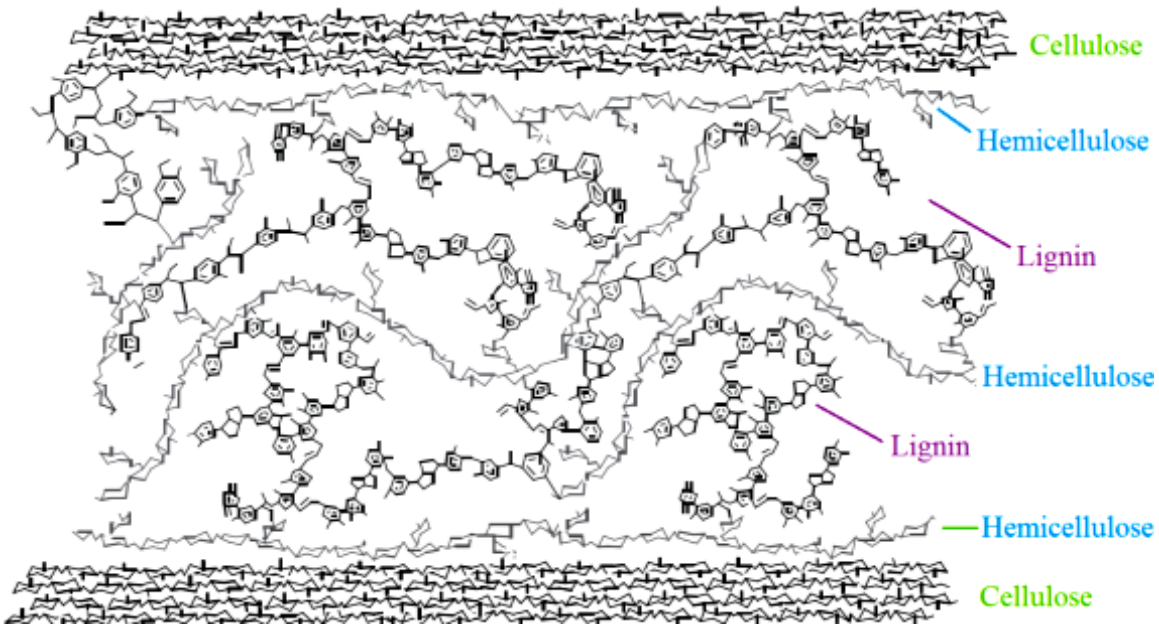

Figure 16: Typical distribution of lignin, hemicelluloses and cellulose in S2 layer of a plant cell wall. Cellulose occurs as crystalline regions of a bundle of (polymeric) cellulose chains sandwiching amorphous regions of hemicelluloses and lignin. Most of the lignin is bonded with hemicellulose as shown but is also known to directly bond with cellulose (*adapted from* [80]).

Composition wise, both softwood and hardwood contain about 40-45% cellulose. However, hardwoods contain more lignin (25-30%) compared to softwoods (15-25%) and less hemicellulose (25-30%) than softwoods (25-35%) [80, 84]. There are many other

anatomical and chemical differences between hardwoods and softwoods than discussed here, but they are not within the scope of this study.

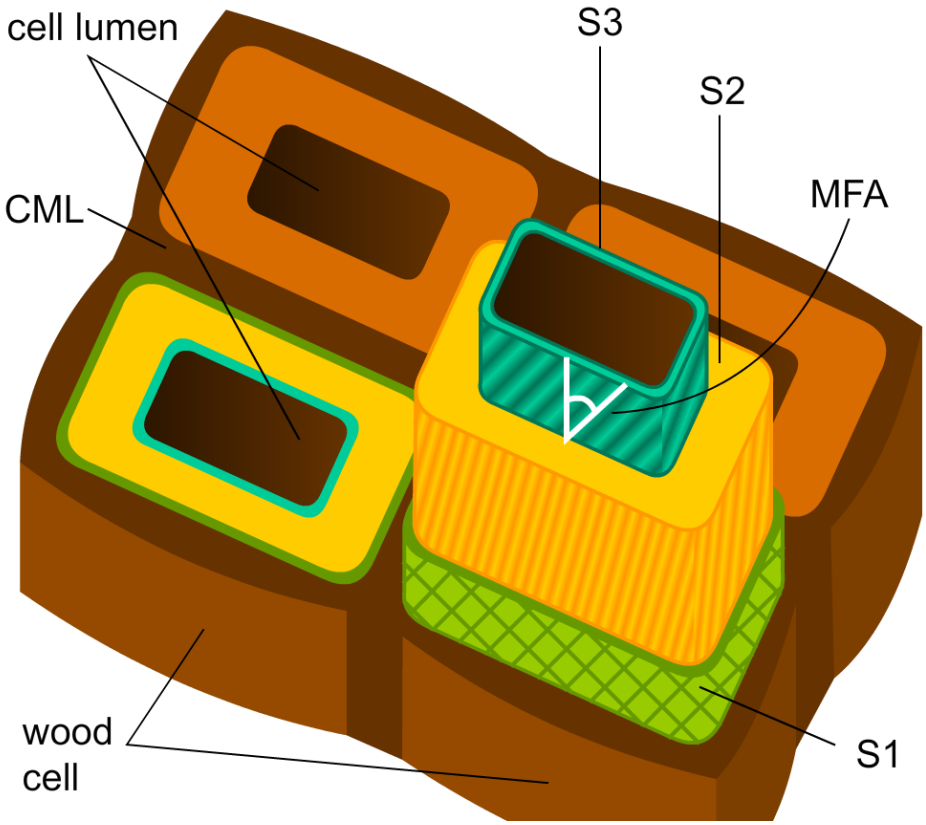

Figure 17: A wood cell wall organization showing cellular lumen, compound middle lamella (CML) and secondary layers (S1, S2 and S3) mainly composed of cellulose. S2 layer has more cellulose content and contributes most to the strength of the fiber. MFA (micro fibrillar angle) is the angle made by oriented cellulose fibers with the axis [86].

3.1.2 The science of papermaking

A typical papermaking sequence starts with debarking and chipping of wood logs. Wood chips then undergo pulping, an operation where the chips are disintegrated into individual fibers [87]. Figure 18 shows the entire papermaking sequence from cutting of

trees to reeling out the finished paper. Kraft pulping is the most common type of chemical pulping where wood chips are chemically ‘cooked/digested’ to make the lignin water-soluble using sodium hydroxide and sodium sulphide [83, 87].

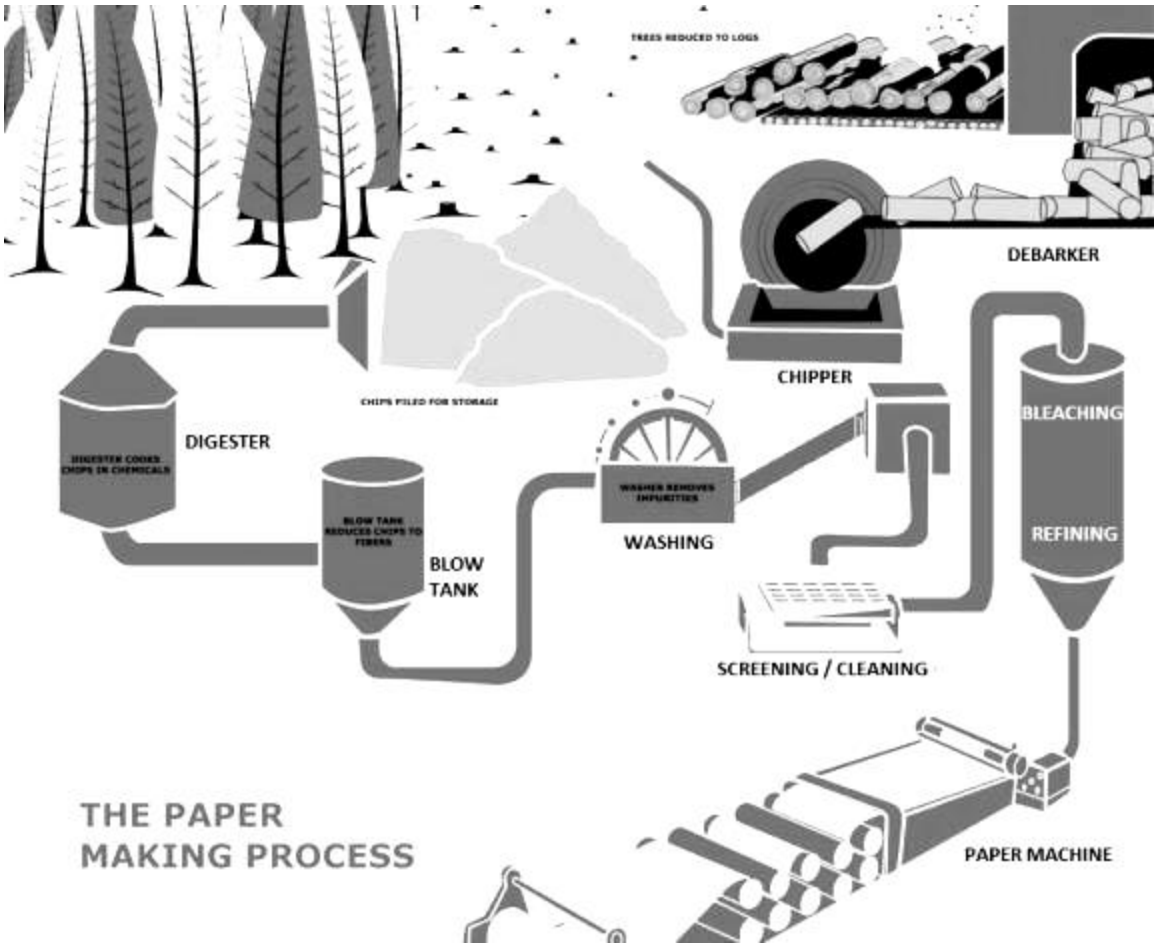

Figure 18: Illustration showing a common papermaking process (Source: http://www.seedesignstudio.com/paper.html)

Pulping chemicals attack the lignin between the cells/fibers and sometimes even the primary cell wall. These chemicals introduce charged groups on the oily lignin macromolecule and help it to float in water, thus dissolving the lignin and separating the

wood fibers from one another [80, 83, 87]. Pulping is followed by many washing stages with water, which wash away the dissolved lignin. Wood fibers are hence segregated exposing the S1/S2 layer which enables them to form inter-fiber hydrogen bonding in paper later [80, 88–90]. Pulping chemicals cannot remove all the lignin present in wood. Some other small impurities like dirt, tar etc. are removed by filtering screens.

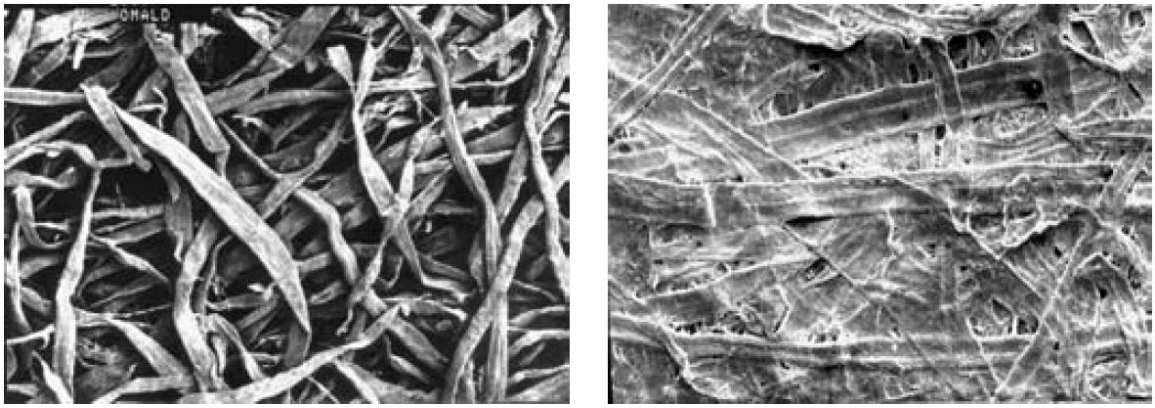

Figure 19: SEM showing fibers before (left) and after (right) refining of the pulp [83]

After pulping-washing-screening, the pulp still contains about 2-5% (by dry pulp weight) of lignin and appears brown in color. Brown color of pulp is due to the presence of chromophores present in the structure of lignin [91, 92]. Paper needed for printing is desired to appear white and bright. Further delignification and brightening is achieved by bleaching of pulp. Bleaching chemicals decompose and get rid of some more lignin that pulping chemicals were not able to remove [93]. Chemicals such as peroxide, chlorine dioxide, oxygen and ozone are commonly used for bleaching [93]. Bleached pulp appears white. As expected, the pulp needs to be washed again after bleaching. Sometimes, to increase the fiber-fiber hydrogen bonding, the fiber surfaces are mechanically stripped

and defibrillated in a process called 'refining' or 'beating' [94, 95]. Refining defibrillates the outer (primary) and S1 sub-layers of the fiber cell wall producing a much larger surface area for H-bonding (see Figure 19 and Figure 20). It also affects the shape of the lumen of the fiber by flattening it out further (flattening also occurs during delignification and later during drying) [95].

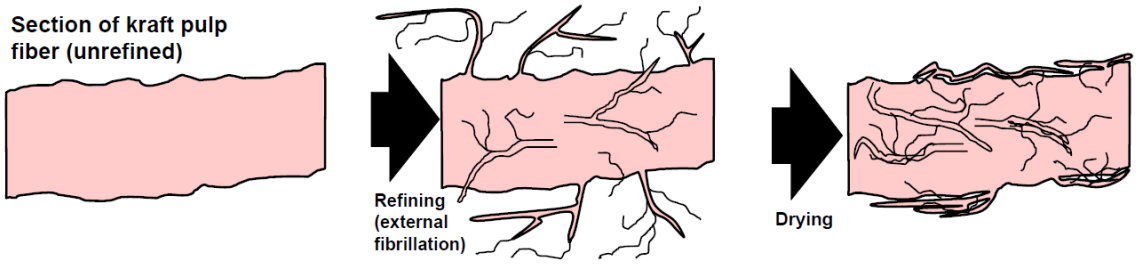

Figure 20: Cell wall fibrillation during refining operation and snapping of fibrils back to surface during drying [95]

Pulping and bleaching (bleaching is optional) are followed by paper formation on a paper machine (see Figure 21). A dilute slurry of pulp is made in water (about 0.1 to 1.0 % by weight) and sprayed (by a device called headbox) on a moving wire (a woven fabric). The fibers in the slurry settle on the moving wire and form a fiber-web while water is drained by gravity through the wire. The direction of movement of the wire is away from the headbox and is called the machine direction. The pulp concentration, the velocity and angle of spraying, the speed and drainage of wire etc. can be varied depending upon the kind of paper in production. By the end of the wire, the fiber web loses about 20% of its water i.e. about 80% water content remains [91]. Water restricts direct fiber-fiber interaction but inter-fiber hydrogen bonds can form whenever the

adjacent fibers contact each other throughout the papermaking process. The web is mechanically transferred from the wire to heavy rolls that press out some more water from the web. After pressing the water content of the web is about 60% [91]. The pressed web is then sent through drying steel rolls that are at a temperature usually above boiling point of water [82, 95]. The dried paper still contains about 5-6% of moisture, which is also close to the moisture content of paper under ambient humidity conditions. Note that by this time, the fiber takes a flattened cross-section (instead of a square/circular cross-section) due to the collapse of lumen, especially during refining, pressing and drying. After drying, paper can be made to undergo calendering [96] (which smoothens the surface) and coating [97, 98] (with specific chemicals) if required.

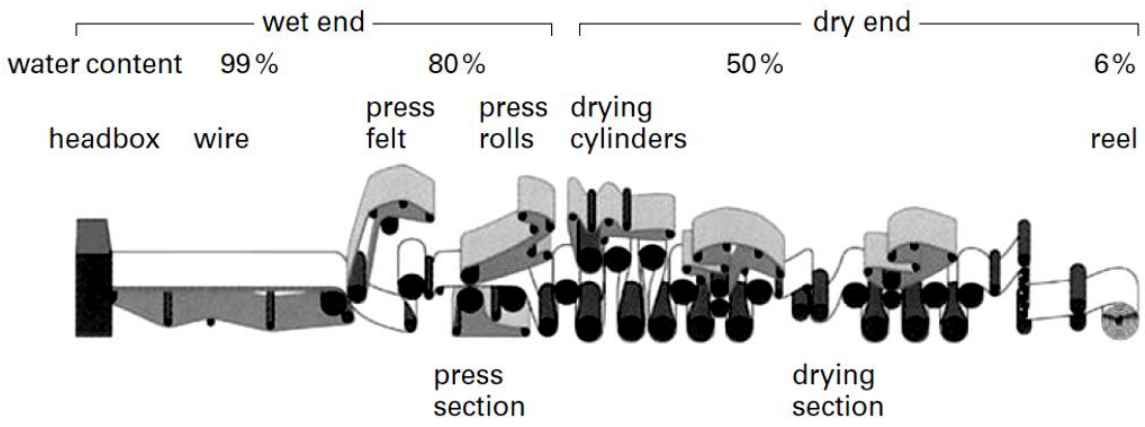

Figure 21: Schematic of a paper machine [83]

Presently, many variations of papermaking processes are used depending upon the end product and requisite paper properties. For instance, printing application requires paper to have a smooth finish (having shorter fibers on surface and using calendering),

high brightness (achieved through bleaching) and high tensile strength along the printing (also machine) direction [89]. Similarly, packaging requirements include high tensile, high tear and burst strengths – along both machine and cross directions but does not require the pulp to be bleached. Many chemicals too are added at different stages – like starch (for dry strength), resins (for wet strength), talc (for brightness and optical properties), dye pigments (for colored paper) etc. [89, 98].

In laboratory, paper can be produced using a small pilot plant that imitates the industrial processes on a smaller scale. For other quick and specific characterizations, laboratory handsheets can be prepared using pulp, a metallic screen and drying in air [99]. Because of major differences in the production processes, properties and structure of handsheets are expected to be different from those of commercially produced paper.

Fibers and pulp obtained directly from wood are called virgin fibers. In modern day papermaking, a lot of fiber is also obtained from already used paper called recycled fiber. Many daily use paper types have little to a large fraction of recycled fibers. Some specialty paper may require the use of virgin fibers only. Recycling of paper can also be done multiple times, i.e. already recycled fibers can again be recycled. Fibers are usually discarded after 3-4 recycle cycles due to their reduced strength. Recycling of used paper involves a different kind of pulping, which is accompanied by operations for removing ink (deinking) and glue (called stickies) etc. [95].

3.1.3 Processing-structure-property relationships in paper

In its simplest description, paper is a nonwoven network of cellulose fibers laid down to form a mat [82]. From the previous section, we know that the fibers are like tubes made up of mainly cellulose and hemicellulose. The fiber wall and the lumen

shrink and flatten during refining and drying [95]. Note that due to delignification during pulping and bleaching, most of lignin and a lot of hemicellulose too is lost and washed away leaving pores on the fiber surface. Some cellulose fibrils are stripped out (more, if refining is done) exposing more cellulose surface. Fiber surface is very rich in hydroxyl groups (–OH) that are present on both cellulose and hemicellulose chains. Under wet conditions, these groups are readily hydrated (surrounded) with water molecules. During drying, water is lost from between the fibers allowing for hydrogen bonding between two fibers. More drying means more bonding between fibers. The fibrils coming out of the fiber surface are flexible and increase the bonding between fibers/fibrils making the resulting paper stronger. Fibrils ripped out of the surface during refining and which hasn't bonded to another fiber/fibril snap back during drying to bond to the same fiber (Figure 20). Too much refining is not good for paper strength. In addition to increasing number of bonding sites, too much refining can break the fibers into shorter ones which decreases paper strength.

Fibers mostly lie in the plane of the paper sheet. There are very few fibers making an end-to-end angle that is more with the horizontal (in-plane) than with the vertical (along thickness), so much so that a paper structure can be approximated by a two-dimensional structure for certain studies [82]. Fibers also have some curl and kink generated during papermaking, which makes 3D modeling of a paper structure difficult. A single fiber can bond with tens of other fibers along its length. Because paper is formed by settling of a dilute water suspension, a single fiber crosses over many other fibers (that had settled before on the wire) along its length and also crosses below many other fibers (that settled after). Although the fiber settling on paper machine is predominantly

random, a directional orientation along machine direction is imparted to fiber suspension and hence to the fibers too by the moving wire. Handsheets prepared in laboratory are formed on a circular screen rather than on a moving wire, hence there is no machine direction orientation of fibers.

Fiber length is also an important structural parameter determining tensile strength of paper. Softwood paper is stronger than hardwood because of the longer fiber length in softwoods (~3 mm long in softwood compared to ~ 1 mm long in hardwood) which allows a higher number of fiber-fiber bonding per fiber [81, 91, 100]. Fiber diameter can range from a few microns to about 30 microns for both softwoods and hardwoods depending upon the type of wood source and processing conditions. Grammage and thickness are two properties that characterize the bulk density and overall bulk of paper sheets [89]. Grammage is the weight of a paper sheet per unit square meter area. Sheets with higher grammage are also usually thicker, but this might not be true if the density of the web is high. Bulk density can be calculated by dividing the grammage by the thickness of the paper sheet –

$$\text{bulk density } (\text{g/cm}^3) = \frac{\text{grammage } (\text{g/cm}^2)}{\text{thickness (cm)}} \tag{6}$$

For an equal thickness, a denser grade of paper will weigh more than a lighter grade. The packing of fibers is tighter and the structure is less porous for a denser grade of paper. By crude approximation, there are about ten fiber layers through the thickness of a copy paper sheet [82]. Paper thickness can be as low as 50 microns (glassine paper and newsprint), about 100 microns for copy paper and can be high as of the order of a millimeter for certain paperboard sheets.

The two in-plane orthogonal directions in paper are conventionally called the machine-direction (MD) and the cross-direction (CD), designated along *x*- and *y*-axis respectively. Cross-direction is the direction perpendicular to the direction of motion of paper machine. The thickness direction is commonly referred to as the *z*-direction or the out-of-plane direction.

3.1.4 Background on auxetic behavior in paper

Despite paper being a ubiquitous material of modern commerce, there has been surprisingly little attention paid to previous reports of its exhibiting auxetic behavior [55–58, 101]. These have shown differing results, dependent to some extent on the type of paper examined. While Ohrn [55], Baumgarten [57], Baum [58] and Stenberg [56] measured the out-of-plane Poisson's ratio for several kinds of paper and found them to be negative, Mann [101] and Baumgarten [57] found in-plane Poisson's ratios of paper to be positive. Öhrn [55], Baumgarten [57], Baum [58] and Stenberg [56] found the thickness of paper to increase when strained along the machine direction or cross direction, although they did not use the term 'auxetic' for this observation. Their key results are tabulated in Table 1, Table 2 and Table 3.

Stenberg found that the increase in paper thickness was greater when paper was stretched along MD than when stretched along CD. He used a tensile machine for straining and a custom designed thickness measuring device with a spherical platen head (attached to displacement transducers) [56] to continuously measure the thickness over about 20 cm^2 area of paper. Figure 22 shows a plot of increase in thickness with strain along MD and CD for an uncoated paperboard sample of Stenberg.

Table 1: Values of Poisson's ratio for different paper samples from Stenberg [56]

Type of paper	**Thickness** *(μm)*	**Grammage** *(g m^{-2})*	**MD** ν_{xz}	**CD** ν_{yz}
Paperboard (uncoated)	458 ± 10	282	-1.9	-1.2
Paperboard (coated)	387 ± 5.5	274	-3.2	-1.8
Liner	286 ± 14	224	-2.3	-0.78
Copy paper	99 ± 3.3	80	-0.24	+0.42
Sackpaper (uncalendered)	89 ± 7.3	70	-0.22	+0.55
Sackpaper (calendered) I	70 ± 5.2	70	-3.0	-0.87
Sackpaper (calendered) II	70 ± 4.7	70	-4.4	-1.2
Newsprint	62 ± 2.3	45	-3.8	-0.38

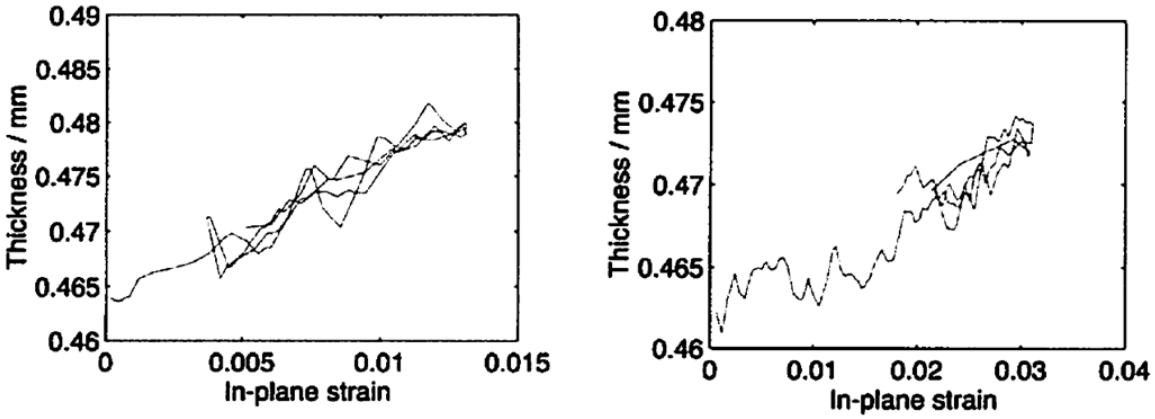

Figure 22: Stenberg's plots of thickness variation in uncoated paperboard with in-plane strain along MD (left) and CD (right) [56]

In both cases, the overall thickness can be observed to increase with strain. Multiple lines in the plot are from the cyclic loading and unloading experiments performed during these tests. As can be seen from Table 1, the magnitude of negative Poisson's ratio is different for different types of paper and it becomes positive for certain

papers (copy paper and uncalendered sack paper) along CD. Stenberg reported Poisson's ratios based on a linear fit of the thickness strain with in-plane strain. The magnitude of Poisson's ratio did not seem to correlate with either the grammage or the initial thickness of the sample and Stenberg did not discuss any relation with the papermaking processes employed.

Öhrn, however, measured thickness change by three different types of instruments – a continuous thickness gauge consisting of a metallic circular platen of diameter 2.7 cm, a mercury dilatometer measuring thickness as a function of volume change of liquid mercury and a microcator which measures thickness during a biaxial bulging of paper by a hemispherical head of a metal rod [55]. Öhrn tested four types of paper and found all of them to show an increase in thickness (except tracing paper along CD) (see Table 2). The thickness increase was found to be almost the same with both the continuous thickness gauge instrument and the mercury dilatometer. A typical plot of thickness increase for Billerud's kraft paper from Öhrn's experiments is shown in Figure 23. Öhrn continued measuring the thickness until sample failure and even after failure. Note that the thickness curve was found to be concave upward for all samples. The strain at break was larger for CD, but the magnitude of thickness increase at break was lower in CD. Öhrn described a possible mechanism of this behavior, which will be discussed in more detail in the mechanism section of this chapter.

Table 2: Increase in thickness of paper samples from Öhrn's work [55]

Type of paper	**Thickness** *(μm)*	**Grammage** *(g m^{-2})*	**Increase in thickness** *(at rupture)*	
			MD	CD
Kraft paper, Billerud	130	75	9 %	5 %
Semi chemical lab handsheet	130	75	5 %	N/A
Tracing paper (grease-proof)	50	57	4 %	-2 %
MG kraft paper, Billerud	100	80	12 %	11 %

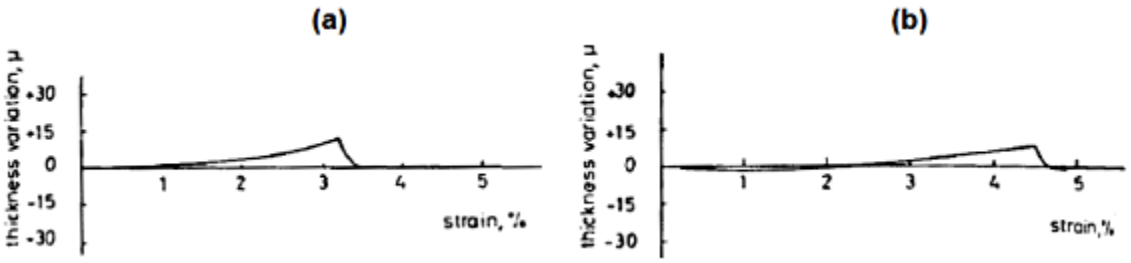

Figure 23: Thickness increase plots with strain (top) for Billerud's kraft paper along (a) machine-direction and (b) cross-direction [55]

Another important study on both the out-of-plane and in-plane Poisson's ratio of paper was carried out by Baumgarten et al. on a wide range of commercial paper and handsheet samples [57]. They used a tensile tester for straining the paper sample uniaxially, and measured the lateral strain (along width) and the thickness strain using mechanical strain gauges and strain transducers. For thickness measurement, two anvils of contact area 1 cm^2 and contact pressure of about 10 kPa were used. Table 3 shows a summary of Baumgarten's key experimental results.

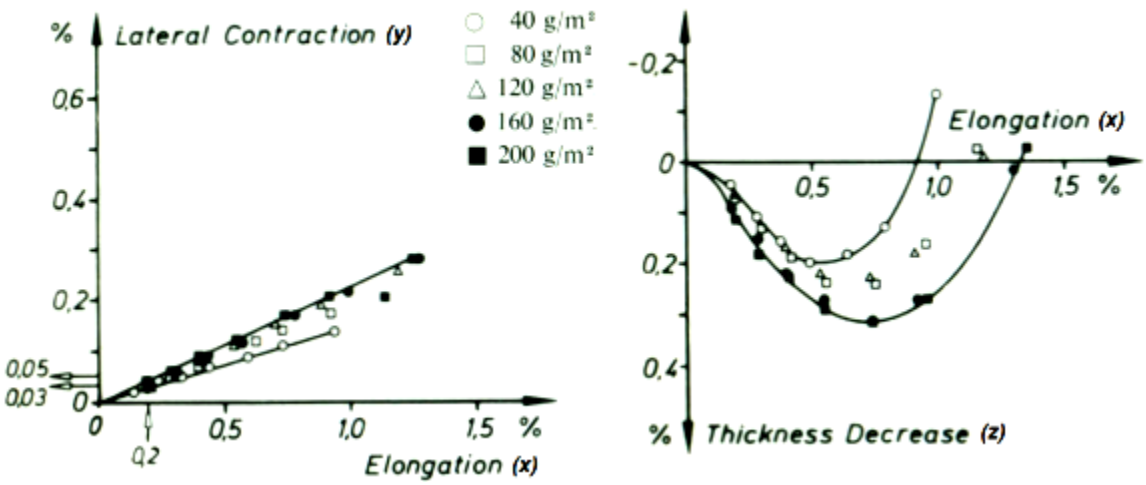

Figure 24: Lateral deformations (left – width change, right – thickness change) with machine direction strains in spruce groundwood handsheets of varying grammage in the work of Baumgarten et al. [57]

In the spruce wood handsheets, lateral contraction increased almost linearly with elongation and also increased as grammage was increased (see Figure 24 left). In the same handsheets, thickness was found to decrease with elongation until it reached a minimum at about 0.2 – 0.3 % strain. Beyond that, thickness increased until fracture (see Figure 24 right). The effective out-of-plane Poisson's ratios reported are positive despite the late thickness increase as they are calculated over only the initial linear strains.

Furthermore, Table 3 also shows that the decrease in width and thickness with strain became larger as refining was increased. Bulk density did not seem to have any effect on in-plane Poisson's ratio in illustration printing paper but caused a thickness increase upon strain for all bulk densities greater than 0.55 g cm^{-3} (see Figure 25a). Similarly, large negative out-of-plane Poisson's ratio values were seen for calendered printing paper and newsprint. Baumgarten noticed the large thickness increases (up to 6%) in certain types of paper and acknowledged Öhrn's results and explanation about the

thickness increase [55]. He added some more to the understanding of negative out-of-plane Poisson's ratio in paper, also with the help of discussions (Faraday's transactions) with Dr. D. H. Page and Dr. H. W. Giertz [57] which shall be utilized in the mechanism section of this chapter.

Table 3: In-plane and out-of-plane Poisson's ratio from experimental works of Baumgarten et al. on handsheets and commercial paper [57]

Type of paper	**Grammage** *(g m^{-2})*	***In-plane Poisson's ratio***		***Out-of-plane Poisson's ratio***	
		ν_{xy}	ν_{yx}	ν_{xz}	ν_{yz}
Spruce ground wood handsheets†	40 to 200†	0.15 to 0.21†	N/A	0.25 to 0.59†	N/A
Bleached spruce sulphite pulp handsheets (varying refining) ††	80	0.17 to 0.32††	N/A	0.15 to 1.19††	N/A
Illustration printing paper (bulk density 0.55 to 0.90 g cm^{-3}) †††	65	0.23		0.26 to –1.0†††	
Illustration printing paper, calendered uncoated	65	0.23	0.09	-2.28	-0.59
Illustration printing paper, calendered coated	55	0.34	0.10	-2.95	-0.41
Machine-finished newsprint	52	0.27	0.08	-2.20	-0.01
Kraft sackpaper	75	0.31	0.10	0.31	1.36
Coated folding boxboard	280	0.16	0.04	-0.08	0.89

† Poisson's ratio values in increasing order with increasing grammage
†† Poisson's ratio values in increasing order with increasing refining
††† Poisson's ratio values in decreasing order with increasing bulk density

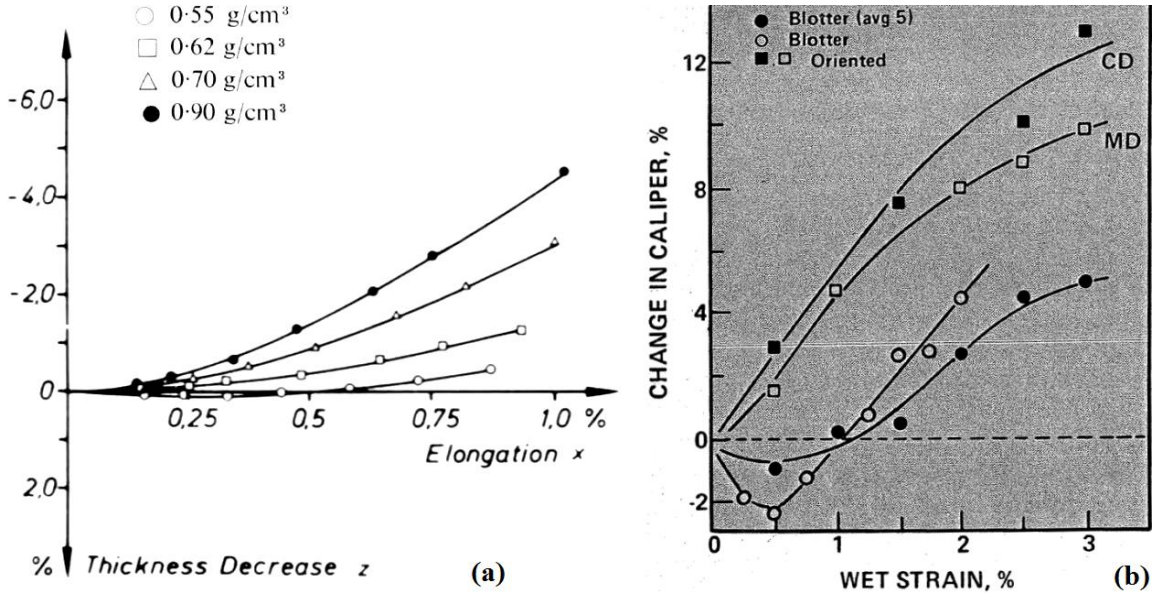

Figure 25: Thickness change with (a) machine direction strain in Baumgarten's illustration printing paper for different bulk densities [57] and (b) with axial strain in Baum's handsheets and oriented sheets [58].

Baum [58] also found thickness increase with strain during his experiments on wet straining on paper. Unbleached softwood kraft handsheets wet strained to about 3 % showed an initial decrease but a subsequent increase in thickness by about 4 % of original thickness. On his test of an oriented sheet, the thickness increase (by about 12 %) was found to be consistent until sample failure (see Figure 25b). In addition to these major reports on paper materials, Schulgasser [102] also supported Baumgarten's results and provided theoretical justification for in-plane Poisson's ratio of nearly 1/3 for most chemical kraft papers. Previously Mann et al. [101] used ultrasonic techniques to measure the nine elastic constants of a heavy bleached kraft milk carton paper (thickness ~680 μm, grammage ~525 g m^{-2} and bulk density of 0.78 g cm^{-3}) and found large positive values for out-of-plane Poisson's ratio varying from +0.59 to +2.45. Recently Yokoyama

and Nakai [103], using an optical extensometer, found the in-plane Poisson's ratio of commercial copy paper, paperboard and sack paper to roughly lie between +0.06 to +0.24. Thus, paper exhibits a positive in-plane Poisson's ratio, which means that its width decreases when it is stretched along its length.

The results on Berhan's auxetic sintered steel nanowires and nanowire composites discussed before [64–66] have conceptual similarity of the network structure of cellulose. In the case of paper, some fusion at fiber crossing points (network points) can be assumed to be provided by strong inter-fiber hydrogen bonding [82, 95]. Because of the benefits to construct composites from auxetic components, the possibility opens then for auxetic paper (like Berhan's steel wire composites), to be a potential candidate for inclusion into composite materials. Baughman's reports on in-plane auxetic behavior of buckypapers made from carbon nanotubes [52, 53] is also noteworthy. Buckypapers can be related to the cellulose network structure of paper in that the process of making paper and buckypaper are similar – both being formed by settling of a dilute suspension of fibers/nanotubes.

Given the extent of worldwide use of paper and the long evolution of the papermaking processes, studies on thickness variations in paper are rather scarce. It is clear from previous reports that all types of cellulosic paper (so far tested) exhibit in-plane contraction but many of them do exhibit a thickness increase (auxetic behavior) when stretched. Some other random fiber networks of steel wires and nanotubes, too, have been found to be auxetic. The rare occurrence of auxetic materials and the ubiquitous use of paper in our daily lives bring value to the study of the origin and nature of auxetic response in paper.

3.1.5 Key research objectives

This research intends to contribute to the understanding of paper's auxetic behavior and to attempt to establish basic processing-structure-property relationship for this behavior. The first primary objective was to examine a range of commercially produced paper samples to investigate the reported out-of-plane auxetic response in paper. It was also desired to produce handsheets in laboratory (which gives more control on production parameters) and examine their auxetic behavior. It was necessary to establish a protocol for accurate measurement of out-of-plane Poisson's ratio of paper. Changes in thickness are of the order of a few microns, which coupled with the rough (and hairy) surface of paper makes thickness measurement a challenging task.

To gain more insight into the origin and the underlying mechanism of auxetic response in paper, imaging techniques like electron microscopy and micro-computed tomography (μCT) were used. It was intended to extend Öhrn's model further and build and analyze a finite element model to relate the effect of fiber properties and processing parameters with the network structure and the observed auxetic response.

3.2 Materials

The types of papers examined can be divided into two broad categories – commercial papers and laboratory handsheets. Six commonly used and commercially produced paper samples were first examined. These were – copy paper, paperboard (used as folders), bamboo paper, cotton paper, filter paper and glassine (weighing) paper. These are listed in Table 4 below. Copy paper was chosen because of its widespread use, and its being made from an extensive sequence of industrial papermaking stages. Pulp for copy

paper is prepared through chemical pulping (likely kraft) which then undergoes bleaching and refining. The bleached and refined kraft pulp is then formed into a web on a paper machine, dried, calendered and rolled off [83]. Several fillers are also added during making of copy paper that make it fit for printing and writing uses. The thickness of our copy paper samples was a little higher than 100 μm and its grammage was about 75 g/m^2. Bulk density of our copy paper sample was calculated to be 0.71 $g\ cm^{-3}$.

Table 4: Measured thickness and grammage (approx.) values for different paper samples along with source. Calculated bulk density values are also shown.

Sample name	**Thickness** *(μm)*	**Grammage** *($g\ m^{-2}$)*	**Bulk Density** *($g\ cm^{-3}$)*	**Source**
1. Copy paper	105±2	75	0.71	Office Max OM98043 Copy Paper, 30% recycled fibers, 92 brightness, 20 lb. wt.
2. Paperboard	270±2	220	0.815	Smead UPC 12043 No. 53LBE 10% recycled fibers, Colored blue folder
3. Bamboo Paper	433±7	295	0.681	Strathmore Bamboo Cards 105-142, acid free, 90% bamboo and 10% cotton fibers
4. Cotton Paper	190±3	120	0.632	Crane & Co. PS8111 Premium Cotton paper, 100% Cotton fibers, 32 lb. wt.
5. Filter Paper	178±4	85	0.48	Whatman Grade I 1001-070 Filter paper, Fibers from cotton linters
6. Glassine Paper	52±2	48	0.92	VWR Weighing Paper, 4 x 4 in. 12578-165
7. PET film	144±2	152	1.06	HP Premium Inkjet Transparency Film, C3834A, 157 $g\ m^{-2}$, 5 mils thickness

Next, a thicker (270 μm) dyed paperboard (also called cardboard) sample used for making folders was examined. The grammage of paperboard sample is higher at 220 g/m^2

and its bulk density is 0.815 g/cm^3. Bamboo paper and cotton paper are made from a process similar to the manufacture of copy paper and paperboard, but they differ in fiber source. Bamboo is technically a grass and cotton is a shrub unlike other common softwood and hardwood fiber sources. Bamboo fibers are more similar to softwoods than to hardwoods in having long fibers in the range of about 1 – 3 mm [104, 105]. Cotton fibers used in papermaking are obtained as linters by cutting around the seeds of the cotton plant, are long up to 10 mm and almost pure cellulose [106, 107]. The cotton paper examined was about 190 μm in thickness and the bamboo paper was much thicker at 433 μm. They both were found to be of lower bulk density than either copy paper or paperboard. All these four paper types (copy paper, paperboard, bamboo paper and cotton paper) are assumed to be bleached (except cotton) and produced on a paper machine, thus showing preferential fiber orientation along machine direction.

Two other kinds of commonly used papers – glassine paper (also known as weighing paper) and filter paper were also examined for their Poisson's ratio. Whatman filter papers are made from cotton linters [108] and have the lowest bulk density (0.48 g/cm^3) among all other paper types, suggesting a more porous network structure. Glassine paper is made from wood pulp but its production involves large compressive forces during supercalendering [109] which makes its surface very smooth and its bulk density very high (0.92 g/cm^3). Glassine paper has small and few pores if any [110], which together with the smooth surface prevents residue retention during weighing of chemicals.

Laboratory handsheets were prepared by the author at the RBI Pulping and Papermaking facility (Georgia Tech, USA) as detailed in Section 3.3.1 using softwood

and hardwood kraft pulps. The process of handsheet production used can be well controlled and accurately described as opposed to the production process of commercial papers, which can only be speculated. Lab handsheets are structurally different from commercial paper. There is no machine direction due to the absence of a paper machine in its formation. Fiber orientation is almost entirely random in the plane. There were no fillers added and there was no calendering or coating action done after the drying step. They are composed entirely of wood fibers, some bound water (chemically bound water that cannot be removed by drying alone [95]) and any other impurities that might have been present in the pulp.

Table 5: Laboratory handsheets examined for their out-of-plane Poisson's ratio along with their measured thickness, approximate grammage and calculated bulk density.

Name	**Details**	**Thickness** *(μm)*	**Grammage** *($g\ m^{-2}$)*	**Bulk Density** *($g\ cm^{-3}$)*
SW1	Softwood, thin	92±2	60	0.65
SW1R	Softwood, thin, refined	78±1	60	0.77
HW1	Hardwood, thin	96±1	60	0.63
HW1R	Hardwood, thin, refined	80±1	60	0.76
SW3	Softwood, medium	269±9	166	0.62
SW3R	Softwood, medium, refined	206±4	168	0.81
HW3	Hardwood, medium	284±5	165	0.58
HW3R	Hardwood, medium, refined	228±4	162	0.71
SW5[†]	Softwood, thick	542±26	220	0.41
SW5R[†]	Softwood, thick, refined	502±23	217	0.43
HW5[†]	Hardwood, thick	586±28	209	0.36
HW5R[†]	Hardwood, thick, refined	526±22	210	0.40

[†]Different pulp batch source, manufacturer SAPPI

Table 5 shows the different handsheets prepared, their mean thickness values, approximate grammage and calculated bulk densities. Industry obtained bleached softwood and hardwood pulps obtained from RBI pulping lab (bought from SAPPI®) were used. Both types of pulps were additionally refined to produce a separate set of refined handsheets for testing (see Section 3.3.1 for details). Handsheets of three different grammages for each pulp type were produced. These are suffixed in SW or HW as 1, 3 and 5 depending on the increasing grammage value. More the grammage, greater was the thickness of resulting handsheet (see Table 5). Refining was performed on each pulp type to produce a new set of refined handsheets (with different grammages and pulp types). Suffix 'R' is used in the sample name to denote a refined handsheet sample. Note that the pulp used to prepare the thick handsheets (SW5, SW5R, HW5 and HW5R) were obtained from a different batch of pulp from SAPPI®.

As a check on the reasonableness of our Poisson's ratio experiments, a transparency film sheet made of poly(ethylene terephthalate) (PET) was also tested. PET is a plastic that like almost all other plastics has been shown to exhibit a positive Poisson's ratio in all directions [111, 112]. The PET film was about 144 μm thick, which was within the thickness range of our paper samples, thus proving to be a suitable comparison sample.

Figure 26 shows scanning electron micrographs (SEMs) of copy and filter paper samples that were examined. From the micrographs of copy paper, the high aspect ratio of cellulose fibers can be seen. Preferential orientation of fibers along the machine direction and a relatively flat 2D structure (rare occurrence of out-of-plane fibers) can be observed. The magnified view shows the non-uniformity of fiber diameter and some

severely broken fibers as well as fibrils, pores and pits on the fiber surface. The micrograph of filter paper shows no preferential orientation of fibers. The magnified view very clearly shows fibril-fibril and fibril-fiber (not just fiber-fiber) contact. Fiber diameter in filter paper is smaller than that in copy paper. SEMs were also taken for selected handsheet samples. Figure 27 shows intact fiber diameters of about 20 μm and a high degree of defibrillation and flattening out of softwood fibers because of refining. Unrefined fibers do not have fibrils coming out of their surface Figure 27a.

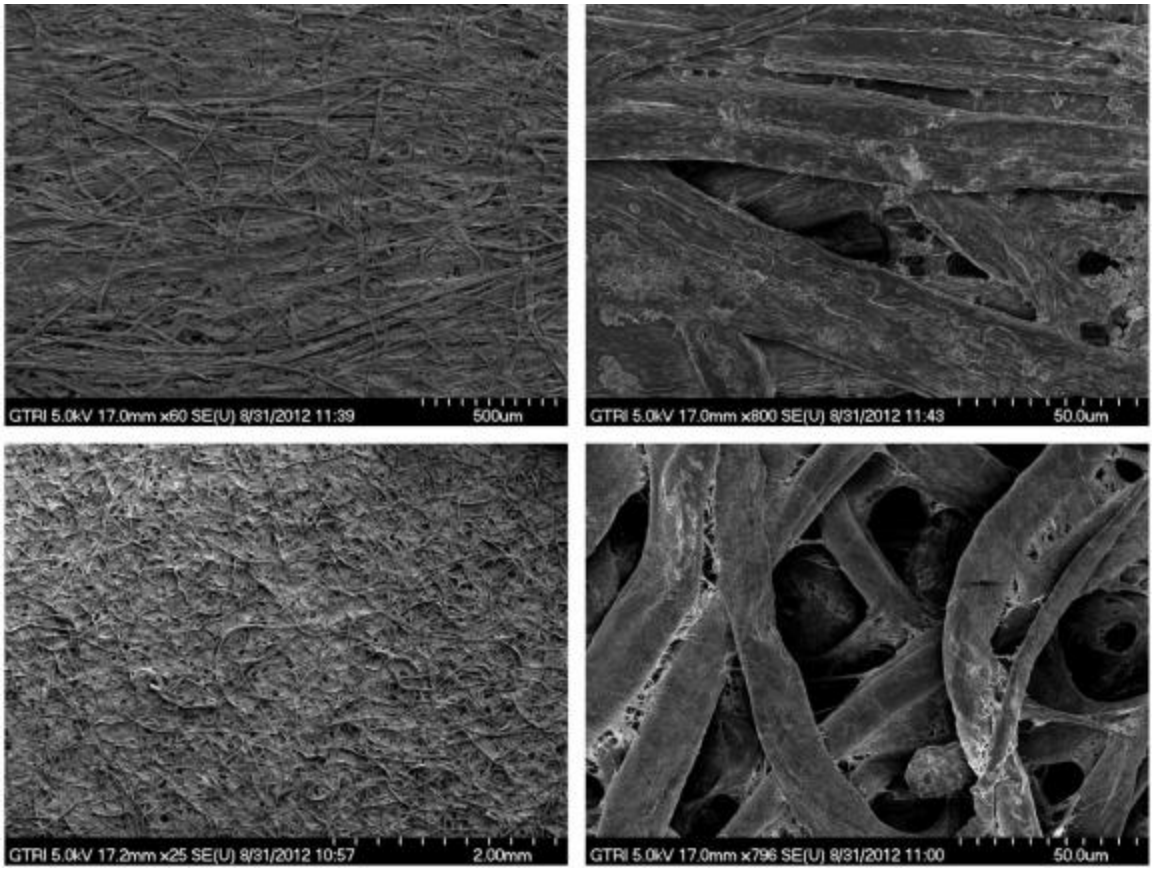

Figure 26: SEM Micrographs of copy paper (top) and filter paper (bottom) at two given magnifications for each sample. These show the cellulosic fiber network structure of papers [30].

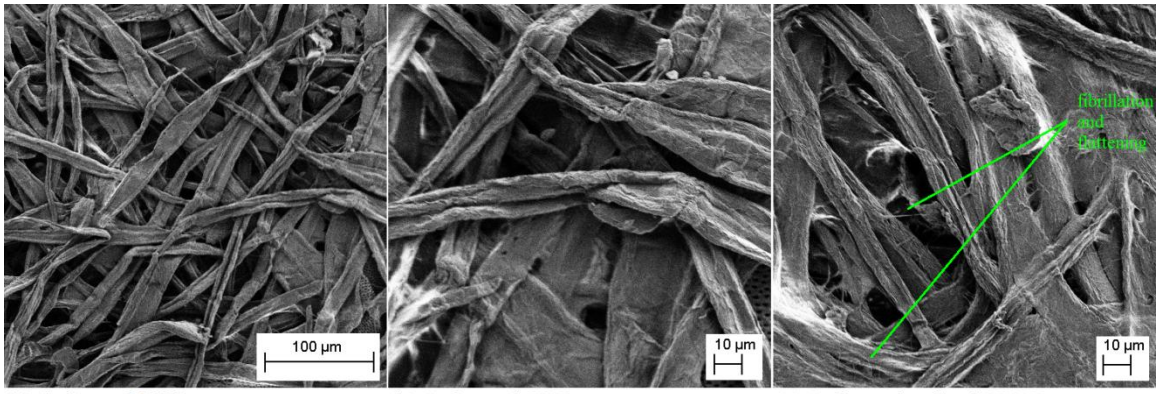

Figure 27: SEM micrographs of SW3 handsheets (a) unrefined handsheet showing intact but somewhat flattened fibers (b) magnified image of SW3 and (c) refined (CSF = 360 ml) SW3R showing defibrillation of fibers, fibril-fiber bonding, ruptured and highly flattened fibers.

3.3 Experimental

3.3.1 Producing laboratory paper handsheets

Hardwood and softwood handsheets were produced in accordance with TAPPI's standard 'T-205' [99] at the RBI Pulping and Papermaking lab at Georgia Institute of Technology, Atlanta (USA). Bleached kraft pulps used in this study were obtained from SAPPI® Ltd. through the courtesy of Dr. Rallming Yang. Below are the steps carried out for the production of a handsheet from the obtained pulps.

3.3.1.1 Calculating moisture content

Commercially obtained pulps contain moisture (moisture content depends on the storage environment) that needs to be calculated precisely to determine the weight of dry fibers. Five samples of about 5 g each were weighed and then oven dried overnight at 120 °C to get rid of all water (except 'chemically bound' water molecules that cannot be removed by heating [95]). Oven dried pulp was weighed again. The oven dried fiber

content, for instance on one occasion, was determined to be 35.92 % in softwood pulp and 94.26 % in hardwood pulp. After moisture measurement, pulp was stored in a dark and cold storage inside sealed bags. Moisture content was determined again if more than a few weeks had passed since the previous measurement. Before beginning to produce handsheets, the oven dry weight of pulp/fibers was determined. Starting with 30 g of oven dry pulp is the normal procedure.

3.3.1.2 Disintegration

Pulp was weighed such that it contained 30 g of dry fibers and diluted to about 2000 ml suspension in deionized water. It was then transferred to a standard disintegrator (see Figure 28) operating at 3000 rpm. The disintegrator disperses/separates the individual fibers from each other [99]. Both kinds of pulp were disintegrated for 30,000 revolutions (for 10 minutes).

Figure 28: Disintegrator used for dispersing pulp fibers, RBI (Georgia Tech)

3.3.1.3 Refining

Note: This step was skipped for handsheets that were to be produced without refining of pulp.

Refining was performed using a PFI mill in accordance with TAPPI Standard 'T-248' [99]. Refining is a term better used for industry-scale refiners that have a different design due to the large amount of pulp they process. Lab-scale refiners come as 'valley beaters' or 'PFI mills' which operate on the same principle as industrial refiners but are popularly known as 'beaters'. However, the term refining will be used for handsheets in the rest of this thesis for the sake of simplicity.

Figure 29: PFI mill used to refine pulp fibers, RBI (Georgia Tech)

The PFI mill requires 30 g dry fibers at a consistency of 10% (total mass, fibers plus water of 300 g). After disintegration, excess water was removed using simple

vacuum filtration and the remaining pulp was diluted to a total of 300 g. It was then evenly distributed along the smooth walls of the PFI mill bowl (see Figure 29). The bowl was closed with the top part of the mill that contains a roll with bars for beating the pulp. The mill was then operated for a given number of revolutions (1000 revolutions in our case) to beat/refine the pulp. After refining, the pulp was taken out for further dilution (described in Section 3.3.1.4) and measurement of freeness (described in Section 3.3.1.5).

3.3.1.4 Dilution

The fiber suspension used to produce handsheets should have a consistency of 0.3 %. Therefore, after disintegration (and optional refining), the suspension was diluted to a total weight of 10 kg in a clean bucket used to store this stock suspension. Because 30 g of fibers were used, a consistency of 30 g in 10,000 g suspension was obtained, which is the equal to the desired 0.3 % fiber by weight.

3.3.1.5 Freeness measurement (Canadian Standard Freeness Test)

Freeness of a pulp is the measure of how much a dilute suspension of pulp can be drained through a screen (a metal plate with holes). A Canadian Standard Freeness instrument (see Figure 30) was used to measure the freeness of pulps according to TAPPI Standard 'T-227' [113]. One liter of a 0.3% suspension of pulp (refined or not refined) prepared in last step was transferred to the chamber of the instrument fitted with a screen at its bottom. The drained/filtered water was collected in a measuring cylinder. The volume of water collected (corrected with a supplied temperature-volume chart) is called the 'Canadian Standard Freeness (CSF)' of the pulp and was reported. We were then left with 9,000 g (or 9 L) of the stock suspension.

Figure 30: A Canadian Standard Freeness testing equipment (left image, RBI, Georgia Tech; right image adapted from http://www.mctec.nl)

CSF values for our softwood pulps were found to be 360 ml (refined) and 460 ml (unrefined) and for our hardwood pulps were found to be 385 ml (refined) and 510 ml (unrefined).

Note: Refining of pulp reduces its drainage-ability because it increases fiber-fiber bonding. CSF is therefore an important property to be measured before and after refining in order to compare the effects and extent of the refining process.

3.3.1.6 Handsheet making

The apparatus prescribed to make handsheet in accordance with the TAPPI Standard 'T-205' [99] is shown in Figure 31. The amount of stock suspension to use depends upon the final mass of handsheet desired. For example, 1 L of stock produces a

handsheet weighing 3 g because it contains that mass of dry fibers. The apparatus consists of a tank (Figure 31.2) which has a mark to which it should be filled. A metallic forming wire (or screen) is fitted at the bottom of the tank. The tank was filled halfway with water first, then the desired volume of stock was added and finally more water was added to fill the tank to the marked height. This new diluted suspension in the tank was mixed well with a perforated metal stirrer. Water was then allowed to drain through the wire/screen such that a fiber web was formed on the screen under the hydrostatic pressure from the tank suspension. The formed handsheet was then covered with blotting papers and pressed with a supplied couch roll (a heavy brass cylinder) (Figure 31.2).

Figure 31: Handsheet making equipment (Source: http://www.lcrl.ppc.ubc.ca/facilities/)

After rolling with the couch roll a few times, the sheet was transferred to a press (again, as prescribed in the standard) (Figure 31.3), covered with a chrome plate and covered with another blotting paper. More sheets were prepared in a similar fashion and stacked over one another in the press. Stacking was such that each handsheet rested upon two blotting papers on the bottom and was covered by a chrome plate on the top. The press was then covered and its heavy metal lid was screwed down. Press was switched on to compress the stack of handsheets under 50 psig for 10 minutes. After this, the press was opened and the wet blotting papers were changed with new dry ones. Another cycle of pressing at 50 psig was performed for 5 minutes. Following pressing, the handsheets were taken out and the blotting papers were discarded. The handsheets were still attached to the chrome plate. Figure 31.4 shows a stack of drying rings with holes on the sides. The handsheets with the chrome plates were put on a drying ring and stacked on top of each other and left for drying in air under ambient conditions for 2 days. Dried handsheets were easily separated from the chrome plates (once dried, the chrome plates do not stick to the sheets) and stored for conditioning.

3.3.1.7 Conditioning

Dried handsheets were transferred to an environmentally controlled room at 23 °C temperature and 50 % relative humidity and stored there for another 48 hours. The samples were then sealed in airtight bags and stored away from heat and light until they were examined to determine their Poisson's ratio.

3.3.2 Measurement of out-of-plane Poisson's ratio

3.3.2.1 Thickness measurement

Precise and accurate measurement of thickness was very important for this study. A digital micrometer (Mitutoyo-369) with a circular contact surface of diameter 2 cm and a resolution of 0.001 mm was used. The contact faces of the micrometer exert a force of approximately 7-9 N during the thickness readout. A relatively constant force ensures repeatability of the thickness values and the large contact area helps to compensate for the roughness of the paper surface and thickness heterogeneity in the sample. This technique works well for both paper and nonwovens. Pressure values for our micrometer are approximately between 20-25 kPa. This value is between the one used by Baumgarten (10 kPa) and suggested value (50 kPa) in the TAPPI Standard 'T-411' [114]. At this pressure the measured thickness is lower than an optically/visually observed thickness due to the yielding of surface fibers. The total thickness change before break for paper was of the order of a few to tens of microns. The resolution of micrometer was therefore limiting for certain grades of paper where the total change was only a micron or two. It still, however, gave a good qualitative indication of overall thickness increase or decrease when the change was considered over the entire strain regime and for several specimens.

3.3.2.2 Measuring grammage of paper

For commercial papers, five square specimens of size 10 cm x 10 cm were cut and weighed on a laboratory balance. Grammage was calculated by dividing the mass by the area of specimen and the mean of five samples was reported. For handsheets, the TAPPI test method 'T-220' was followed to calculate the grammage. Five handsheets were weighed. Grammage is ten times the mass of five handsheets expressed as g m^{-2}. This utilizes the fact that the approximate area of a handsheet is 200 cm^2.

3.3.2.3 Determination of machine direction

For commercial paper samples (Sample 1 – 4 and 6, Table 4), tensile testing was carried out to determine the machine direction. Strips of width 2 cm and length 15 cm (gage length 10 cm) were cut along the sheet length (0°) and along angles 30°, 60° and 90° to the sheet length. All strips were tested for a uniaxial stress-strain experiment on an Instron tensile testing machine. The strip that showed maximum tensile strength was selected as the one that was cut along the machine direction. It was found that the machine direction was actually the length direction for all our commercial papers (copy paper, paperboard, glassine paper, bamboo paper and cotton paper).

3.3.2.4 Specimen preparation

Rectangular specimens of 2 cm width and 15 cm length were cut out for both commercially available papers and lab handsheets. A gage length of 10 cm was marked (see Figure 32). Except for glassine paper for which gage length of 6 cm and a total length of 7.5 cm was used due to its smaller size. Handsheets were conditioned at 23 °C and 50% relative humidity for 48 hours and then sealed in airtight bags until tested. Testing was only done along the machine direction (MD) of papers that had one. For MD testing, specimens were cut such that their length was along the machine direction. Papers not having a machine/cross direction, like handsheets, were cut along an arbitrary direction. Note that the handsheets and filter paper were circular in shape. Five specimens of each type, each specimen cut from a different paper sheet, were examined to allow calculation of statistical deviations. Each specimen was marked with a circular region (with 2 cm diameter) at its center where the thickness would be measured (Figure 32). This ensured that the same area was measured for thickness each time.

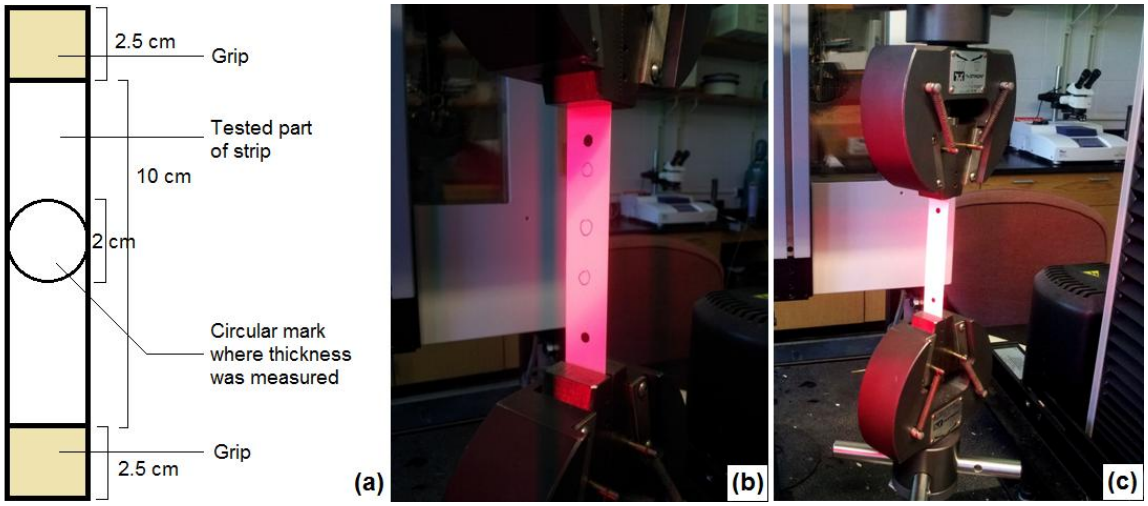

Figure 32: Testing procedure for measurement of out-of-plane Poisson's ratio (a) preparation of a test specimen showing gripped area and circular area where thickness is measured (b, c) the test specimen gripped and strained in an Instron

3.3.2.5 Measuring thickness change with extension

Specimens were clamped at the ends of their length in the jaws of an Instron testing machine (model 5566, 10 kN load cell). Uniaxial strain was applied along the length of a specimen at a constant rate of elongation of 0.5 mm/min. Extension was paused at regular intervals of strain until sample failure to allow for manual thickness measurements. Thickness values at each pause were recorded at the marked circular region using the micrometer and plotted against the corresponding extension values from the Instron's crosshead. Each sample was tested until failure and one last thickness value was recorded approximately one minute after failure to check for the reversibility of thickness change. All tests were done at room temperature and ambient (not controlled) humidity conditions. PET films were tested like paper samples as stated before.

3.3.2.6 Tensile properties of paper

During the thickness versus extension experiment, Instron also recorded the load applied on the specimen. Two important tensile properties of paper, as per TAPPI standard 'T-494' [115] can be derived from the load-extension curves obtained for paper specimens –

Tensile strength was obtained by dividing the maximum tensile force developed in the specimen (right before failure) by the width of the sample (20 mm) and expressed in kN/m. Note that the rate of elongation used for these experiments was 0.5 mm/min.

Tensile stiffness was obtained by dividing the maximum tensile force developed in the specimen within the tensile region (linear part of load-extension curve) by the width of the sample (20 mm) and expressed in kN/m. Note, again, that the rate of elongation used for these experiments was 0.5 mm/min. For the sake of ambiguity in identifying the linear strain regime, tensile stiffness was calculated from the load at 0.25% strain for all samples, unless otherwise noted.

All these properties were measured and reported in the machine direction (MD), for samples that had a distinct MD.

3.3.2.7 Calculating out-of-plane Poisson's ratio

Strains in the axial and thickness directions were calculated at each pause (data-point) using original sample thickness and gage length respectively. These were used to calculate the effective Poisson's ratio values at each step using formula given in Equation (4) and are tabulated in the next section (3.4). Thickness strain versus axial strain data was also fitted using straight lines and second degree polynomials (Section 3.4) to analyze Poisson's ratio in other ways.

3.3.3 Imaging of paper samples

In order to understand the origin of auxetic response, an insight into network architecture was needed. Techniques like optical microscopy, SEM and μCT (Appendix A) were used to get a snapshot of fiber arrangement in the network. Objects of interest were network contact points, pore structures and sizes, occurrence of reentrant cells or ribs, fiber shape, fiber diameter and fiber bonding.

3.3.3.1 Scanning electron microscopy (SEM)

SEM was used to image the surface of paper for select samples – copy paper, filter paper and some handsheets. SEM was found to be the best technique to look at the fibers on the surface of paper. It had better depth resolution and focusing capability for paper when compared to optical microscopy. Paper samples were mounted on carbon tape covered SEM stages and sputtered with gold using a Quorum® Q150T ES sputter-coater for durations of 30s to 2 min coating a layer of gold 10 nm to 30 nm on the surface of paper. SEM was performed using a LEO 1530 model at accelerating voltages anywhere between 2 and 10 kV.

3.3.3.2 Micro computed tomography (μCT)

μCT imaging was performed for a few samples on a Scanco Medical μCT50 instrument using a scanning tube of inner diameter 5 mm and an X-ray source energy of 45 kVp (details of a μCT scanning procedure has been given in Appendix B). For imaging of paper, a small strip of approximate width 5 mm and length about 1 cm was cut from the sample and put in the scan tube. Upon scan completion, a rectangular (cuboidal) subsection of the resulting images was chosen for 3D-reconstruction. The 2D axial images were stacked and global thresholding applied to segment fibers from surrounding air and noise and produce binarized 3D images. All scans were performed at

a voxel resolution of 2 µm. A voxel can be thought of as the smallest unit volume (cube) defined in the 3D structure.

3.3.4 Finite element analysis (FEA) of paper network structure

A simple geometrical network model was developed for paper (Figure 44) to explain the out-of-plane auxetic response. Finite element analysis was carried out in addition to simple geometrical calculations on the model (assuming rigid body mechanics). Modeling was done using the Abaqus® CAE software. Nine wavy fibers and nine straight transverse fibers were fused together in the software to mimic the model. The fibers had circular cross-sections (of diameter 10 units) and were given isotropic elastic properties with a Young's modulus of 5 MPa and a Poisson's ratio of +0.3. The center-center separation between two fibers was set at 40 units.

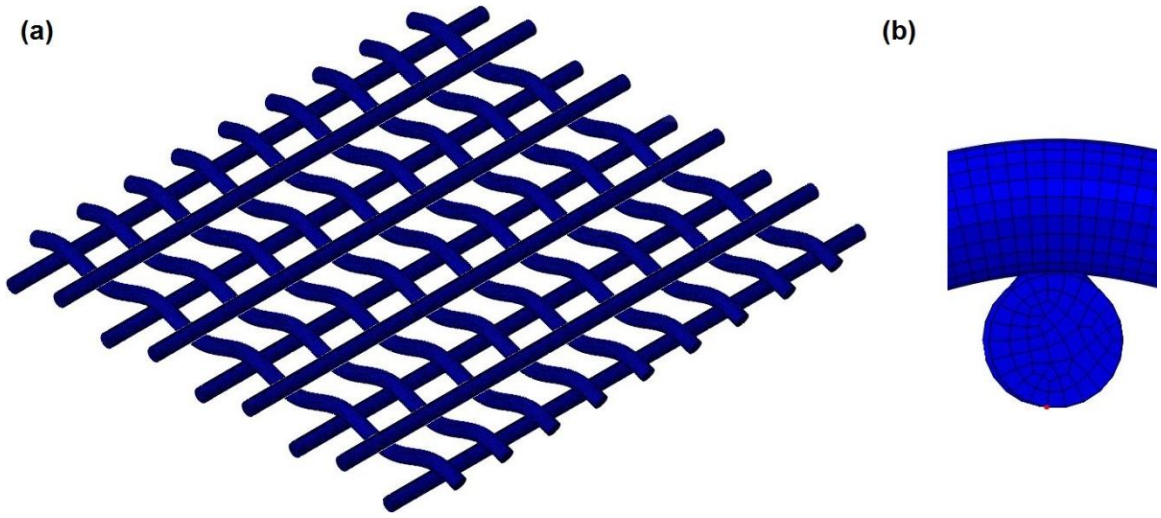

Figure 33: (a) Paper network model composed of nine wavy and nine straight transverse fibers built for the purpose of finite element analysis (b) Close up showing the mesh and the fixed contact point between the wavy and the straight transverse fiber (no relative motion between fibers was allowed).

Resulting network was converted into a mesh suitable for tensile FEA. Wavy fibers were strained up to 4% strain from one end while the other end was fixed and the resulting mechanical deformation of the network was analyzed. Transverse fibers were attached to (fused with) wavy fibers at network contact points. The change in the thickness of the network with respect to the axial strain was observed and reported.

3.4 Results and discussion

3.4.1 Determination of machine direction

Tensile tests in different directions were performed on different commercial paper samples as described in Section 3.3.2.3. Figure 34 shows the results on copy paper only for the sake of brevity. Maximum tensile strength was found along the 0° direction (which is along the length of a commercial copy paper). Similar results were found for other commercial samples and it was determined that the length direction was indeed the machine direction for copy paper, paperboard, cotton paper and bamboo paper samples. Machine direction for glassine paper, which was a square sample, was also determined in a similar fashion.

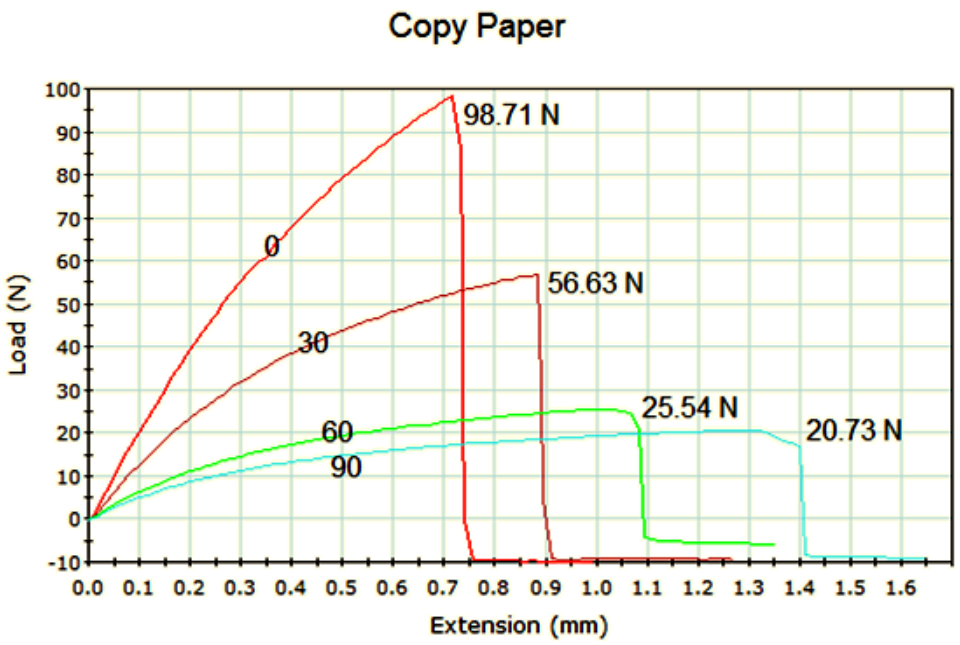

Figure 34: Tensile tests carried out on copy paper in various directions (0°, 30°, 60° and 90°). Result show that the 0° direction, which is along the length of the sheet of paper sample is the machine direction.

3.4.2 Tensile properties of paper

A typical load versus extension curve obtained from the Instron looks like the one shown in Figure 35 for a paperboard sample. Rate of elongation for all paper specimens was set at 0.5 mm/min. Some stress relaxation was observed at each pause that was taken for thickness measurement. The plateau in the load at about 50 N between extension levels of about 0.4 mm to 0.9 mm occurs likely due to grips of the Instron tightening and adjusting themselves. This was seen in all kinds of samples and can be attributed to a particular Instron machine's load-cell/grip combination. This plateau region was subtracted from axial extension values for all measurements of Poisson's ratios.

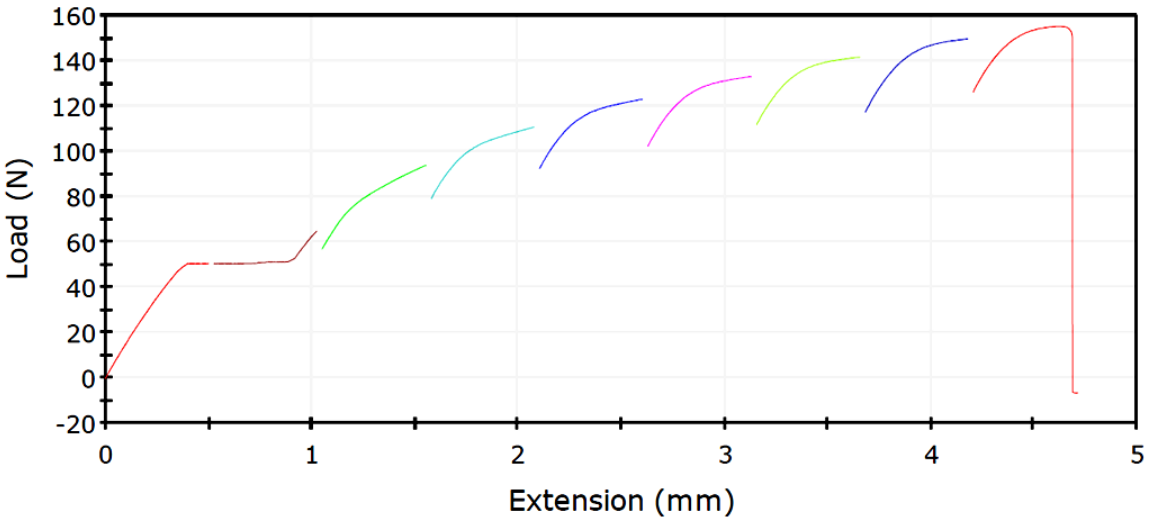

Figure 35: A typical load-extension curve obtained from the Instron during the thickness versus extension experiments (with pauses for thickness measurement). This plot shows the curve for a paperboard sample strained in machine direction. Notice the stress relaxation at each pause and note that the rate of elongation for experiments on paper specimens was 0.5 mm/min.

Table 6: Tensile properties – approximate values of tensile strength, tensile stiffness and strain at break of commercial paper samples examined for their auxetic response. Note that the rate of extension was set at 0.5 mm/min for all paper samples.

	Sample name	**Tensile Strength** *kN/m*	**Tensile stiffness** *kN/m*	**Strain at break** *%*
1.	Copy paper	4.2 ± 0.4	1.4 ± 0.1	1.1 ± 0.2
2.	Paperboard	7.2 ± 0.3	1.8 ± 0.1	4.0 ± 1.0
3.	Bamboo Paper	9.9 ± 0.5	3.4 ± 0.2	1.3 ± 0.1
4.	Cotton Paper	4.3 ± 0.5	1.1 ± 0.1	2.5 ± 0.4
5.	Filter Paper	2.1 ± 0.2	0.76 ± 0.1	1.6 ± 0.2
6.	Glassine Paper	3.5 ± 0.2	1.1 ± 0.1	1.0 ± 0.1

Table 6 and Table 7 list important tensile properties of tensile strength, tensile stiffness and strain at break for all paper samples examined. These properties were

calculated from the load-extension curves obtained by the Instron (see Section 3.3.2.6). The significance of the observed values will be discussed at appropriate parts in later sections while discussing the mechanism of auxetic response.

Table 7: Tensile properties – approximate values of tensile strength, tensile stiffness and strain at break and elastic modulus of laboratory produced handsheets examined for their auxetic response. Note that the rate of extension was set at 0.5 mm/min for all handsheets.

	Sample name	**Tensile Strength** *kN/m*	**Tensile stiffness** *kN/m*	**Strain at break** *%*
1.	SW1	1.9 ± 0.1	0.9 ± 0.1	2.2 ± 0.2
2.	SW1R	2.8 ± 0.1	1.5 ± 0.1	2.8 ± 0.3
3.	HW1	1.4 ± 0.1	0.6 ± 0.0	1.2 ± 0.1
4.	HW1R	2.0 ± 0.1	1.1 ± 0.1	1.4 ± 0.2
5.	SW3	4.5 ± 0.3	1.5 ± 0.1	2.7 ± 0.1
6.	SW3R	9.0 ± 0.5	2.2 ± 0.1	3.8 ± 0.1
7.	HW3	2.4 ± 0.1	1.0 ± 0.1	1.2 ± 0.1
8.	HW3R	5.6 ± 0.2	1.8 ± 0.1	2.7 ± 0.1
9.	SW5	6.1 ± 0.6	1.8 ± 0.2	2.3 ± 0.5
10.	SW5R	7.4 ± 0.5	2.0 ± 0.2	2.8 ± 0.5
11.	HW5	2.5 ± 0.1	1.4 ± 0.2	0.7 ± 0.0
12.	HW5R	3.1 ± 0.2	1.6 ± 0.2	0.7 ± 0.0

3.4.3 Out-of-plane auxetic response in commercial papers

Figure 36 shows thickness versus length plots along with bars showing standard deviations for all six commercial paper samples examined. Copy paper (Figure 36a) and paperboard (Figure 36b) both showed a significant increase in thickness until failure. The similarity in their auxetic behavior might be a result of their being made from very similar sequence of papermaking processes. Paperboard fails at a much larger strain of

about 4% when compared to copy paper that breaks at 1% strain (Table 6). Thickness increase in copy paper is almost linear which is probably because the strains are still within the elastic regime (below 1% strain). Also, after failure, all copy paper samples returned to their original thickness values, which supports the idea of thickness increase being an elastic/reversible change in copy paper. This observation is in agreement with Öhrn's [55]. Paperboard specimens undergo some permanent thickness change and do not return fully to the original thickness after failure. The curve for thickness increase is also concave up for paperboard, similar to the plots obtained by Öhrn [55].

Filter paper and cotton paper also increase in thickness when strained, but the increase was not as pronounced as in the case of copy paper or paperboard samples (Figure 36 c, e). The observed effective Poisson's ratio in this case lies roughly between 0 and –0.7. Fiber source for both these paper types is cotton. Both these papers are also on the lower side of bulk density when compared to other paper types (see Table 4). Poisson's ratio values for bamboo paper oscillated around zero, varying from slightly positive to slightly negative. Limited testing of the bamboo fiber based papers, however, restricts us from commenting anything conclusive about the behavior of bamboo papers in general.

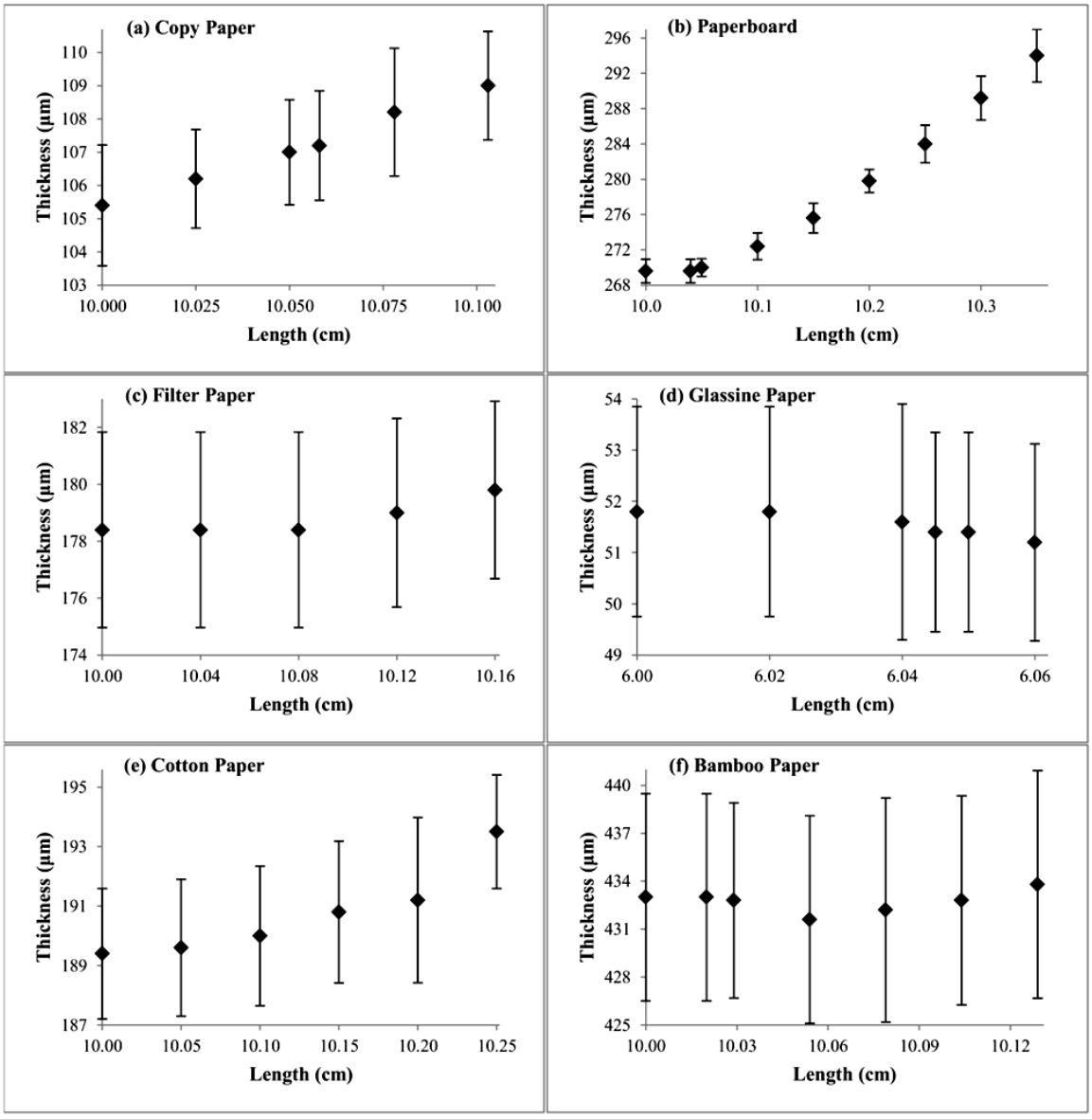

Figure 36**:** (a-f) Plots of thickness (µm) vs length (cm) data for different types of paper samples. Standard deviation was calculated over five samples of each type [30].

On the contrary, glassine paper showed a positive Poisson's ratio. Although glassine paper is made from ordinary wood pulp, it is thin and has been subjected to heavy refining and calendering. Glassine paper was found to thin out like an ordinary plastic material exhibiting positive value of Poisson's ratio (+0.6 in the initial strain

region), which was a strikingly different behavior when compared to other paper types. We suspect that supercalendering may be limiting the ability of fibers in glassine paper to expand in tension (more in Section 3.5).

One should also take note of the large error bars associated with the thickness readings, mostly owing to the heterogeneity of thickness among five paper specimens. In a qualitative sense however, the difference between either thickness increase or thickness decrease was clearly observed in each specimen individually. Referring to the behavior of copy paper, it can be hypothesized that compressive forces and fiber orientation imposed by the paper machine plays an important role in inducing auxetic characteristics to paper.

PET film exhibited ordinary Poisson's ratio values varying from +0.2 to +0.5 in initial strain region, as would be expected from a polymer film (Figure 37). The result on PET film helped us to confirm that the method developed for determination of out-of-plane Poisson's ratio was reasonable for such ‘film/sheet like’ paper samples.

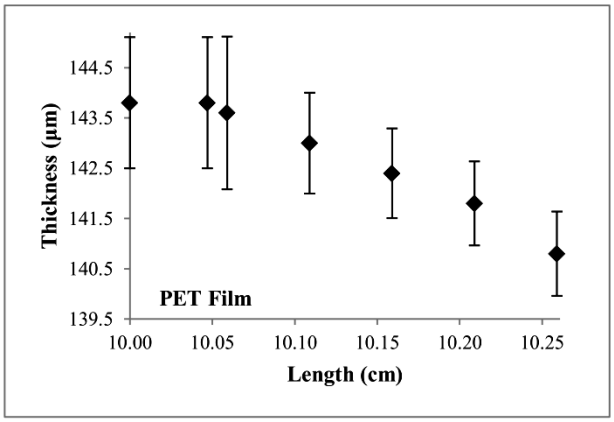

Figure 37: Plot of thickness (µm) vs length (cm) data for a PET Film sample. Standard deviation was calculated over five samples [30].

To summarize the results on commercial paper samples, a thickness strain versus axial strain plot has been shown in Figure 38. Dashed lines represent second order polynomial fits of all data points in a given sample series. Out-of-plane Poisson's ratio is the negative of the slope of this plot and helps us to compare the magnitude of auxetic response among different paper samples. To understand the variation of Poisson's ratio with axial strain, Poisson's ratio values was calculated in various ways.

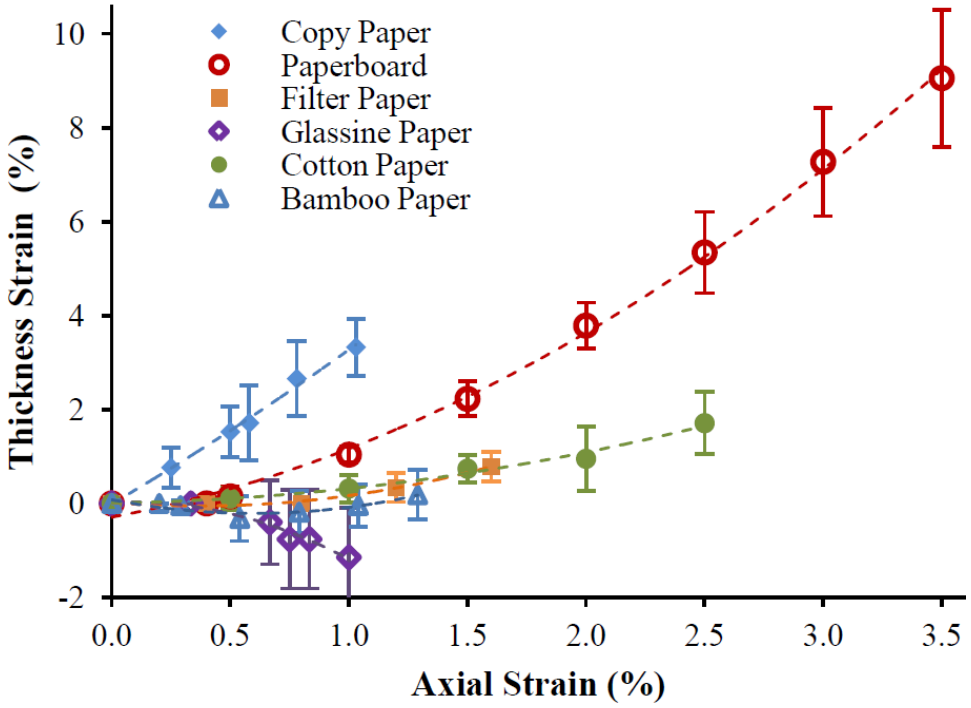

Figure 38: Plot of thickness strain (%) vs axial strain (%) for the eight paper samples. Each series has been fit using a second degree polynomial (dashed lines) [30].

Table 8 summarizes Poisson's ratio values for each paper sample calculated using various methods. A 0.7% strain was chosen below which samples were assumed to be within the elastic regime. This was judged from the near linear appearance of curves

below this strain regime for most samples. Note that this value can be different; for instance Baumgarten [57] found linear behavior of his handsheets only under 0.2 % strain which he then chose to be the limit of elastic regime. Effective Poisson's ratio value was calculated from the experimental data-point lying just below 0.7% strain and is shown in Column (a). Poisson's ratio values were also calculated from the slope of linear fit of data points lying within 1% axial strain and are shown in Column (c).

Table 8: Values of Poisson's ratios for paper samples calculated at highest strain data-points below 0.7% strain (a) and at highest strain data-point before break (d), both calculated using Equation (4). Values of Poisson's ratios from second order fits (b, e) are calculated from the slope of the fitted curves of Figure 38. Poisson's ratios were also calculated from the slope of linear fit (c) obtained using data points up to about 1% axial strain (elastic region) [30].

	Poisson's ratio values				
Sample name	(a) experimental value at below 0.7% strain	(b) 2^{nd} order fit at below 0.7% strain	(c) linear fit of elastic region	(d) experimental value at highest point	(e) 2^{nd} order fit at highest point
Copy paper	-3.0 ± 1.4	-3.3	-3.3	-3.2 ± 0.6	-3.6
Paperboard	-0.3 ± 0.4	-1.5	-1.1	-2.6 ± 0.4	-4.5
Bamboo Paper	0.6 ± 0.9	0.1	0.1	-0.1 ± 0.4	-1.1
Cotton Paper	-0.3 ± 0.5	-0.3	-0.3	-0.7 ± 0.3	-1.2
Filter paper	0.0 ± 0.0	-0.04	-0.3	-0.5 ± 0.2	-1.4
Glassine paper	0.6 ± 1.3	1.7	1.2	1.1 ± 1.1	2.7
PET Film	0.2 ± 0.5	0.5	0.5	0.8 ± 0.2	1.4

Because several samples clearly showed a concave up shape for their thickness increase, it was deemed reasonable to fit the experimental data with a 2^{nd} degree polynomial curve. All curves were fit using such a polynomial (dashed lines in Figure 38). The slope of the 2^{nd} degree polynomial curve at the experimental data point just

before 0.7% strain was used to calculate the Poisson's ratio and is shown in Column (b). The same slope was also calculated at the data-point right before sample failure and is shown in Column (e). As expected, the values in Column (e) are the most negative as the thickness increase rate is most rapid just before the sample fails. Effective Poisson's ratio was also obtained from the highest data point, shown in Column (d). Values in columns (a) and (d) were calculated using Equation 4.

By examining effective and instantaneous Poisson's ratio at each strain, further insight into the variation of Poisson's ratio and hence the nature of auxetic response with strain can be studied. This works best in cases where the thickness strain is nonlinear and will be used more when discussing handsheets and nonwovens.

3.4.4 Out-of-plane auxetic response in laboratory handsheets

Individual ‘thickness strain versus axial strain’ plots for Poisson's ratio experiments on laboratory made handsheets have been grouped and reported based on their grammage. Figure 39 shows this plot for the thick (SW/HW-5) handsheet samples. Similarly, Figure 40 and Figure 41 show the plots for medium thick (SW/HW-3) and thin (SW/HW-1) handsheets respectively. Figure 42 shows the variation of instantaneous Poisson's ratio values (calculated using Equation 3) with axial strain for all handsheets. Instantaneous Poisson's ratio is suitable to study the nature of thickness increase for highly non-linear dimensional changes, like in this case. It is easier to discuss the key features of handsheets by studying all the plots together.

Most striking observations related to thickness change in handsheets are listed as follows –

1) ‘Thick’ handsheets with high grammage (above 200 g m^{-2}) and low bulk density (about 0.4 g cm^{-3}) were found to be most auxetic (Figure 39 and Figure 42). These were followed by the medium and the thin handsheets (which were also denser), not all of which were not found to be auxetic. Poisson's ratio values as low as -4.0 were obtained in the initial strain region.
2) Refining caused the thickness to increase more rapidly in thick handsheets (Figure 39). Thus thick refined handsheets had a more negative Poisson's ratio (Figure 42). However, this effect was reversed in the case of medium and thin handsheets.
3) All thickness strain versus axial strain plots had a concave upwards curve, meaning that thickness increases more rapidly as strain increases, consistent with Öhrn’s [55] and our model [30], described in the next section.
4) In medium handsheets, similar to Baumgarten’s results [57], first an initial decrease in thickness and then a rapid increase in thickness was observed which finally exceeded the original thickness value of the specimen before failure. This effect may be due to the presence of coiled (not taut) fibers between contact points. Because hardwood fibers are shorter than softwood, this effect is almost only seen in SW3 and SW3R but not so much in HW3R and not at all in HW3 (see Figure 40).
5) Refining caused the thin samples to stop being auxetic. Unrefined thin specimens were found to be slightly auxetic but refined samples (SW1R and HW1R) actually decreased in thickness with strain (see Figure 41). This observation was analogous to behavior of glassine paper. Too much refining in thin samples may cause breaking and splitting of fibers and result in dense sheets that behave like an ordinary plastic.

6) In general, softwood samples failed at a larger strain than hardwood samples – very likely due to longer fibers in softwood samples. Similarly, refined handsheets failed at a larger strain when compared to their unrefined counterparts and also showed a higher tensile strength, suggesting increased fiber-fiber bonding due to refining.

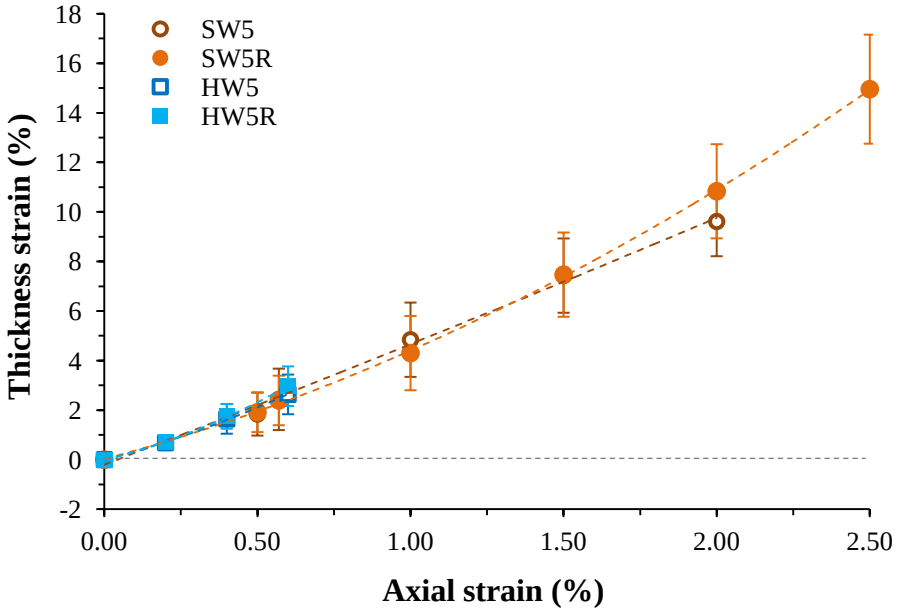

Figure 39: Plot of thickness strain (%) versus axial strain (%) for the thick handsheet samples (SW5, SW5R, HW5 and HW5R). Each series has been fit using a second degree polynomial (dashed lines) to serve as a guide to the eye.

Apart from these general observations, it is difficult to relate all parameters of papermaking accurately to the auxetic response in paper. Sometimes, factors such as refining can act to either increase or decrease the auxetic response depending upon other factors. For instance, too much refining can beat and break the fibers, causing them to open up and behave as a plastic sheet instead of a rigid fiber. Although this will increase the strength of the sheet, it will not contribute to an enhanced auxetic response as per our

model. Similarly, a low amount of refining that will only act in increasing the network contact points and connecting loose fibers should theoretically lead to a larger auxetic response.

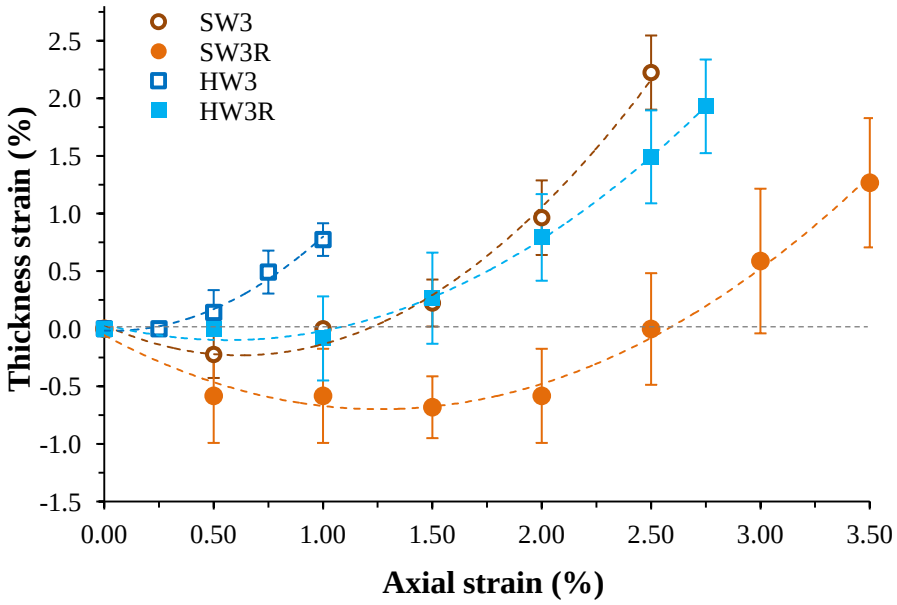

Figure 40: Plot of thickness strain (%) versus axial strain (%) for the medium thick handsheet samples (SW3, SW3R, HW3 and HW3R). Each series has been fit using a second degree polynomial (dashed lines) to serve as a guide to the eye.

These results on commercial and laboratory papers indicated that the value of Poisson's ratio and mechanism of auxetic behavior depend not only upon fiber and network characteristics but also on processing conditions employed during papermaking. Modification of fiber and fiber surface characteristics by pulping, bleaching chemicals, refining, fillers and calendering [83, 89] make the deconstruction of auxetic behavior a rather complicated subject. In an attempt to elucidate this behavior, a geometrical and a finite element model was built. It was clear that the magnitude of Poisson's ratio increases

(rate of change in thickness increases) with increasing axial strain in paper. This observation supports the quadratic fits applied to the data sets and is in agreement with Öhrn's observations. Our mathematical model for a simplistic network described in the Mechanism Section (3.5) below also showed a 2nd degree rise in thickness. A simple mechanism of auxetic response can be easily understood using this model and analysis of some complex structure-property relationships regarding auxetic response was also made possible.

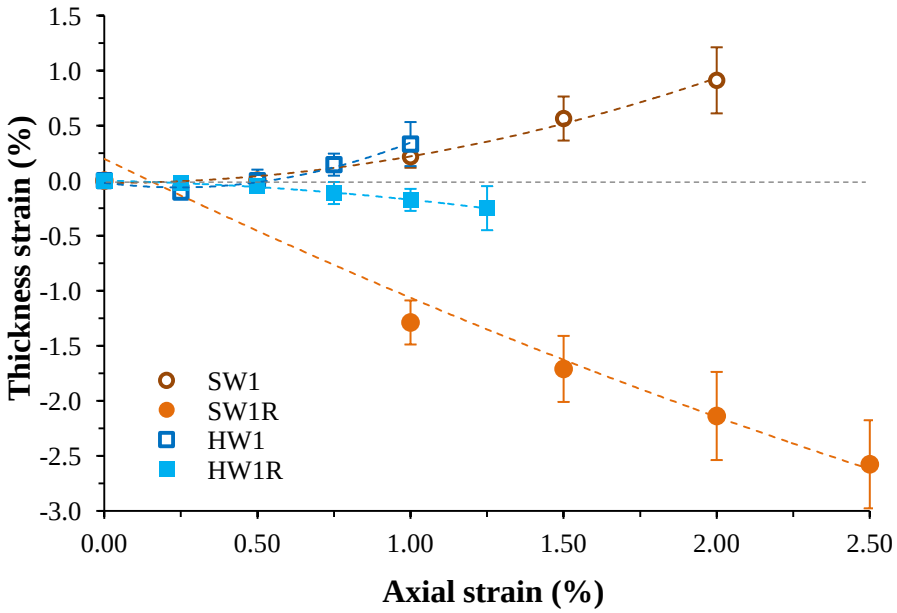

Figure 41: Plot of thickness strain (%) versus axial strain (%) for the thin handsheet samples (SW1, SW1R, HW1 and HW1R). Each series has been fit using a second degree polynomial (dashed lines) to serve as a guide to the eye.

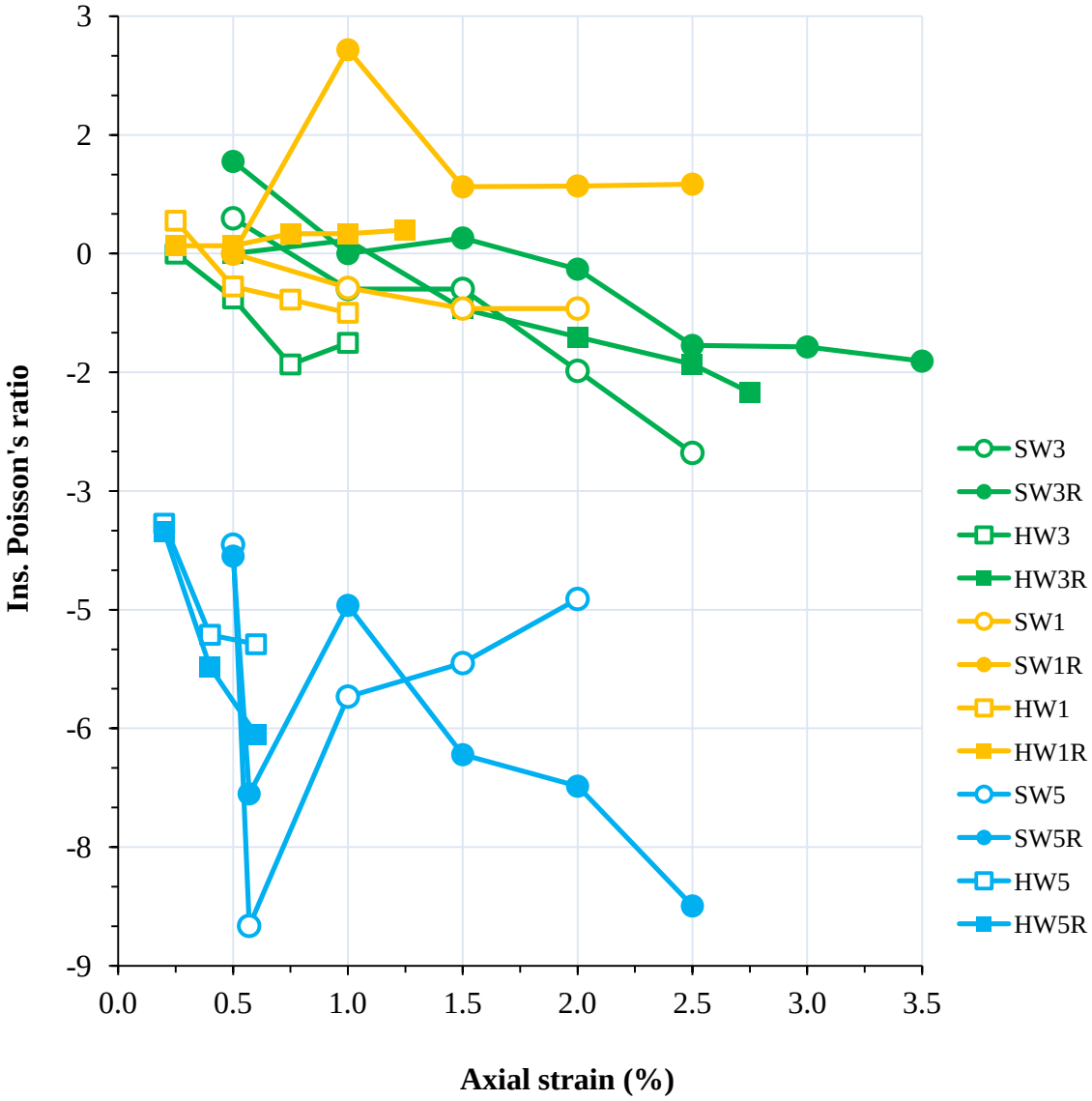

Figure 42: Plot of instantaneous Poisson's ratio for laboratory handsheets with respect to axial strain (%). Circles denote softwood while squares denote hardwood. Solid symbols denote handsheets made from refined pulp while the colors blue, green and yellow denote the thick, medium and thin handsheets respectively.

3.5 Mechanism of auxetic response in paper

Öhrn [55] proposed a plausible explanation for thickness increase in paper sheets under tension. He used a simplified network structure that expands in thickness similar to

modern theories of opening up of acute angles. Öhrn's model makes more sense when compared with SEM images of paper. Certain fibers can be seen organized in the way Öhrn describes. His mechanistic interpretation seems valid and was accepted fully by Stenberg [56] and partly by Baumgarten [57]. Baumgarten argued, based upon earlier reports by Ranger and Hopkins [116], that the increase in thickness may be caused by lateral contraction of CD fibers during MD straining. Öhrn had earlier disagreed with Ranger and Hopkin's theory of lateral compression of CD fibers, going by his own results using biaxial stretching of paper on his microcator device. In the microcator device, CD contraction of paper was inhibited but it still resulted in a thickness increase. Baumgarten and Page [57] agreed that more conclusive results and explanation were needed to explain this phenomenon. Technology has evolved immensely since then with the introduction of higher resolution strain measuring devices and better imaging techniques. Introduction of computational technology in orthotropic and random fiber networks has also allowed for modeling of these systems. It has been attempted in this study to add to the current understanding by also considering fiber surface chemistry and papermaking processes. We believe that hydrogen bonding at fiber joint is decisive in imparting this magnitude of auxetic behavior in paper.

Presence or absence of anisotropy (or machine direction) in the in-plane orientation of fibers is not thought to affect the overall mechanism but could in principle affect the value of v_{zx} against v_{zy}. During papermaking, fibers are laid out on top of each other and also interweave at some places along a fiber's length. This local interweaving where a fiber crosses over a fiber and then goes below another fiber is crucial for this mechanism (see Figure 43). During web formation and drying, water is lost from in

between the fibers allowing for inter-fiber hydrogen bond formation. New bonds are formed and the attachment strengthens as more and more water is lost. The end to end vectors of fibers mostly lie in the *x*-*y* plane.

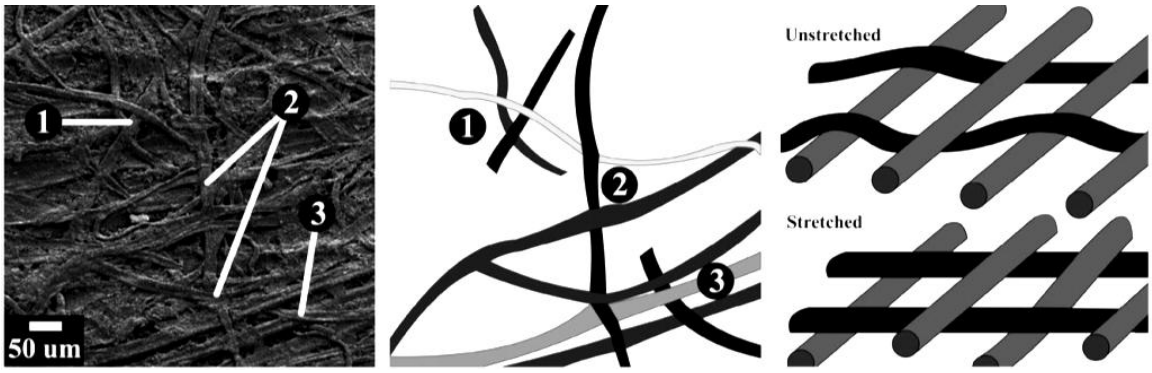

Figure 43: (left, a) SEM Micrograph (cropped from Figure 26) of copy paper – labels 1, 2 and 3 highlight the fibers that run from above a fiber to below a fiber. Each network contact is assumed to be 'fixed' through hydrogen bonds. (Center, b) Schematic analogue of the SEM picture showing some of the key fibers that would take part in inducing auxetic behavior and (right, c) a model of fibers (shown as rods) in *x* and *y* directions showing the auxetic effect on stretching [30].

SEM images show the fibers as flexible and somewhat flattened cylinders. Fibers are both over and below other fibers along their length and hence are not in a fully extended state in a finished paper. However this can change with processing conditions like refining, calendering and with mechanical properties of fibers themselves. On application of an in-plane force, these flexible fibers are stretched and start to get extended between network points. This results in pushing of fibers lying both above and below them (Figure 43, b and c), whether bonded or merely in contact, thereby increasing the thickness of the sheet. This push along *z*-direction is much pronounced when the network points are H-bonded. If the fibers are not bonded, they can slide past each other

on application of force and might occupy empty spaces – thus not leading to any or little increase in thickness.

3.5.1 Geometrical model

A simplified network arrangement of fibers is modeled based on the above observations. Consider a 3D-network of cylindrical fibers as shown in Figure 44. In an ideal scenario, assume that the fibers are infinitely long cylinders, inextensible and fixed at network (junction) points. The cylinders can be assumed to be flattened, so that the cross-section is elliptical rather than circular. The lowest (first) layer is formed of transverse (*y*-axis) fibers laid out parallel to each other at a separation of $2x_0$. The second layer of fibers is then laid on top and perpendicular to the first layer along the axial direction (*x*-axis). At every junction point, the fibers are considered attached through hydrogen bonds. The fibers are flexible enough to slack between two junction points and have a wavy nature in the model. The third layer of fibers is again oriented along the *y*-axis, but the fibers are now placed in between the spacing of the first-layer-fibers. We will call this three-layered structure a "stack" (see Figure 44a).

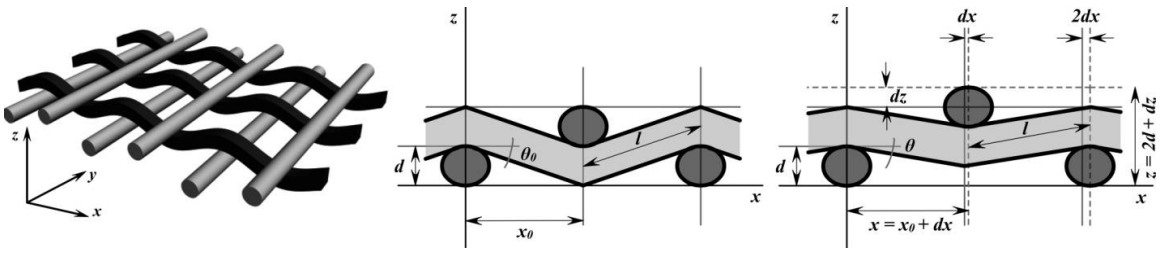

Figure 44: (left, *a*) Simplified fiber network arrangement – single 'stack' of three layered fiber structure. (center, *b*) the cross-sectional view of the geometrical model in its unextended original state and (right, *c*) model showing the change in thickness, *dz* as a result of extension, *dx* along *x*-direction [30].

To form an ideal paper sheet, stacks made up of these three layers are put on top of each other congruently, and repeated along the *z*-direction. When the fibers of second layer are pulled axially, they push the fibers in third layer upwards (towards positive *z*-axis). Thus a single stack of fibers can simulate the auxetic phenomenon. A geometrical model showing the *x*-*z* plane cross-section of the network is shown in Figure 44b. We further assume that the fibers are in fully extended state between network points (not coiled) and cannot be strained further. In this cross-sectional view of the stack, '*d*' is the fiber diameter (along minor axis of the elliptical cross-section), '*l*' is the length of fiber between network points, '$2x_0$' is the spacing between transverse fibers in a given layer and 'θ' is the angle the second layer fibers make with the *x*-axis.

Extending the axial fiber by '*dx*' along *x*-direction causes the stack thickness to increase by '*dz*'. Consider in Figure 44b, the length of the fiber between nodes, *l*. We can have

$$l^2 = d^2 + {x_0}^2$$

Similarly, from Figure 44c, we can have the same length of fiber, *l*, written as

$$l^2 = (d - dz)^2 + (dx + x_0)^2$$

Equating l^2 in the two equations and simplifying it for *dz*, we get the dependence of *dz* on *dx*, x_0 and *d* to be

$$dz = d - \sqrt{d^2 - 2x_0.dx - dx^2}$$

This equation gives $dz = 0$ when $dx = 0$ and $dx = l\text{-}x_0$ when $dz = d$ (i.e. at full extension), as one would expect from the model shown in Figure 44. The plot of thickness direction strain ($dz/2d$) vs axial strain (dx/x_0) is shown in Figure 45, for a chosen value of *d* (30 μm) and x_0 (100 μm). It is interesting to note that the shape of this

curve (second degree) is similar to the experimentally obtained curves for papers (as also noted and discussed by Öhrn [55]) – with the magnitude of negative Poisson's ratio increasing with strain. With increasing strain, the angle 'θ' in Figure 44c decreases causing the thickness to change more rapidly as governed by the equation. The curve shown in Figure 45 is part of a circle where the starting value of θ can be greater than the θ_0 shown in Figure 44a. In those cases the network stack will first decrease in thickness for $\theta > \theta_0$ and then increase in thickness for $\theta < \theta_0$.

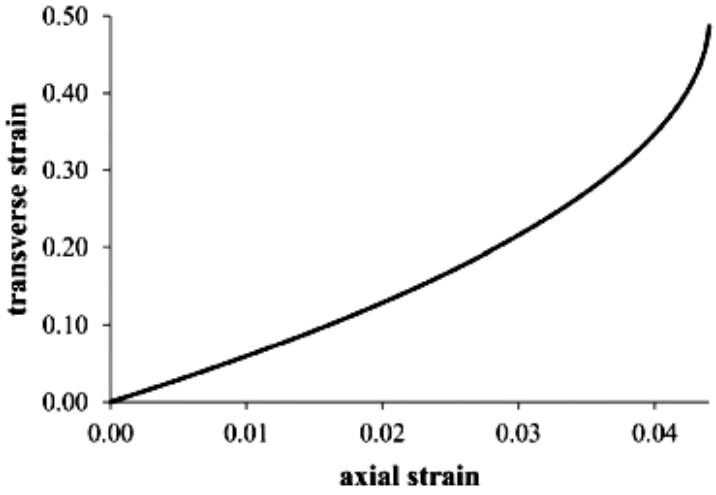

Figure 45: Theoretical plot of thickness (transverse) strain ($dz/2d$) vs axial strain (dx/x_0) for the geometrical model shown in Figure 44. Here we used d = 30 μm and x_0 = 100 μm [30].

3.5.2 Finite element analysis

Several attempts were made to build and simulate (computationally run uniaxial tensile calculations on the model) a suitable model. Modeling and simulation were first done on a 3 axial and 3 transverse (3 x 3) fiber system and then on a 9 x 9 fiber system

(see Figure 46). Transverse fibers were modeled as both fused to the axial fibers and merely in contact with the axial fibers. In one simulation, transverse fibers were pinned at their ends to restrict motion in the *z*-direction. Network parameters were changed and computational time was observed (to get a computational time that was less than overnight) several times until the following model and parameters were found, that yielded reasonable results.

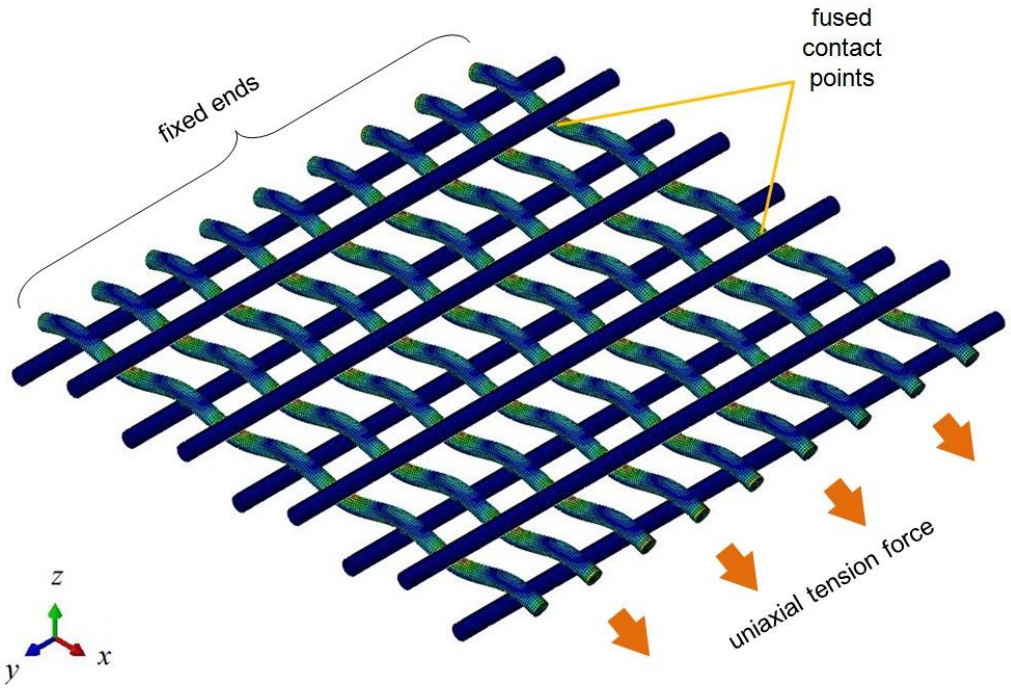

Figure 46: Finite element model under tension. The shaded regions show stress concentration in the mesh. One end of wavy fibers is fixed while the other is strained uniaxially. The transverse fibers are fused to the wavy fibers.

The results reported here were calculated on a network model build on 9 axial and 9 transverse fibers. Each fiber was assumed to have a circular cross-section for simplicity. Axial fibers were modeled to have a wavy nature such that the distance

between the top of the peak to the bottom of the well is twice the diameter of the fiber (see Figure 44 on which the FE model was based). Transverse fibers were assumed to be in permanent contact (fused) with the wavy fibers, attached on top of the wells and at the bottom of the peaks. The distance between two contact points (along *x*-direction) was set at 40 units and the fiber diameter was set at 10 units for this simulation. These values are of the order of fiber diameter and separation in real papers. Fiber modulus of 5 MPa and Poisson's ratio of +0.3 were used.

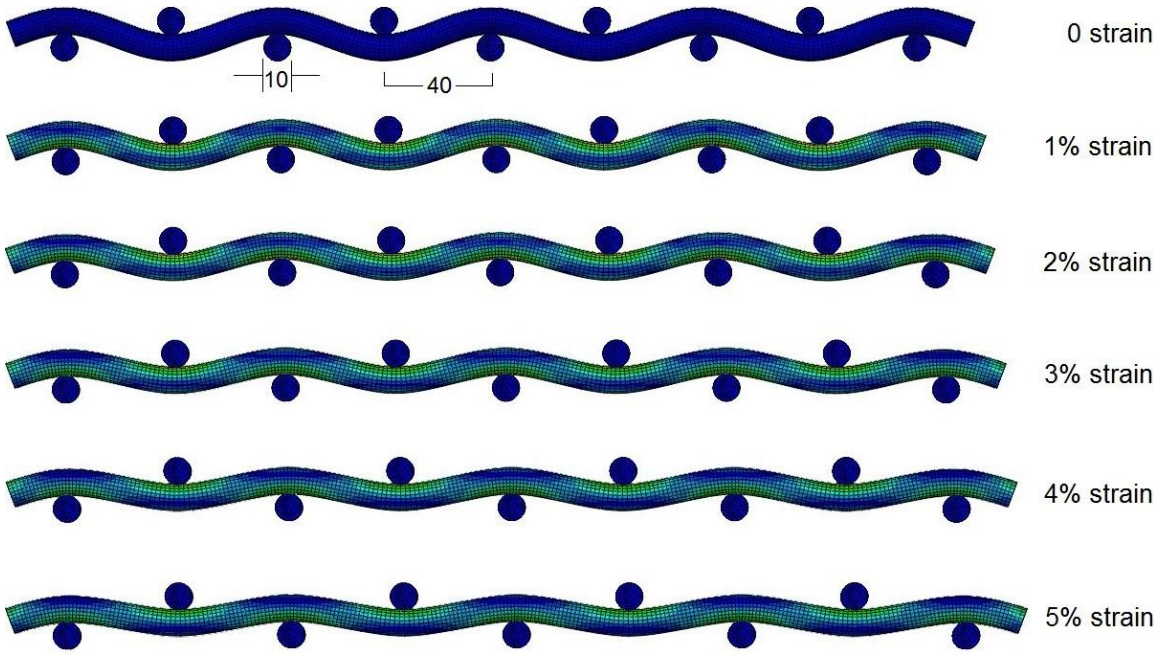

Figure 47: Uniaxial straining of the finite-element paper network model using Abaqus CAE software. The model was strained to 5% and thickness changes were measured at 1%, 2%, 3%, 4% and 5% axial strain values.

One end of the wavy fibers was fixed (motion restricted in *x*, *y* or *z*-directions) while the other ends were pulled uniaxially in the *x*-direction. The finite element model

was computationally strained using Abaqus CAE software and the Force Cluster (Georgia Tech, USA) up to 5% strain. Figure 47 shows the result of the simulation as five snapshots at 1%, 2%, 3%, 4% and 5% strain of the sideview of the network. Effective Poisson's ratio values obtained from the result of this simulation along the thickness direction are tabulated below. The values of Poisson's ratio obtained (close to –4.9 in the initial strain region) are reasonable for the given network. The geometrical and the finite element model also help to understand the strain dependent variation of Poisson's ratio in paper. While the geometrical model of inextensible fibers (Figure 44) suggests an increase in auxetic response with strain, the finite element model does not (Table 9). In the latter case, the fibers themselves are stretchable (extensible) and the Poisson's ratio values can thus be of lower magnitude, especially at higher strain levels.

Table 9: Out-of-plane effective Poisson's ratio values from the simulation results on the finite element model of the paper network for up to 5% uniaxial strain.

Axial strain %	**Thickness strain %**	**Poisson's ratio ν_{zx}**
0	0	-
1	4.9	-4.9
2	9.9	-4.9
3	14.4	-4.8
4	18.4	-4.6
5	21.8	-4.4

For future researchers, the next step in the finite element modeling of paper would be to introduce randomness in the planar orientation of fibers. While the ideal network shown here helps to understand the deformation mechanism in the neighborhood of a

hydrogen bonded contact point, real paper does not have such contact points arranged in a periodic fashion. Fiber orientations, starting angles (θ_0), contact separations and fiber diameters and shape are suggested to be randomized within reasonable limits. Moreover, the modulus of fiber and other mechanical and viscoelastic properties can be varied and their effect on auxetic response can be studied through further finite element analysis.

3.5.3 Advanced discussions on auxetic response in paper

Due to the variations in processing conditions, for a finished paper, the cellulose fibers may not be fully extended between network points. They are also extensible and the layout is not regular. In real commercial papers, a lot of filler material, pigments, recycled content etc. are also present. Therefore, the proposed geometrical or FE model is expected to be qualitatively consistent with the auxetic response of paper and will need further refinement to be quantitatively consistent.

However, many of the results obtained in the previous section can be explained with the help of this model. A lower θ angle at the start means that the thickness increase will be more rapid as suggested by the theoretical plot. This can occur in paper that has been compressed and stretched during calendering. If the paper is thick and has a low bulk density, the expansion in one layer might not efficiently get transferred to the above layer, thereby dampening the auxetic response. Thinner fibers will contribute to a lower thickness increase and so will flexible fibers that are not taut between two network points. This might be the cause of feeble thickness increase in cotton and filter papers.

In glassine paper, refining and supercalendering effectively destroys the fiber network – flattening out all fibers and closing in any pore spaces. The bulk density of glassine is quite high. Also glassine is semi-transparent, which is characteristic of thin

paper that has been beaten and calendered so much that the pore sizes have been reduced to lower than the order of a fiber diameter [89]. Glassine paper thus does not resemble the model fiber network. Instead, it is more like a continuous medium of cellulose. Thus its behavior is plastic-like.

Large auxetic behavior in thick handsheets can be attributed to their resemblance to the ideal network and lack of fillers. They have not been calendered and might have an optimally spaced fiber-fiber bonding. Close bonding sites (lower separation between contact points) will generally cause the auxetic response to increase – given that the paper has not been supercalendered or heavily refined. The thick handsheets might have an optimum structure to generate such a large auxetic response. It is however, not straightforward to comment upon its differences with thinner handsheets, again, due to the complexity of network structure and the various parameters in operation.

This model, in addition to explaining the auxetic response in paper, can also help in the development of new networks made out of entirely different fibers and processes. The model is independent of length scale and material type and is a novel and simple design to be used in creating new auxetic materials.

3.6 Conclusions

A technique to measure the out-of-plane Poisson's ratio of paper using a pressure sensitive digital micrometer and an Instron has been developed. Changes in thickness of paper sheets with respect to axial strain could be measured accurately to one micron. It was found that the Poisson’s ratio of some commonly used and commercially available papers had a negative value (auxetic) when measured in the thickness direction. A

negative Poisson's ratio value as large as –3.0 was observed for copy paper. This out-of-plane auxetic behavior was also observed in many laboratory made handsheets. For example, handhseets with higher grammage (> 200 g m^{-2}) and un-refined handsheets with lower grammage (lower than 200 g m^{-2}) were found to exhibit auxetic behavior. For some higher grammage handsheets, the negative Poisson's ratio was found to be as large as –3.5 in the initial strain regime while for some other kinds of handsheets the thickness first decreased and then increased only at higher strains.

The difference in the values of Poisson's ratio for different types of paper suggests a strong correlation with the fiber-network structure and the processing conditions employed during papermaking. Strong hydrogen bonds between fibers at junction points and the interwoven organization of fibers, albeit irregular, are thought to be critical elements in the tensile deformation mechanism leading to auxetic response. Fiber length, fiber morphology, fiber orientation and various papermaking parameters such as bleaching, refining, calendering and coating etc. affect the fiber network structure and consequently the nature and extent of auxetic response.

A simple geometrical model was used to qualitatively explain the increase in thickness upon strain and the second degree shape (concave up) of the observed 'thickness strain versus axial strain' curves. A finite element model was also built and it was found that such a network should produce auxetic responses in not just paper but any other system based on a similar network design. The model was independent of the length scale and the fiber type.

3.7 Suggested future work

For commercial exploitation of the auxetic behavior that we found in paper, a series of experiments carried out on paper produced on pilot paper plants (that mimic industrial production) might provide additional understanding of the origin and extent of auxetic response. Also, it will be interesting to examine this effect in non-cellulosic papers. Papers made from natural fibers that are not cellulose or paper made from synthetic fibers which might have a similar network structure but say, no H-bonded contacts, might produce interesting results. In the finite element analysis, additional sophistication for the model may be achieved by incorporating additional network properties such as orientation and fiber properties such as viscoelasticity etc.

CHAPTER 4

AUXETIC BEHAVIOR IN NEEDLE-PUNCHED NONWOVENS

4.1 Background

4.1.1 What are nonwoven fabrics?

The nonwovens industry is a very profitable industry owing to the low cost of polymer fibers as raw materials and due to their global use in applications including, but not limited to apparels, medical bandages and scaffolds, hygiene disposables, carpets, automobile lining, roofing materials, filters and geotextiles [117, 118]. Nonwoven fiber-based assemblies are annually produced in large volumes (1.95 million tons produced in 2012 worldwide) and are of considerable commercial importance [119]. Ranging from newsprint and fine papers to surgical gowns and filtration materials, nonwoven fabrics are ubiquitous in daily life. Understanding the mechanical behavior of nonwoven fiber systems is an important and challenging problem.

A nonwoven fabric is made from a collection of fibers held together by either mechanical entanglements or by some kind of thermal or chemical binding [120, 121]. Contrary to woven or knitted fabrics, nonwoven fabrics do not have a regular or a uniform arrangement of fibers or yarns, nor do they undergo yarn preparation [121]. The fibers in nonwovens are simply filaments of a synthetic or a natural polymer. Nonwovens are planar network structures that are consolidated to produce a robust fabric by above mentioned techniques [122, 123]. This bonding is necessary to impart strength to the fiber web (batt). The fibers can be staple (up to a few inches long) or continuous (as in

case of spunbonded nonwovens) and can be either oriented along a given direction or randomly laid in the mat [121].

4.1.2 Production of nonwovens

Production of a nonwoven fabric can be mainly divided into three stages –

1. Fiber manufacture
2. Web forming and
3. Web bonding

Natural fibers such as cotton, jute, cellulose, wool, silk etc. [121, 124, 125] and synthetic fibers such as polyester [124], nylon [126], polyolefins [76], etc. and even metal wires [64] can be used to make nonwovens. Nonwoven industries usually buy their fibers from fiber manufacturers as raw materials. Sometimes the process of fiber production and web formation is continuous and has to be integrated into a single process, for instance in spunbonded nonwovens [120].

4.1.2.1 Web formation

Taking the fibers and laying them down into a mat before they can be bonded constitutes the process of web formation [120, 121]. (In case of staple fibers, they can first be cut to desired lengths). This is followed by the process of carding (combing of fibers by metallic wires/teeth), which helps to separate and disentangle the fibers. Different kinds of fibers can be blended together to form a web. Blending is usually done in air. Following are the three methods in which a web can be formed –

a) Dry-laid web formation
b) Wet-laid web formation
c) Polymer-laid web formation

In dry-laid web formation, the fibers are laid into a web without the use of any suspension, solvent or a liquid medium. In wet-laying of fibers, a suspension of fibers is prepared (almost always in water) and is allowed to drain through a wire (or screen) while the fibers settle down to form a web. This process is inspired from the traditional papermaking process. Polymer-laid formation refers to the process where a web is formed directly from continuous polymer filaments being extruded or spun. The most common methods of polymer-laid web formation are spunbonding and meltblowing.

The web is usually formed on a wire (or a screen) which is in continuous motion. The web forming part of the nonwoven loom (loom is the machinery for nonwoven production) can have another stage of carding which combs, disentangles and aligns fibers again while the web is in motion [121]. Thus the fibers have a preferential orientation in the direction of motion of the machine. Because the strength of the finished fabric will be higher in the direction in which the fibers are oriented [127], it is often desired (when strength uniformity in different directions is needed) that the orientation is more random in the plane of the fabric. One way this is usually achieved is through cross-lapping [121]. In this process a layer of formed web is overlapped with another layer at an orthogonal direction. Other angles and multiple layers can be used to achieve the required mechanical properties. Air-laying (a type of dry-laying) ensures more isotropic orientation of fibers as opposed to methods that involve a lot of carding [121].

4.1.2.2 Web bonding

The variety of web forming processes are followed by bonding of the web [120, 121]. Without bonding, the web has little mechanical integrity which makes it unfit for practical use. Fibers can bond to each other through surface chemical bonding as in case

of hydrogen bonding between cellulose fibers in paper. But for majority of other fibers, bonding is achieved through chemical binders, adhesives, solvents, needling, stitching, high pressure air or water jets, heat or heated calendaring etc. [121, 128, 129]. This bonding can be achieved using one of the following methods –

a) Chemical bonding

b) Thermal bonding

c) Mechanical bonding

In chemical bonding, a chemical is mixed with the fibers or the web at some previous stage and then subsequently made to react through heat or light to enable bonding between binders and the fibers [122]. In thermal bonding, the fibers are heated to their softening temperatures, usually at certain spots (through heated patterned metal rollers) that cause the fibers under them to soften and fuse together [130–132]. Mechanical bonding is the oldest bonding technique that now uses barbed needles to repeatedly punch through the fiber web, thus locking the fibers together. Water jets can also be used instead of needles. It is then called 'hydroentanglement' or 'spunlacing' [120]. Stitching together of layers of wovens, nonwovens and other materials in various combinations is also a method of mechanical bonding. Any of these bonding techniques is not exclusive to any of the web forming process.

4.1.2.3 Some definitions

In the remaining text, the term 'batt' will stand for the web of fibers that will subsequently be needle punched or otherwise bonded. The term 'fabric' will be used for a finished nonwoven. 'Basis weight' or 'grammage' of a nonwoven fabric or web is its weight per unit square meter area. Also, similar to the nomenclature in paper, the

direction in which the batt moves (direction of movement of batt in the loom) will be called the ‘machine direction’ and the orthogonal direction will be called the ‘cross direction’.

4.1.3 Motivation for examining auxetic response in nonwovens

In Chapter 2, it was seen that auxetic behavior can be induced in commonly used materials through special processing conditions or using clever structural designs. Apart from the early reports of auxetic response in paper [55–58] (considering paper as a special case of nonwovens), Berhan’s steel mats [65, 66] and Baughman’s buckypapers [52], the common nonwoven materials have rarely been studied for their auxetic behavior. It is likely that there are advantages in producing auxetic behavior in all kinds of nonwoven materials, because of the following reasons –

a) Nonwovens are inexpensive materials that are produced and used in huge quantities across the world. They could be very profitable as raw materials in producing smart materials such as auxetics.

b) Nonwovens have fiber components and network microstructures that have the potential to be tailored into designs characterized by acute angles that would open up on application of stress – the fundamental mechanism of an auxetic response.

c) Almost all parameters of the production of a nonwoven fabric – fiber types and characteristics, bonding technology, matt density and thickness, orientations etc. can potentially be changed as desired to achieve the requisite mechanical properties, including Poisson’s ratio.

Needle-punched nonwovens are a major type of nonwovens (going by their volume of production) and have interesting internal structure produced by the needling

process that can have a great potential to be converted into auxetic materials. Apart from needle-punched nonwovens, any nonwoven bonded at network contact points could possibly be able to mimic the mechanism of auxetic response in paper, given they have sufficient density and strength. These other nonwoven types are however, beyond the scope of our research. We now discuss the structure and production of needle-punched nonwovens in some detail.

4.1.4 Needle-punched nonwovens

Needle-punched nonwovens find their applications in geotextiles, filtration devices, paddings, flooring, automobile fabrics, thermal and noise insulations, blankets, wipes, roofing materials etc. [117, 121].

4.1.4.1 Raw materials

Needle-punching is one of the oldest techniques of making textiles [133]. Natural sources such as jute, hair, tree leaves, rags etc. have been traditionally used to make needle-punched nonwovens [121]. Nowadays, these fabrics are mostly manufactured using polyester, polypropylene, aramid, polyacrylic fibers and other advanced fibers for specialized applications. Both staple and continuous fibers are used [134].

4.1.4.2 Production sequence

Needle-punching in nonwoven manufacture is a line operation wherein typically the staple fiber web is first carded to disentangle and orient individual fibers and then punched through its thickness with a large number of needles on needle-boards as the batt moves through the loom [121, 135, 136]. This needle-punching process creates columns (or bundles) of vertically oriented fibers (perpendicular to the plane of batt) by barbs on the needles which grab fibers at the top of the batt upon entry and pull these fibers

through the thickness of the batt [135, 137]. Upon needle retraction, these fiber bundles remain in place reflecting the mechanism of fiber transfer from the top surface to the bottom. This process creates fiber entanglements, decreases the thickness of the fiber batt, and greatly increases the mechanical integrity and strength of the batt [135, 136].

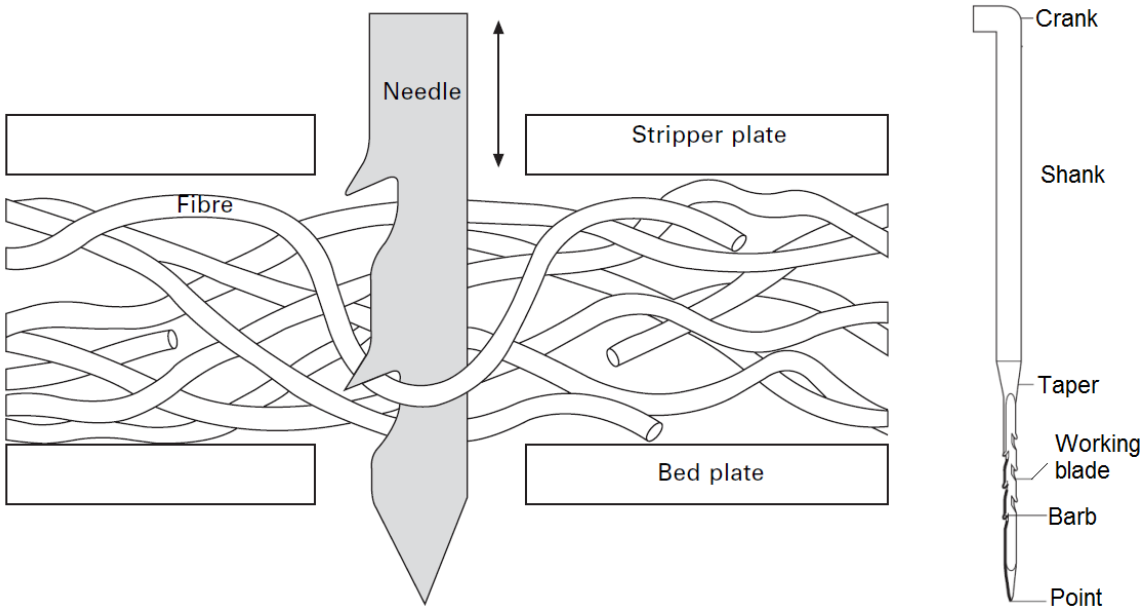

Figure 48: Fiber capture by a barbed needle as it moves through the thickness of the nonwoven web (left) and the detailed structure of a barbed needle (right) [121]

Although needle-punched nonwovens can be produced in very specific ways, a typical series of steps for their manufacture is given below –

a) Fiber stock is prepared from staple fibers. Virgin or recycled fibers, as well as blends of two or more kinds of fibers can be used. Continuously extruded fibers, instead of staple fibers, can also be needle punched.

b) The collection of fibers is separated by mechanical means and/or carding to reduce entanglements and clumping prior to the needling process.

c) Web is formed through dry-laying, wet-laying or polymer-laying (in case of continuous fibers). This process can include the carding of web.

d) Multiple layers of formed web can be cross-laid or parallel-laid or laid at certain angles to each other depending on the orientation distribution of fibers required.

e) This multi-layer of webs is bonded by the use of needles. As the web moves forward down the loom, it is punched through its thickness by an array of barbed needles. See Figure 49.

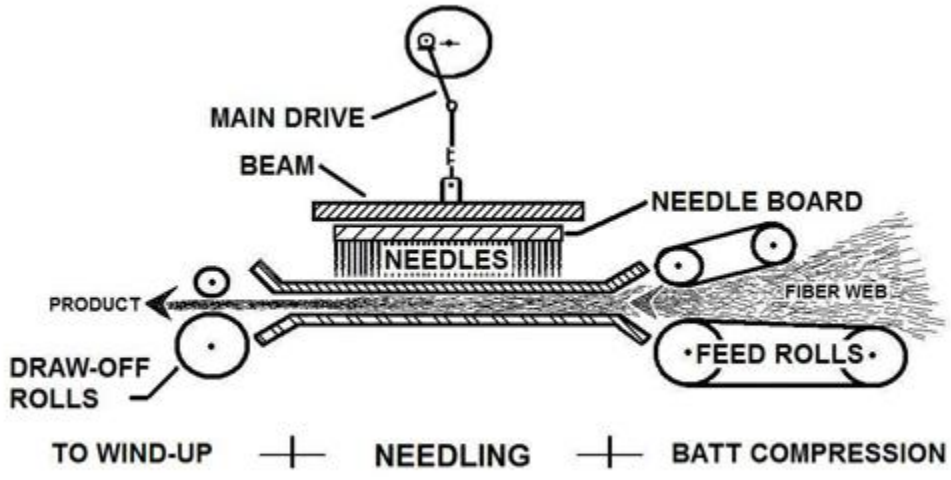

Figure 49: Process diagram of needle-punching. Formed fiber web is compressed to requirement and pushed forward through feed-rolls for needling. One needle board penetrating from top to bottom is shown in the figure. Needle-punching greatly reduces the web thickness and increases the mechanical strength (Source: http://www.dvc500 .com/needle-punched-fabrics.html)

f) Needle boards as wide as the width of the web hold an array of barbed needles and can repeatedly penetrate the entire thickness of the batt. More than one such board can be used as the web keeps moving forward along the loom [138].

g) Figure 48 shows the action of a typical barbed needle in carrying a fiber from the top of the web downward along the thickness direction. This repeated action catches several fibers and orients them perpendicular to the plane of the web – thereby entangling the fibers and consolidating the web [137].

h) Needles penetrate the entire thickness of the web. However, the number of barbs engaged can be changed by changing the depth through which the needle penetrates. Needle punching can be done from top-down as well as from bottom-up. There is a stripper plate with holes between the needle board and the web to prevent fibers being pulled up too far while the needle retracts [139].

i) Different needle boards can have different kinds of needles (although all needles on a particular board can be identical), different punching density per unit area (tens to thousands of punches/cm^2), different number of penetrations per minute (up to thousands of punches/min), and can hit the web at different angles (although penetration perpendicular to the web is very common). The needles themselves can vary in their thickness, length, number and shape of barbs, barb spacing and shape of cross-section etc.

j) After the needling process, the finished fabric is cut off, picked up mechanically and rolled for storage and distribution.

4.1.4.3 Structure

Needling greatly increases the density and strength of the web [138]. Penetration of barbed needles orients the fibers lying mostly in the top part of the web creating bundles of fibers along the thickness direction [137]. The presence of these fiber bundle columns is a distinctive structural element and is unique to needle-punched nonwovens when compared to other common nonwovens. Usually needling is done in one direction only such that the finished fabric shows distinct top and bottom surfaces. Modern needling machines can also perform needling from both the top and bottom surfaces of the batt [135, 136]. Due the movement of the barbed needle from the top to the bottom surface, more fibers are caught from the top region as compared to the middle or the bottom region of the batt. As a result, entanglements of fibers produced during formation of the fiber columns are concentrated significantly in the top section of the batt and would be expected to play a major role in mechanical deformation behavior in these nonwovens. In such fabrics, where only unidirectional needle-punching has been performed, the top surface appears smoother than the bottom surface. The bottom surface has less number of entanglements but a high number of loose fiber segments or loops formed due to the needle action [137].

4.1.5 Background of mechanical deformation studies in nonwovens

Mechanical properties of nonwovens are determined mainly by their anisotropy and fiber orientation [130, 140, 141]; fiber diameter, packing density, fiber length, batt thickness and basis weight [141]; and the nature and strength of inter-fiber bonding [140]. Fibers mostly lie in the plane of the batt with a preferential orientation along the carding direction and/or along the machine direction (the direction of movement of fiber batt during nonwoven production).

In-plane Poisson's ratio of nonwovens has been reported to be positive (lateral contraction) by a number of laboratories [127, 142–146]. Like any other common material, the dimension of a nonwoven strip decreases along its width when it is strained along its length. Rawal et al. [144] found the in-plane Poisson's ratio for some thermally bonded and spunbonded nonwovens to vary between about +0.25 to +4.0 at varying strain levels and in different loading directions. Highest values of Poisson's ratio were obtained when the fabric was stretched along machine direction as majority of the fibers are aligned in the machine direction. Figure 50 shows the Poisson's ratio values of a polyester-based thermally bonded nonwoven from Rawal's studies. The grammage for this particular nonwoven was about 30 g/m^2 and its thickness was about 0.44 mm [144, 147].

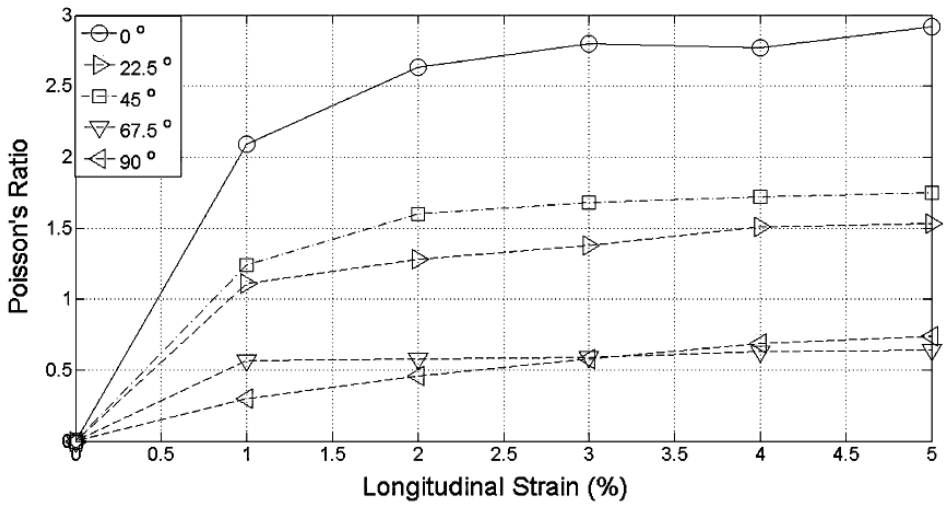

Figure 50: Relationship between in-plane Poisson's ratio and longitudinal strain for a thermally bonded nonwoven fabric in different loading directions [144].

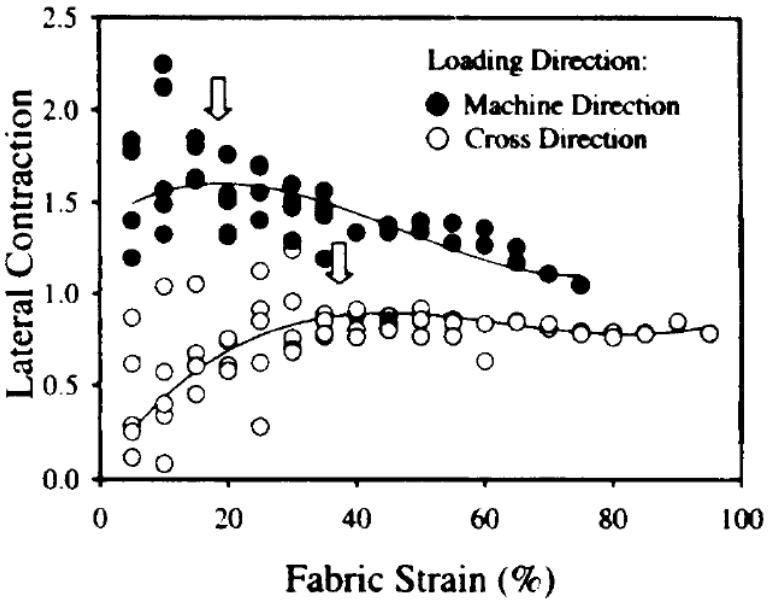

Figure 51: Lateral contraction variation with longitudinal strain in a thermally point bonded polypropylene nonwoven [142]

Kim et al. [142, 148] also found in-plane contraction in their thermally point bonded polypropylene nonwovens for various loading directions. These fabrics had a grammage of 24 g/m^2. Again, the contraction in width when strained along machine direction is much larger than when strained along cross direction (Figure 51). Mitra et al. [127] report in-plane Poisson's ratios of their needle-punched polypropylene nonwovens in the range of about +1.5 to +3.0, again for varying testing directions (Figure 52).

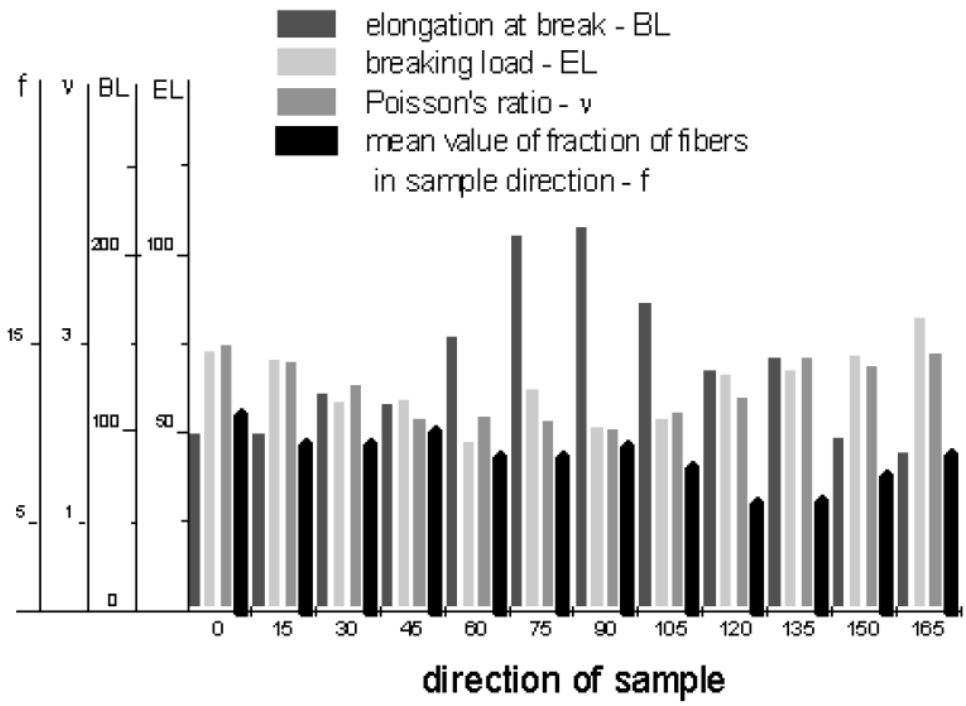

Figure 52: Note the variation of in-plane Poisson's ratio of a polypropylene needle-punched nonwoven with longitudinal strain along different directions [127].

Similar results were obtained showing conventional behavior (positive in-plane Poisson's ratio) of nonwovens in the works of Adanur et al. [143] and Bais-Singh et al. [145]. These examples help establish that most commonly used nonwovens (all kinds) display ordinary (positive Poisson's ratio) behavior in the planar directions.

Besides use in tension, nonwovens are also subject to varying degrees of compression. Kothari et al. [149] characterized the energy loss and compressibility of needle-punched, adhesive bonded and thermobonded fabrics with respect to mass per unit area, needling parameters etc. They found that their needle-punched fabrics were more compressible than thermobonded fabrics and that they exhibited a higher percentage of energy loss when compared to continuous filament fabrics. Effect of compression on pore

size distribution of a hydroentangled nonwoven has also been quantitatively analyzed by Jaganathan et al. [150] and it was found that the distribution became narrower and the pore diameter decreased exponentially with increasing compressive load (see Figure 53). Compressional and recovery behavior was also studied for highloft (low density) nonwovens and it was found that fiber-fiber bonding played an important role in determining the compression behavior [151].

Also, Afshari et al. determined suitability of high tenacity poly(ethylene naphthalate) (PEN) fiber based nonwovens compared to Kevlar 49 armors for ballistic protection [152]. They found that on increasing the tenacity of PEN fibers, the weight ratio of PEN to Kevlar 49 decreased for the same amount of ballistic protection. Although compression effects on nonwoven structure have been studied, we are unaware of any reports on their out-of-plane Poisson's ratio. Apart from certain Baughman's buckypapers [52], which happen to be a very special case of nonwovens, an in-plane auxetic behavior in any kind of nonwoven has not been observed or induced. Similarly, out-of-plane auxetic behavior has also not been observed for any kind of nonwoven so far (except paper).

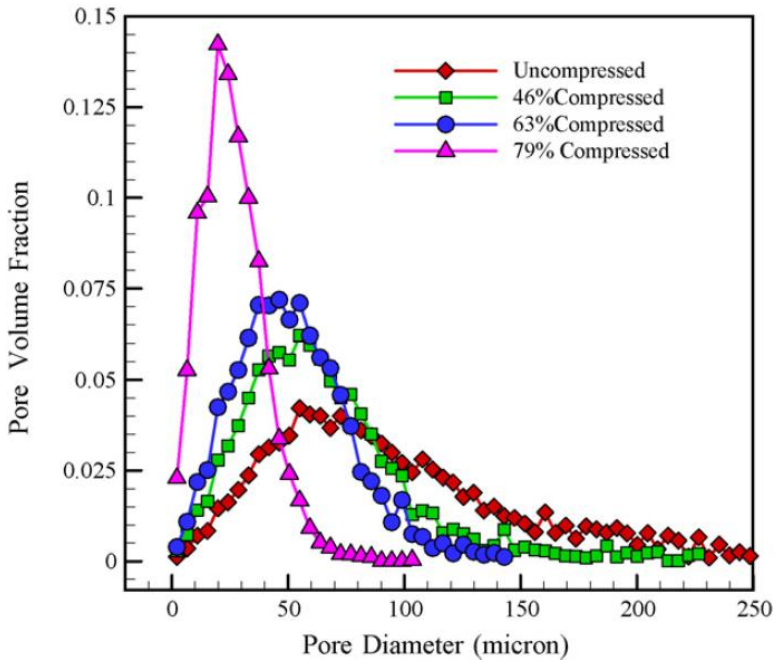

Figure 53: Pore size distribution for compressed hydroentangled polyester nonwovens obtained with the help of calculations from DVI images of these nonwovens. More compression makes the distribution narrower and decreases the average pore diameter [150].

Woven and knitted fabrics however, have gained intense research emphasis in recent years to impart auxetic behavior in them by tailoring the network patterns [62, 73, 152, 153]. These fabrics are different from nonwovens in both – the nature and type of fibers used and in having a more defined geometrical network structure. Studies on auxetic behavior in these kinds of fabrics are not a part of this research.

4.1.6 Key research objectives

Commercially produced nonwovens behave mechanically as common materials in the sense that their in-plane and out-of-plane Poisson's ratio are both positive. Taking

inspiration from the processing conditions of heat and compression during papermaking, that likely are responsible for the out-of-plane auxetic behavior of paper, it was desired to investigate potential auxetic behavior in nonwovens using a combination of heat and pressure. Other methods of producing auxetic response in PE, PP and PTFE also utilized related processing. Nonwovens, specifically needle-punched nonwovens were identified as test materials to study their auxetic behavior. Presence of rib-like fiber columns along the thickness direction in needle-punched nonwovens was also an interesting structural feature separating needle-punched nonwovens from other kinds of nonwovens.

A primary objective was to establish a protocol for accurate measurement of out-of-plane Poisson's ratio of needle-punched nonwovens. The changes in thickness were expected to be of the order of a millimeter. Rough (and hairy) surface of these nonwovens made accurate and repeatable thickness measurement a challenging task.

An additional objective was to find a processing protocol that could induce out-of-plane auxetic properties in these nonwovens.

To understand the nature of structural deformation during treatment and during mechanical strain, the technique of optical microscopy and micro-CT imaging was used. The final objective was to establish a processing-structure-property relationship to explain and predict the mechanical deformation behavior of these nonwovens.

4.2 Materials

All needle-punched nonwoven fabrics in this study were obtained from TenCate Protective Fabrics (Senoia, Georgia, USA). Two kinds of polyester fiber needle-punched

nonwovens and one aramid fiber needle-punched nonwoven were examined. The polyester nonwovens are referred to as NW1 and NW2 while the aramid polyester is referred to as NW3 (see Table 10). NW1 and NW2 were made from 3 inch long virgin poly(ethylene terephthalate) (PET or simply polyester) staple fibers. NW3 was made from a blend of different kinds of 1 inch long aramid fibers; 50% fibers were virgin meta-aramids, 20% were virgin para-aramids and 30% were recycled para-aramids. The mass per unit area of NW2 (30 oz. per square yard) was greater than that of NW1 (20 oz. per square yard), which was greater than NW3 (approximately 5 oz. per square yard). These grammage values were provided by TenCate (except for NW3, which was estimated) but were also calculated for each sample as shown in Table 10. Mean thickness of NW1 was 4.40 ± 0.14 mm, of NW2 was 5.32 ± 0.25 mm and of NW3 was 1.34 ± 0.02 as measured from five specimens of each nonwoven.

All fibers used in the nonwoven production by TenCate were originally crimped. Crimping increases the cohesion between the fibers and hence their ability to entangle with other fibers [154]. The carding direction and machine direction were also the same for all of the nonwovens. After carding, multiple layers of fiber were parallel-lapped to form the batt and then bonded by needle-punching. The speed of movement of batt on the machine was higher for NW3 than for NW1/NW2 [155] which resulted in slightly inclined needle-columns in NW3 when compared to nearly vertical needle columns in NW1/NW2. The approximate number of fiber columns produced by the needle penetrations was found to be about 300 columns per square inch as estimated by the authors from μCT images for all nonwovens. The total number of needle penetrations per

square inch was likely to be considerably larger. This is because multiple and repeated needle-penetrations along the loom can together form one single column.

Table 10: Measured thickness and grammage (approx.) values for different nonwoven samples along with composition. Calculated bulk density values are also shown.

Sample	**Thickness** *(mm)*	**Grammage** *($g\ m^{-2}$)*	**Bulk Density** *($g\ cm^{-3}$)*	**Composition**
NW1	4.40±0.14	678	0.15	Virgin polyester 3 inch long crimped staple fibers
NW2	5.32±0.25	1017	0.19	Virgin polyester 3 inch long crimped staple fibers
NW3	1.34±0.02	150	0.11	Blend of 20% virgin para-aramid, 30% recycled para-aramid and 50% virgin meta-aramid 1-inch long staple fibers

Due to the similarity of the fiber-type and network structure between NW1 and NW2 and also them showing very similar mechanical behavior, the NW1 sample was chosen and used consistently as archetype for all experiments.

4.3 Experimental

4.3.1 Heat-compression protocol for nonwovens

All nonwoven samples were compressed in the thickness direction at a chosen pressure and temperature for 20 hours. A square fabric of size 20 cm x 20 cm was cut for this purpose (Figure 54). A Carver® auto series (model no. 4389) benchtop press with heated platens (heating optional) was used for this treatment. After 20 hours, heating was discontinued (if used) and the fabric sample was allowed to cool under full pressure for

another 4 hours. These will subsequently be called 'heat-compressed' samples. Once the sample was at ambient temperature, i.e. after 24 hours of total compression, it was removed from the press.

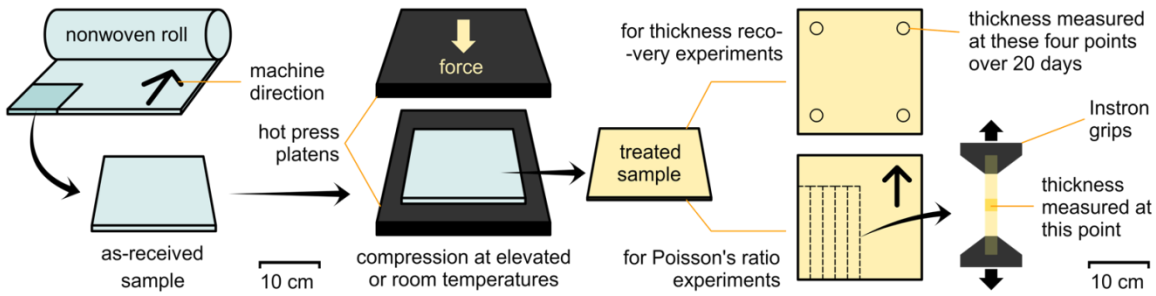

Figure 54: Diagram showing the processing treatment of as-received samples in a Carver® hot press to produce 'compressed' and 'heat-compressed' samples. Following the treatment protocol, samples were examined for thickness recovery over a period of 20 days. A separate set of samples were prepared in the same way for use in Poisson's ratio experiments (thickness change versus extension) [61].

A temperature close to the lower edge of the glass transition temperature (T_g) of the PET fibers [156], i.e. 70 °C was chosen for the treatment of NW1 and NW2 (heat-compressed samples). For comparison with PET fabrics, same temperature of 70 °C was also chosen for the treatment of NW3. The pressure used for compression was 2.45 MPa (10 metric tons over 400 cm^2 area and assuming acceleration due to gravity to be g = 9.8 m s^{-2}) for all nonwovens.

Additional test samples for each of the three nonwovens were also prepared by compression without using heating, i.e. at room temperature on the same press. In this case, they were compressed under the same pressure as above for 24 hours and then removed from the press. These will subsequently be called 'compressed' samples. Lower

pressures of 0.5 MPa and lower compression times of 4 hours (2 hours of heating) were also used in some cases to narrow down to ideal processing conditions. The processing conditions will be hereafter represented in the format of "**[force(tons).temperature(°C). time(hours)]**". For example, "10T.70C.24H" means that the nonwoven was compressed under a force of 10 tons at a temperature of 70 °C for a total duration of 24 hours.

For each treated nonwoven (heat-compressed or compressed), two different 20 cm x 20 cm square samples were prepared by identical compression protocol – one for the 'thickness recovery' experiment and another for the 'Poisson's ratio' experiment which are described below.

4.3.2 Measuring thickness change with time (thickness recovery)

Compression treated nonwoven samples have a tendency to spontaneously recover some of their thickness after they are taken out of the press. Different temperature/pressure conditions during treatment lead to different amounts and rates of thickness recovery in different nonwovens. To monitor this recovery, samples were prepared using the treatment conditions described above and their thickness was measured over a period of 20 days to determine the time required to attain a constant thickness value. As shown in Figure 54, each 20 cm x 20 cm square sample was marked with four circular regions (each of diameter 2 cm). Thickness values in these four circular regions were measured with the micrometer and their mean reported.

4.3.3 Measuring thickness change with extension

After determining the time required for treated samples to attain a constant thickness, an additional and new square sample (20 cm x 20 cm) was prepared using the same compression protocol and left for unconstrained recovery for the required number

of days. It was then examined for Poisson's ratio. Rectangular strips (or specimens) of size 2 cm x 15 cm were cut from the treated square sample with their lengths along the machine direction (see Figure 54). Machine direction was known in the nonwoven rolls and was not needed to be determined experimentally through tensile tests. All samples (‘as-received’, ‘compressed’ and ‘heat-compressed’) were deformed uniaxially in tension along their lengths and the thickness change was recorded using a digital micrometer. The gage length was set to 10 cm. These specimens were strained along their length until failure using an Instron® universal testing machine (model no. 5566, load cell 10 kN) at a constant rate of 10 mm/min and paused at regular strain intervals to allow for manual thickness measurement.

Initially, each specimen was marked with a 2 cm x 2 cm square in the middle along with a center point for positional reference. Despite their transformation during tensile extension, these marks served as a good aid for ensuring thickness measurement of the same area of specimen. Thickness was measured using a digital micrometer (Mitutoyo 369-350, same as used in paper experiments) with a flat circular disk-platen of diameter 2 cm. The micrometer was set by the manufacturer to give a thickness readout at a near constant pressure of 20-25 kPa. This constant pressure helps to ensure the repeatability of measured thickness values and minimizes the potentially misleading effect from a few fibers extending out normal to the surface. The large diameter of platen faces compensates for the heterogeneity of the nonwoven surface. Five specimens of each type – as-received NW1, NW2 and NW3, compressed NW1, NW2, heat-compressed NW1, NW2 and NW3 – were examined and their mean thickness was calculated. All measurements were performed at room temperature and ambient humidity (not

controlled) conditions. The values of instantaneous Poisson's ratio were calculated for each i^{th} strain level using Equation (3).

4.3.4 Testing reversibility of thickness change

These tests were performed to gain insight into the reversibility of auxetic response. In the low strain regimes (especially below 5%) some elastic and reversible behavior was expected. It was desired to examine whether the thickness change upon strain in treated nonwovens was reversible at low strains.

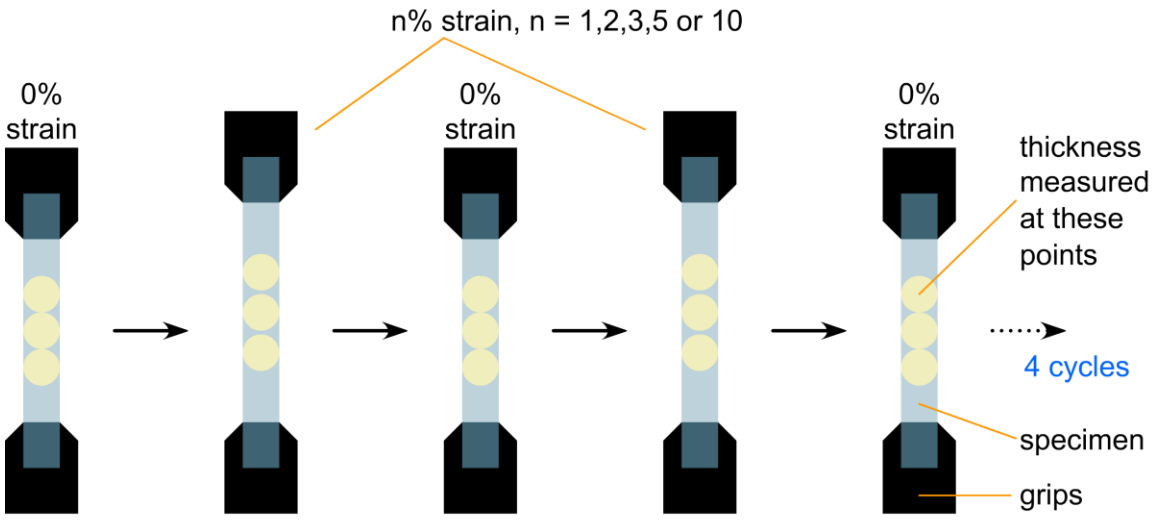

Figure 55: Experiment to examine the reversibility of thickness change upon uniaxial straining of treated nonwoven samples. NW1 heat-compressed sample were strained to different strain levels (n %) repeatedly over four cycles (2 cycles shown) and their thickness change was recorded.

Heat-compressed NW1 samples treated at 70 °C were chosen for this study. Specimens were strained to 1%, 2%, 3%, 5% or 10% of their gage length at a rate of 10 mm/min and then brought back to their original lengths almost instantaneously. This

cycle of applying a given strain and then removing the strain was repeated four times. Thickness was measured at three marked regions on the specimen before the strain was applied, at the maximum given strain level and then finally after the strain was removed for each of the four cycles. For each strain level (1%, 2%, 3%, 5% or 10%), percent change in thickness was plotted over the four cycles.

4.3.5 Optical microscope imaging

DinoLite® handheld microscope was used to take images of the surface and the side-view (thickness) of nonwovens at about 50X and 200X magnifications. Microscopic videos were also recorded of the side-view (thickness) of NW1 during extension and compression to help see the transformation of needle-columns during specimen deformation.

4.3.6 Micro-CT (µCT) Imaging

µCT imaging was performed on a Scanco Medical µCT50 instrument using a scanning tube of inner diameter 5 mm (Figure 56a) and an X-ray source energy of 45 kVp (details of a µCT scanning procedure has been given in Appendix B). For imaging of nonwovens, a small specimen of approximate diameter 5 mm was cut from the sample (as-received or treated) and press fit in the scan tube (Figure 56 b, c). A certain height of the sample (bound by white dotted lines in Figure 56d) was chosen for the actual X-ray CT scanning. Upon scan completion, a cylindrical sub-section of the resulting axial images (a little smaller than 5 mm diameter) was chosen for 3D-reconstruction. The instrument captures slice-by-slice 2D images of the sample separated by the resolution of scan (here 2 µm) until it scans the entire height of the sample. For instance, if the white

lines in Figure 56d contain a height of 1 mm, then the number of slices scanned will be 1 mm divided by 2 µm, which comes out to be 500.

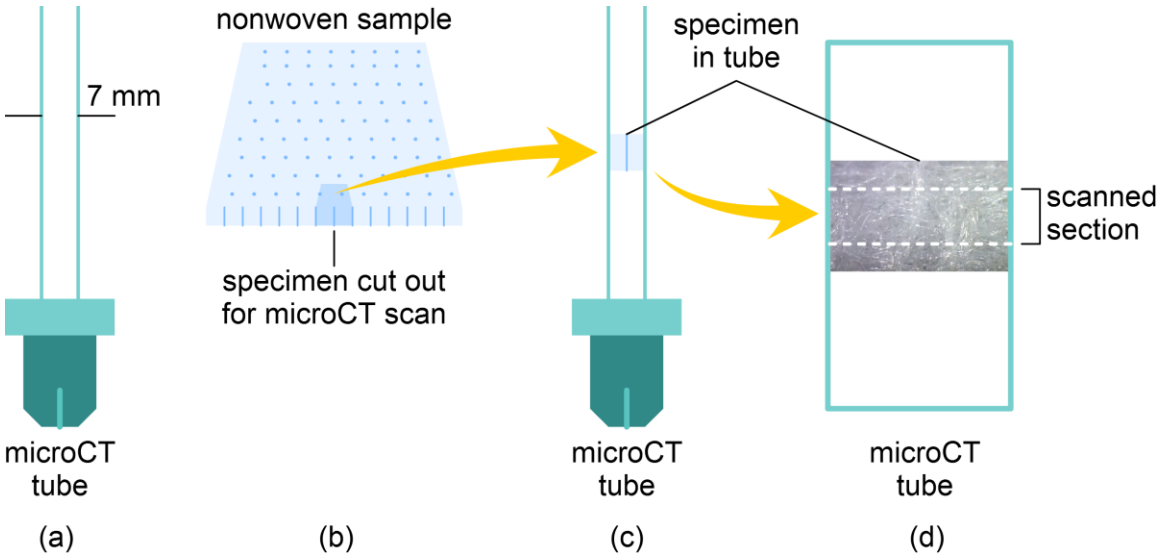

Figure 56: Steps in the preparation of a sample for µCT scanning (a) a sample holder tube of outer diameter 7 mm and inner diameter 5 mm (b) cutting of a 5 mm size specimen from a nonwoven sample (c) placing the specimen in the tube and (d) selecting a section of the specimen for actual scanning.

Thresholding is a process of selecting the fiber material from the surrounding air which is done manually based upon the material density cues from a histogram. The 2D axial image slices were stacked and global thresholding applied by Scanco's computer software to segment fibers from surrounding air and noise and produce binarized 3D images. All scans were performed at a voxel resolution of 2 µm. A voxel can be thought of as the smallest unit volume (cube) defined in the 3D structure. The voxel size in our case is a cube of side 2 µm which is also the error associated with the edge detection of the fibers. Due to sample and instrumental limitations, images of the exact same location

on a given sample both before and after treatment could not be easily obtained. Instead, separate as-received, compressed and heat-compressed samples were prepared for scanning. The 3D images were examined for structural features by viewing the whole image from different angles or at any vertical or horizontal section through the bulk of the sample.

4.3.7 Effect of fiber length on entanglements and thickness recovery

The average spacing between two needle-columns was about a millimeter in our nonwoven samples, and the staple length of fibers was 3 inches for PET nonwovens. Since the staple fiber length was much longer that the needle-column spacing, a single fiber could be associated with more than one needle-column, leading to an additional type of fiber entanglement. Entanglement between fibers (in the planar direction and within the column) imparts strength to the fabric and plays a role in defining its thickness. To examine the role of these entanglements on the thickness of the sample, strips of 2.5 cm x 16 cm were cut for NW1 and NW2. A set of as-received samples and another set of heat-compressed [70 °C, 10 tons, 24 hours] samples were used. The strip was marked with regions at every 2 cm length and thickness was measured at each of the 8 resulting regions (Figure 57). The strip was then cut with scissors into half and the thickness was measured again at each region. Cutting and thickness measurement was continued until the strip was cut down to individual 2 cm x 2.5 cm pieces (Figure 57). The variation of thickness with strip length was reported for each as-received and heat-compressed NW1 and NW2 sample.

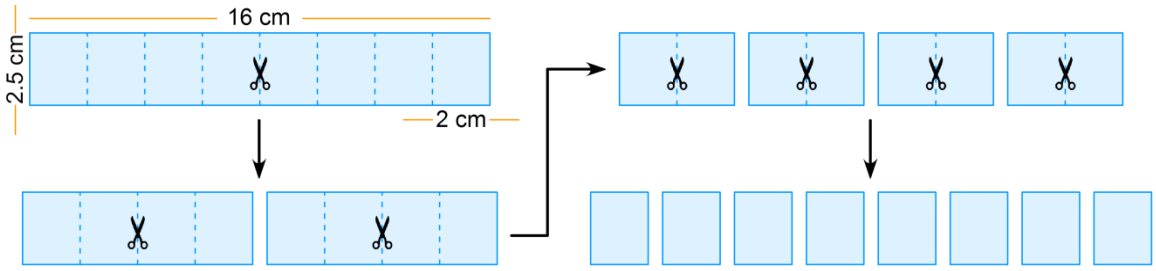

Figure 57: Cutting a strip (16 cm x 2.5 cm) of as-received or a treated nonwoven sample to examine the effect of fiber length on entanglements and thickness of the nonwoven.

4.4 Results and discussion

4.4.1 Thickness recovery with time

Prior to determination of Poisson's ratio for treated nonwovens, it was necessary to establish thickness versus time recovery profiles (time after removal from the press) in order to allow for any spontaneous thickness recovery to occur. Figure 58, Figure 59, and Figure 60 show percent thickness (original as-received sample thickness as 100%) as a function of time after removal from the press, for NW1, NW2 and NW3 respectively. Different processing conditions were tried for the treatment protocol by changing the force, temperature and time parameters. Because all samples measured 20 cm x 20 cm, specifying the force will specify the pressure and vice versa. It should be noted that as soon as the sample is removed from the press (i.e. almost instantaneously), even before the first thickness measurement (at t = 0) is made, it recovers some of its thickness. Hence, different samples have a different starting thicknesses (or % of original thicknesses) at time = 0. Recovery was also observed to be rapid in the first few hours after removal from the press and then slowed down considerably.

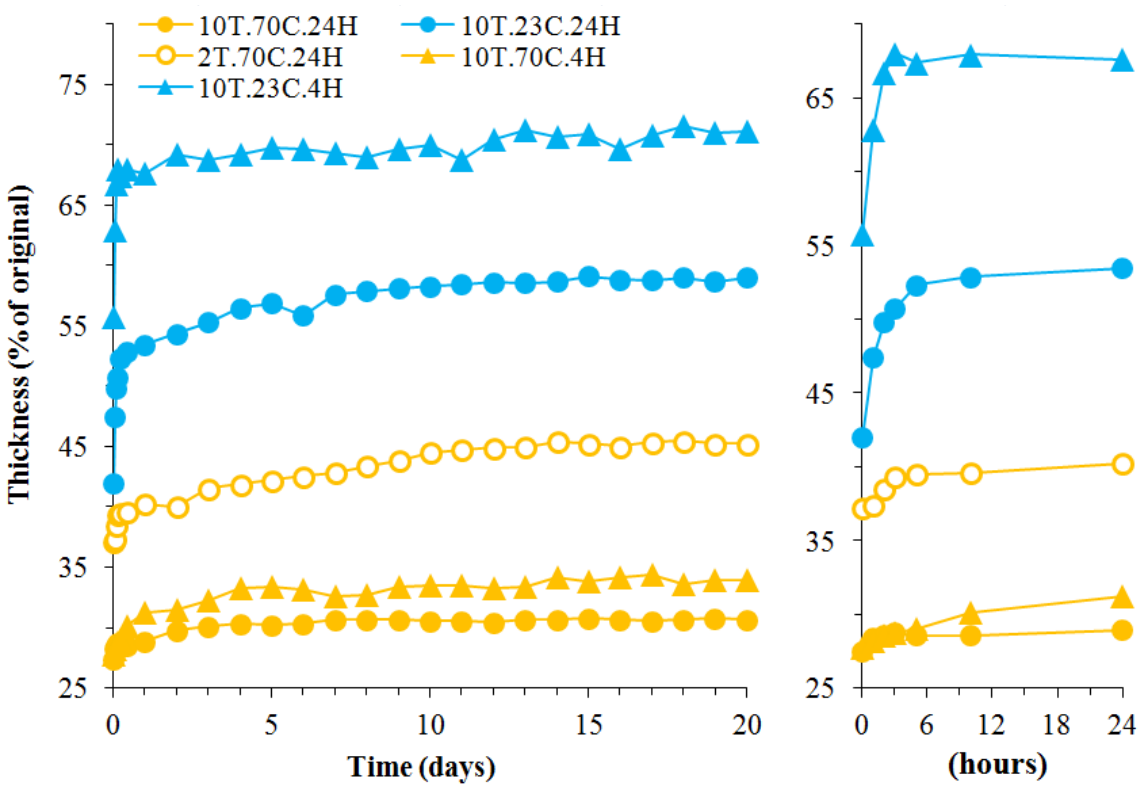

Figure 58: Thickness recovery with time after treatment for NW1 samples over a period of 20 days (left) and for the first day (right). Each data point represents the mean thickness (expressed as a percentage of original thickness of sample) of four distinct regions on a nonwoven fabric of dimension 20 cm x 20 cm (*parts from [61]).*

Figure 58 shows thickness recovery curves for five differently treated NW1 samples. It is clear that a higher temperature results in a larger compression set. NW1 treated at 70 °C (near T_g) showed maximum compression set. It was compressed down to 27 % of its original thickness and recovered to just about 30 % of its thickness. It was also found to attain a constant thickness within 7 days after taking out from the press. Elevated temperature for the heat-compressed samples likely reduces the crimp on the fibers and renders the fibers more susceptible to deformation and densification during the heat-compression treatment. Increases in both entanglements and fiber-fiber contacts

might also contribute to greater retention of compression set in the heat-compressed samples.

Reducing the time of compression to 4 hours (2 hours heating and 2 hours cooling down) from 24 hours only slightly increased the steady state thickness for samples treated at 70 °C (compare 10T.70C.24H with 10T.70C.4H). However, the steady state thickness was much greater in the case of 4 hours than in 24 hours when compression was done at room temperature (compare 10T.23C.24H with 10T.23C.4H). A similar effect was also seen on decreasing the force from 10 tons to 2 tons. On comparing 10T.70C.24H with 2T.70C.24H, the steady state thickness was again much higher for sample compressed at the lower pressure. Overall, higher temperatures, longer times and higher pressures resulted in a greater and more permanent compression set.

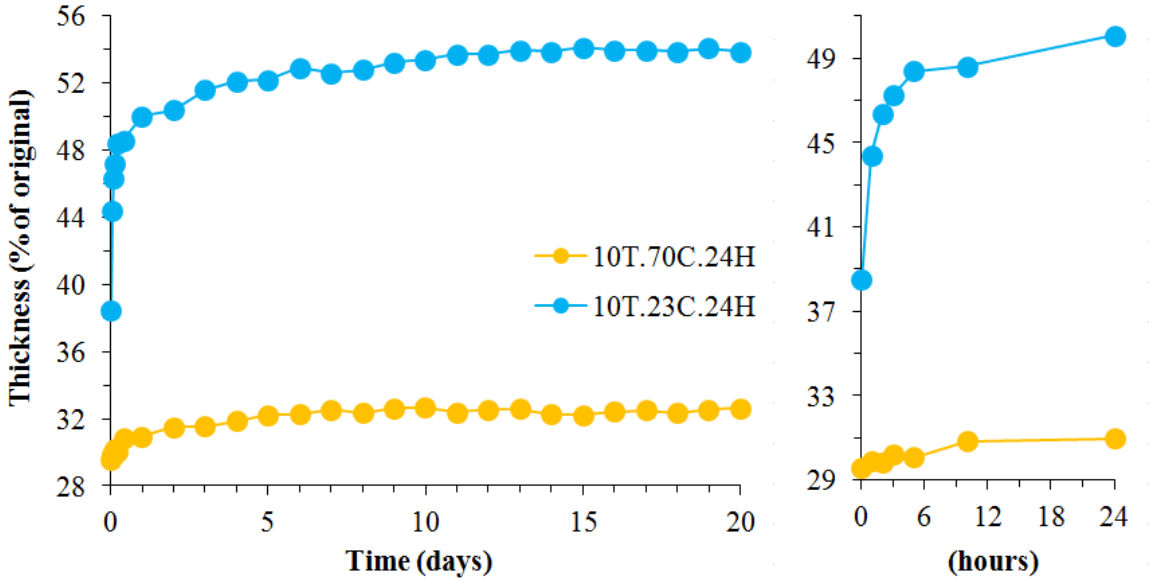

Figure 59: Thickness recovery with time after treatment for NW2 samples over a period of 20 days (left) and for the first day (right). Each data point represents the mean thickness (expressed as a percentage of original thickness of sample) of four distinct regions on a nonwoven fabric of dimension 20 cm x 20 cm (*adapted from [61]).*

A more permanent compression set and a faster recovery to steady state thickness are desirable to produce stable treated samples – an important property for commercial applications. Also, a greater compression set produces a larger auxetic response (which will be seen later) as it has more margin of thickness to recover. It was concluded that a 10 tons force (2.5 MPa pressure) results in a greater and more permanent compression set than a 2 tons force and was thus selected as a standard for remaining experiments. Similarly, 24 hour compression caused a more permanent and greater compression set than a 4 hour compression and was again, chosen as a standard for remaining experiments.

Using the results for NW1 as a guide, thickness recovery for NW2 was only measured at two conditions of treatment – room temperature and 70 °C (with force and time kept constant at 10 tons and 24 hours respectively). As expected, higher temperature resulted in a higher and a more permanent compression set (Figure 59).

Aramid based nonwovens also showed thickness recovery after treatment with time. NW3 was heat-compressed at 70 °C. Figure 60 shows that the thickness recovery in case of aramid nonwovens was much larger (33% to 48%) compared to heat-compressed PET nonwovens. This was likely due to shorter fiber length used in aramid nonwovens which makes it easier for fibers to get disentangled and perhaps also due to higher stiffness of aramid fibers. Also, the recovery in case of aramid nonwovens treated at 70 °C was found to be close to 15%, which was similar to the recovery shown by PET nonwovens compressed at room temperature – about 14% for NW1 and 15% for NW2. Thus, it is reasonable to compare the behavior of NW3 treated at 70 °C (which is way below the T_g of aramid fibers) with NW1/NW2 treated at room temperature (which again,

is way below the T_g of PET fibers). Recovery study was also attempted for room temperature compression (not shown) for aramid nonwovens – but the sample sprung back to its original thickness as soon as it was taken out from the press. It can be speculated that pressure (for a prolonged time) alone is not sufficient to cause any permanent compression set in aramid based needle-punched nonwovens.

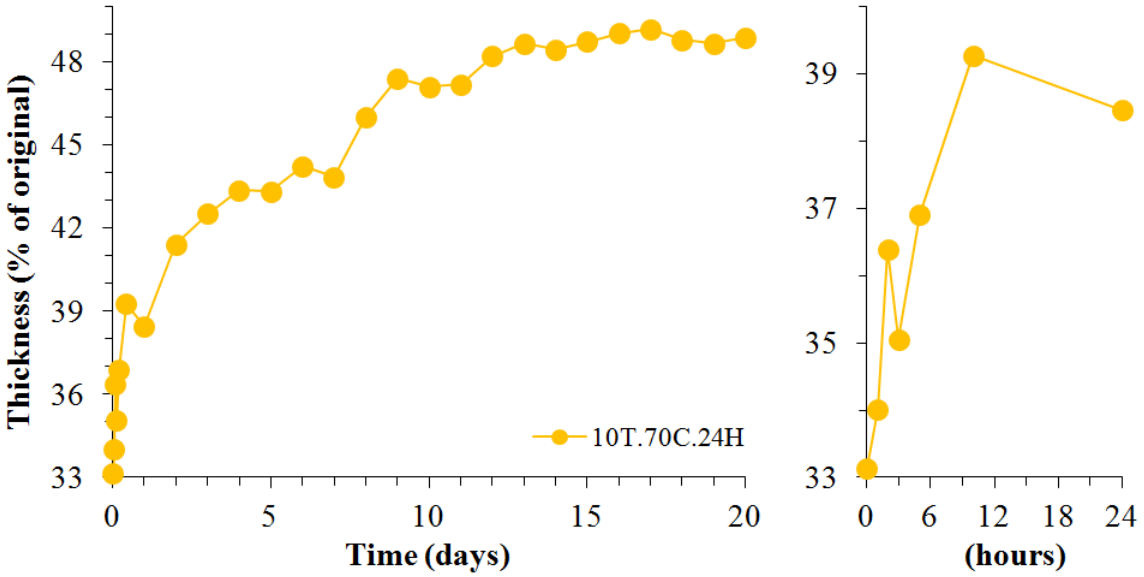

Figure 60: Thickness recovery with time after treatment for NW3 samples over a period of 20 days (left) and for the first day (right). Each data point represents the mean thickness (expressed as a percentage of original thickness of sample) of four distinct regions on a nonwoven fabric of dimension 20 cm x 20 cm.

Table 11 lists the sample name along with the processing conditions, the number of days after which it attained a constant thickness value, the change in percent thickness and the percent thickness at 0^{th} time and on the 20^{th} day. Experiments to determine out-of-plane Poisson's ratio (Section 4.4.2) were performed on the day after which samples had attained a constant thickness value.

Table 11: Important thickness recovery data for treated NW1, NW2 and NW3 samples – mean initial thickness, time to attain an apparently constant thickness value (n days), change in the percentage of original thickness between the time sample is take out of press (t = 0) to the time it takes to attain constant thickness value (t = n), and the percent thickness on 20th day. All thickness values are average of four measurements taken from the 20 cm x 20 cm treated sample.

Sample	**Mean initial thickness** *(mm)*	**Time required to attain constant thickness** *(t = n)*	**Change in % thickness from t = 0 to t = n** *(%)*	**% thickness on 20th day** *(%)*
NW1.10T.070C.24H	4.506	7 days	3.20	30.67
NW1.10T.023C.24H	4.488	10 days	16.31	59.02
NW1.02T.070C.24H	4.444	14 days†	8.24	45.27
NW1.10T.070C.04H	4.562	10 days	5.68	33.93
NW1.10T.023C.04H	4.491	5 days†	14.01	71.06
NW2.10T.070C.24H	5.220	7 days	2.95	32.61
NW2.10T.023C.24H	5.396	10 days	14.92	53.91
NW3.10T.070C.24H	1.352	14 days†	15.31	48.89

† thickness of these samples likely did not reach a steady state value within 20 days, but the increase was much slower after the reported '*n*' number of days

4.4.2 Out-of-plane auxetic response

For the uniaxial tension experiment, thickness values are plotted against specimen length during extension for as-received and treated samples. Figure 61, Figure 62 and Figure 63 show these plots for NW1, NW2 and NW3 respectively. Instantaneous Poisson's ratios based on these data and calculated using Equation (3) are plotted in Figure 64, Figure 65 and Figure 66 respectively. Data are shown until the strains after which specimens failed. All as-received nonwoven samples (PET or aramid based) showed a consistent decrease in thickness with extension (except for the first data point in NW3). The corresponding Poisson's ratios were positive varying between +0.1 and +0.5,

mostly around +0.2 for all of them. It is the point-to-point nature of the calculation of instantaneous Poisson's ratio that leads to these variations.

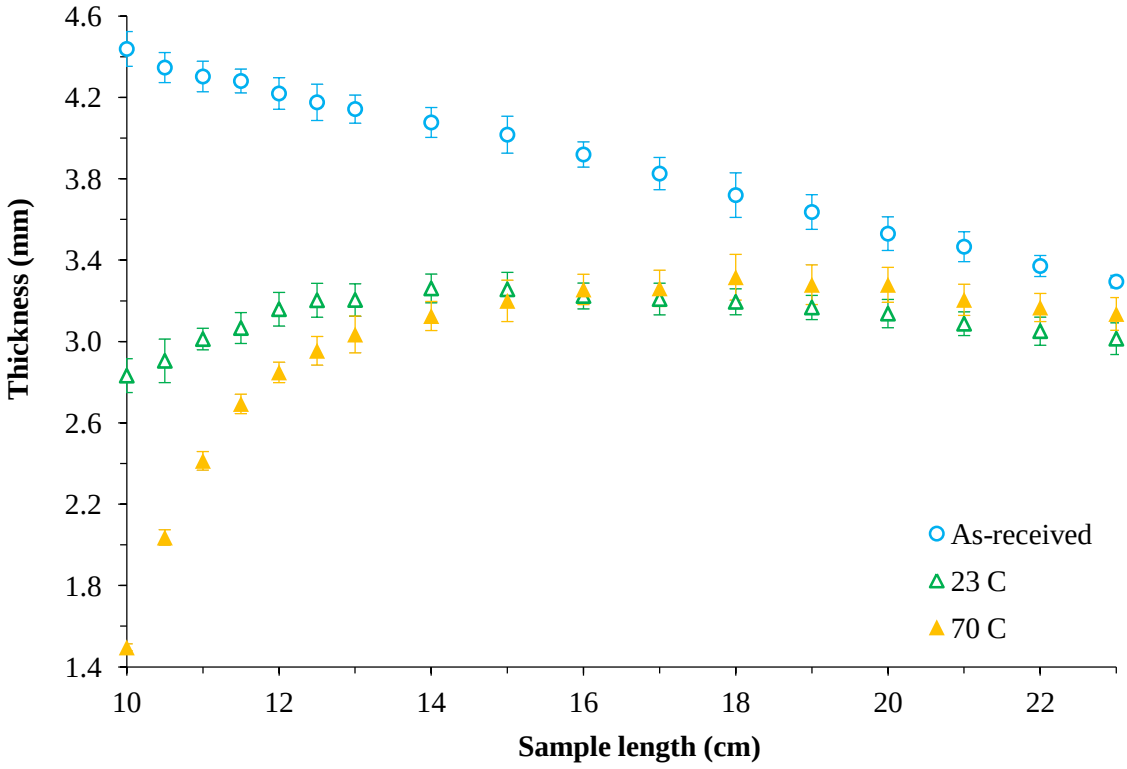

Figure 61: Plots of thickness (mm) versus specimen length (cm) for as-received, compressed and heat compressed NW1 needle-punched nonwoven samples tested along the machine direction. Error bars represent the standard deviation in thickness at each strain level calculated over five specimens of each type (*adapted from [61]).*

Thus, as-received needle-punched nonwoven samples whether composed of PET fibers (differing grammages) or composed of aramid fibers; both showed a consistent decrease in thickness like other common materials. As-received needle-punched nonwovens were therefore not found to be auxetic. One exception to this was the thickness of aramid based as-received NW3 which increased slightly (mean increased

from 1.344 mm to 1.348 mm) for the first 5% strain value and decreased thereafter for all five specimens tested. The corresponding value of Poisson's ratio at 5% strain was –0.06. This initial increase in thickness can be attributed to the slight inclination of the needle-columns in aramid nonwovens (described more in Section 4.5 with µCT images).

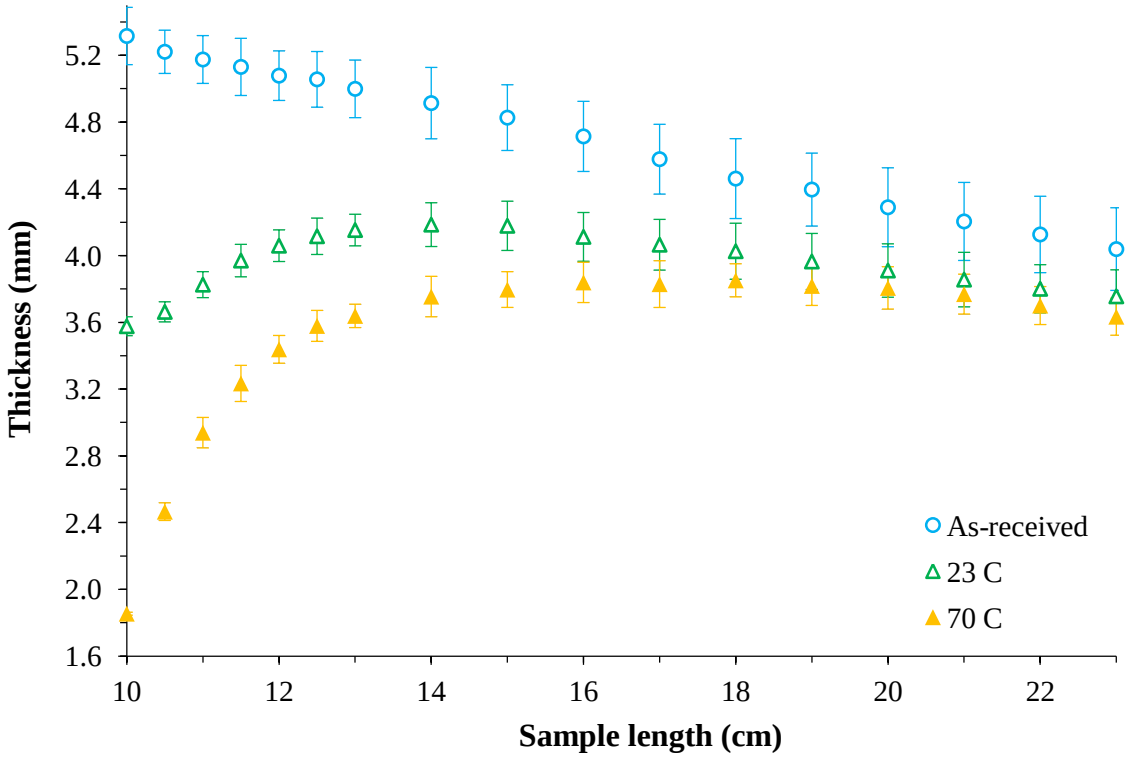

Figure 62: Plots of thickness (mm) versus specimen length (cm) for as-received, compressed and heat compressed NW2 needle-punched nonwoven samples tested along the machine direction. Error bars represent the standard deviation in thickness at each strain level calculated over five specimens of each type (*adapted from [61]).*

Compressed (no heat used) NW1 and NW2 samples were examined for their Poisson's ratio on 10^{th} day after treatment (Table 11). In the case of compressed NW1 and NW2 samples, thickness increase was notable and rapid up to about 40 % strain after

which the thickness began to decrease, rather steadily, until sample failure at around 130 % strain. Instantaneous Poisson's ratio in the initial strain regime was as low as –0.9. The magnitude of negative Poisson's ratio decreased with increasing strain until it reached a positive value after 40 % strain (after the maximum thickness was achieved). NW3 samples retained no permanent compression set when they were treated at room temperature and hence could not be examined for their Poisson's ratio following a no-heat compression.

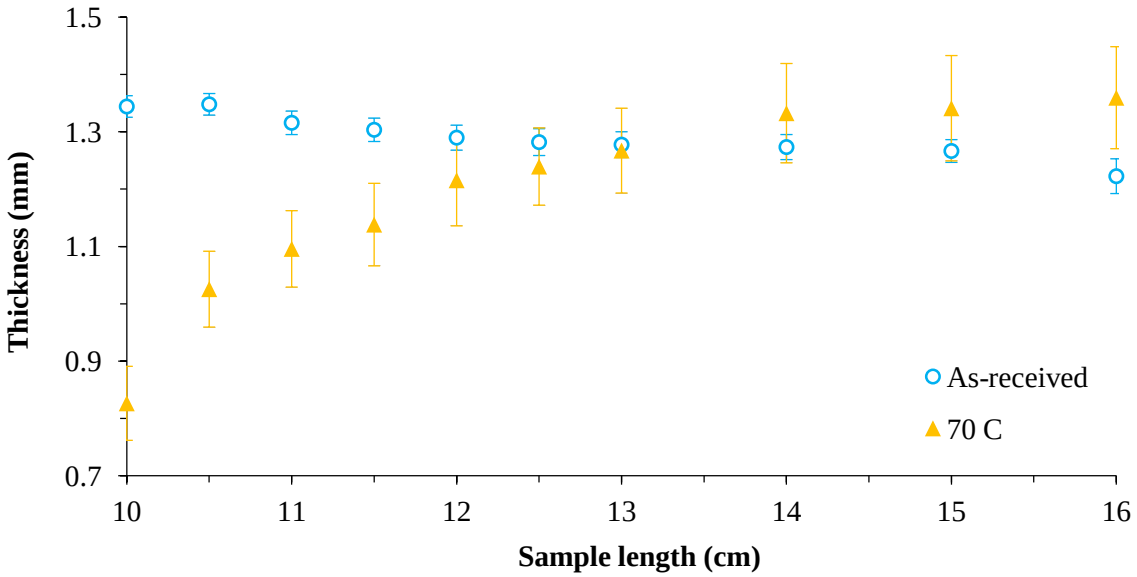

Figure 63: Plots of thickness (mm) versus specimen length (cm) for as-received and heat compressed (at 70 °C) NW3 needle-punched nonwoven samples tested along the machine direction. Error bars represent the standard deviation in thickness at each strain level calculated over five specimens of each type.

In case of heat-compressed fabrics, all nonwovens showed a remarkably steep increase in thickness when stretched, especially in the initial 30 % strain region. Even after 40 % strain, the specimens continued to increase in thickness, but at a slower rate,

until they attained their maximum thickness at approximately 80 % axial strain (NW1 and NW2). Thereafter, the specimen thickness began to decrease at a much slower rate (as compared to the initial increase) until the web structure began to fail. This failure occurs at slightly different strains for different specimens but none below 130% strain for NW1 and NW2. NW3 heat-compressed samples failed after 60% strain, at which point, they achieved their maximum thicknesses. Thus NW3 samples continued to increase in thickness until failure (described more in Section 4.5). For all nonwovens (as-received or treated) web fracture was difficult to observe visually. However, it could be detected by sudden and obvious load drops during strain.

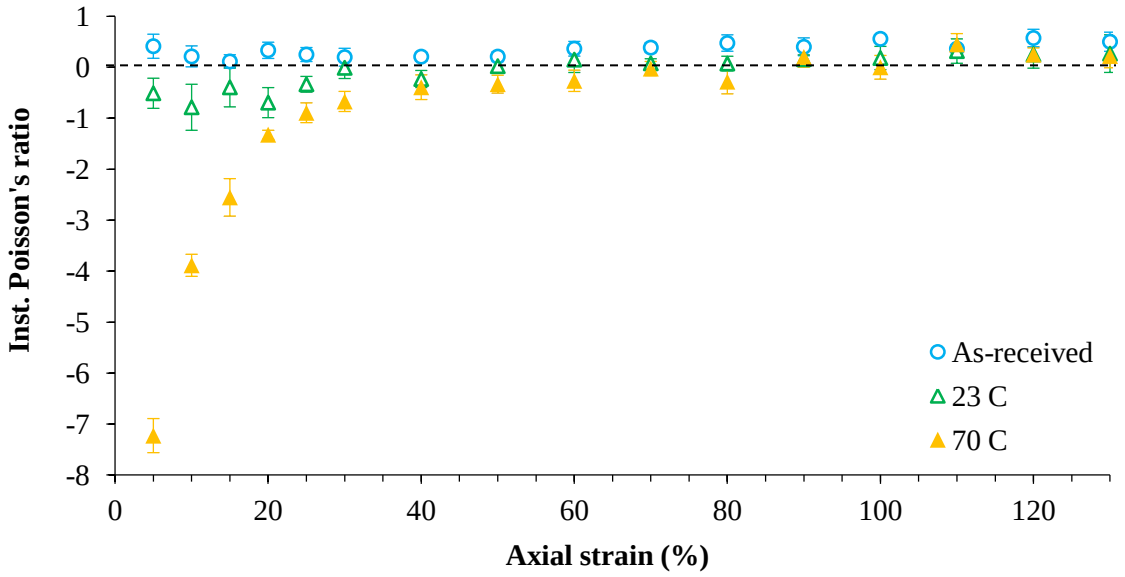

Figure 64: Variation of instantaneous Poisson's ratio with respect to axial strain for as-received, compressed and heat-compressed NW1 needle-punched nonwoven specimens tested along the machine direction. Error bars represent the standard deviation in Poisson's ratio at each data point as calculated over five specimens of each type (*adapted from [61]).*

The instantaneous Poisson's ratio for heat-compressed samples is shown in Figure 64, Figure 65 and Figure 66. It is highly negative at small strain values, again reflecting a rapid increase in thickness. The Poisson's ratio was –4.8 for NW3, –7.2 for NW1 and –6.6 for NW2, corresponding to 5% strain. Similar to compressed NW1 and NW2 samples, the Poisson's ratio for heat-compressed samples became positive after the specimen had attained its maximum thickness (at approximately 80 % strain).

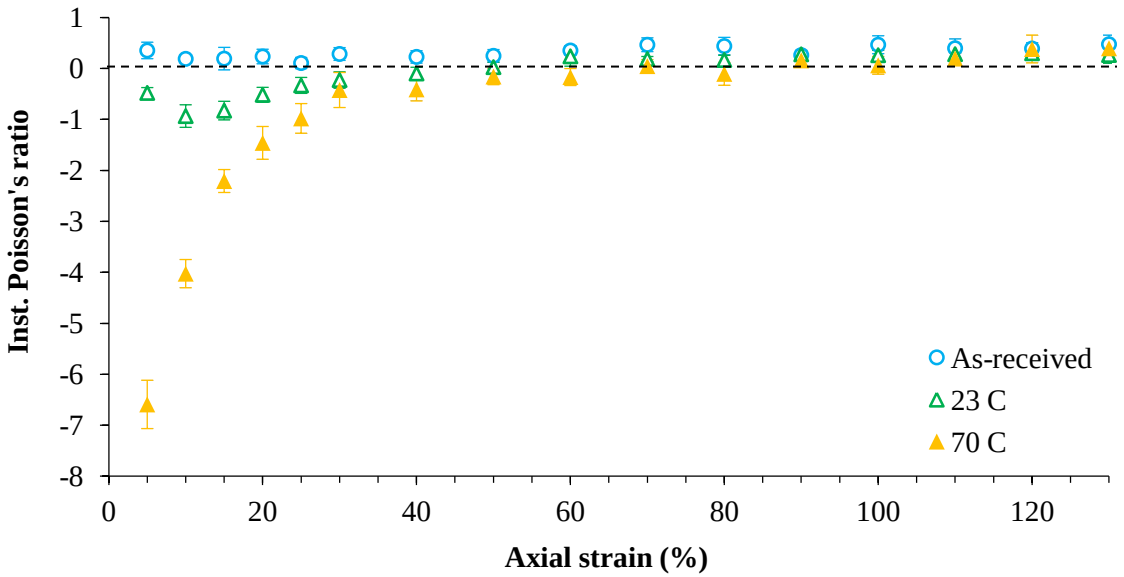

Figure 65: Variation of instantaneous Poisson's ratio with respect to axial strain for as-received, compressed and heat-compressed NW2 needle-punched nonwoven specimens tested along the machine direction. Error bars represent the standard deviation in Poisson's ratio at each data point as calculated over five specimens of each type (*adapted from [61]).*

As a comparison of the two Poisson's ratio calculations (Equation 3 and Equation 4) in the small strain region, data for 'instantaneous' Poisson's ratio of heat-compressed NW1 is as follows with the 'effective' Poisson's ratio in parenthesis: 5% strain, –7.2 (–

7.2); 10% strain, –3.9 (–6.1); 15% strain, –2.6 (–5.3); 20% strain, –1.3 (–4.5). Due to the curvature in the thickness vs. extension curve, the instantaneous Poisson's ratios are generally less negative (implying a diminished auxetic response) for our heat-compressed samples. Since the instantaneous Poisson's ratio captures the response at smaller deformations, we feel that it is the instantaneous Poisson's ratio that most appropriately describes the out-of-plane mechanical response in these systems.

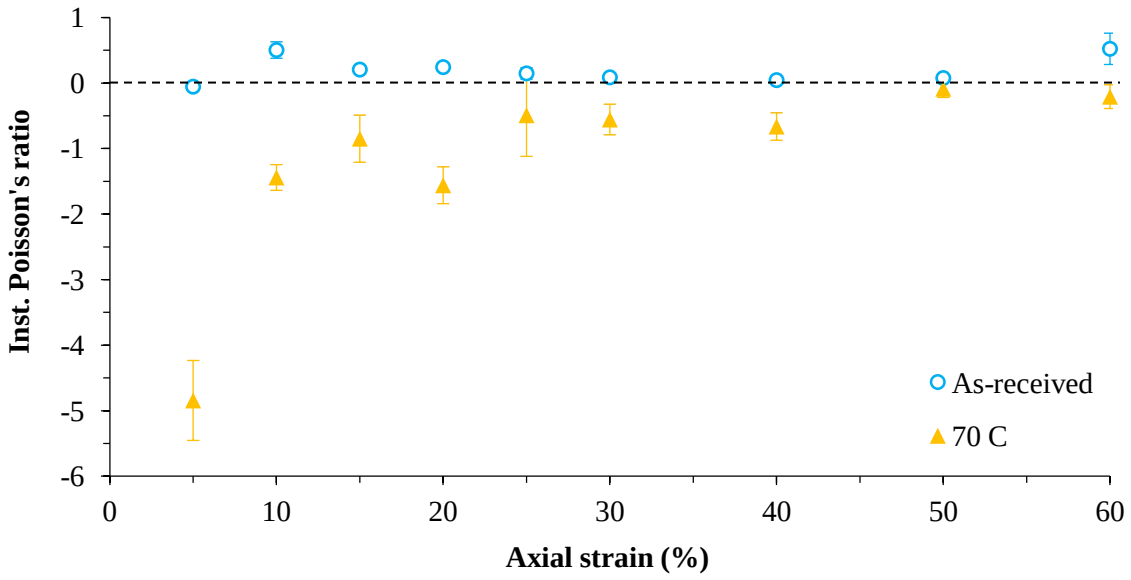

Figure 66: Variation of instantaneous Poisson's ratio with respect to axial strain for as-received and heat-compressed (70 °C) NW3 needle-punched nonwoven specimens tested along the machine direction. Error bars represent the standard deviation in Poisson's ratio at each data point as calculated over five specimens of each type.

Heat-compressed nonwovens showed a large auxetic response compared to that of the compressed nonwovens. Heating at a temperature near and above the glass transition renders the fibers more flexible allowing for increased bending, densification, and reconfiguration of fiber-fiber contacts. Subsequent cooling while the fabric is still under

compression acts to lock-in the effected structural changes. Greater auxetic response in heat-compressed samples is partly due to the fact that, after processing, these samples recover less thickness compared to compressed samples (see Table 11). Heat-compressed samples, therefore, have a greater capacity for thickness recovery when axial strain is applied. As will be described below, we feel that the higher degree of inclination of fiber columns and the increased number of fiber-fiber contacts in the heat-compressed fabrics both play a role in producing a more rapid thickness increase in subsequent axial strain experiments.

So far, all experiments showed the effect of straining along the machine direction of a nonwoven. For completeness, a series of same experiments was performed in cross-direction as well for PET nonwoven samples. In Figure 67 below, thickness versus extension and instantaneous Poisson's ratio versus axial strain has been plotted for as-received and heat-compressed NW1 and NW2 and tested along CD. It can be easily seen that the qualitative auxetic behavior for testing along CD is very similar to MD. This was expected, as the compression of nonwovens can tilt/buckle the fiber column in any direction. The mechanism of thickness increase (explained in detail later), that is likely caused by fibers pulling on the entanglements with these columns, can therefore be effected by a fiber lying in any direction.

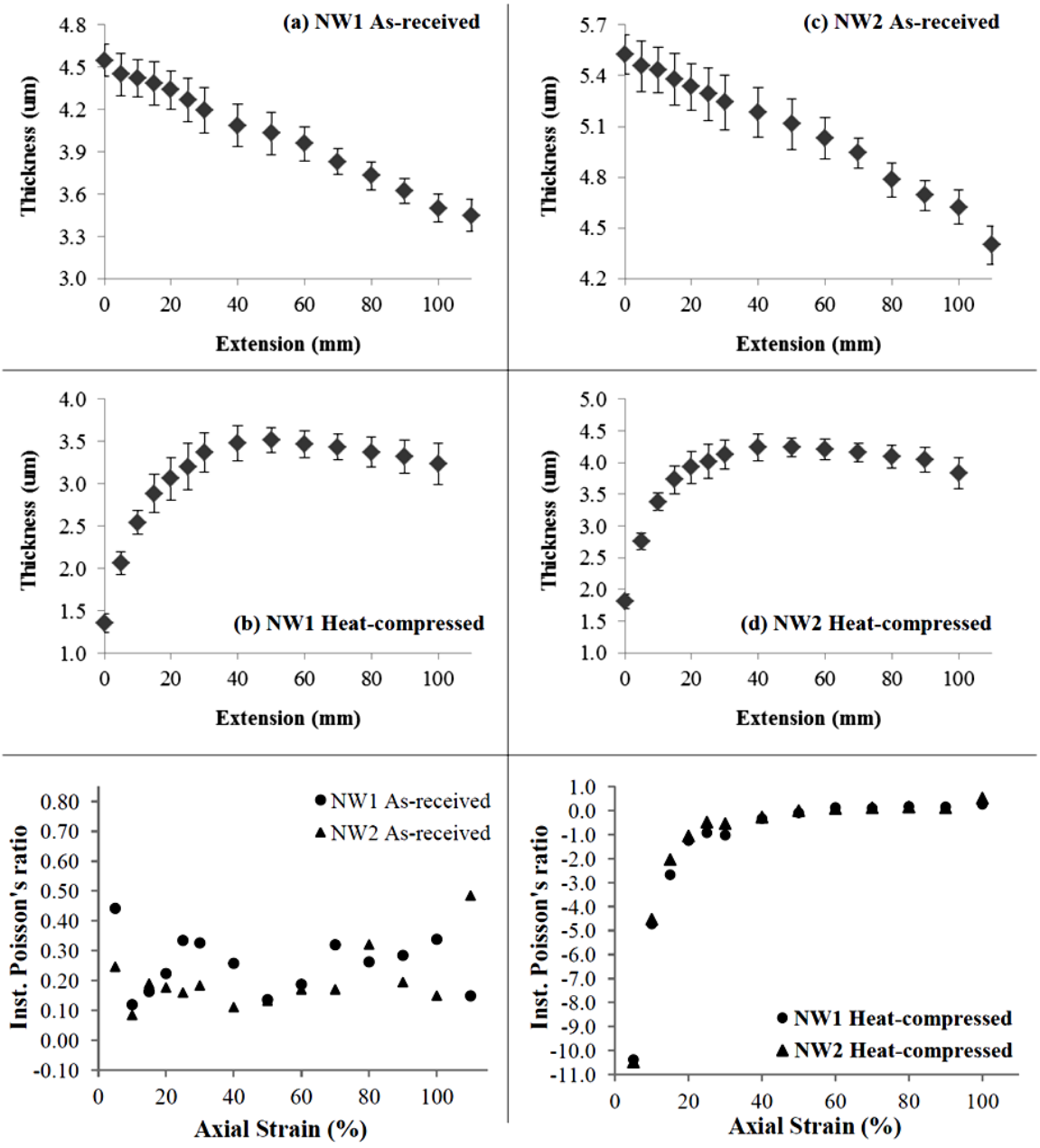

Figure 67: Cross-direction testing – plots of thickness (mm) versus extension (mm) and instantaneous Poisson's ratio versus axial strain for as-received and heat compressed NW1 and NW2 needle-punched nonwoven samples. Error bars represent the standard deviation in thickness at each strain level calculated over five specimens of each type.

4.4.3 In-plane Poisson's ratio values

It should also be mentioned that all of these nonwovens, as-received and treated, showed a conventional decrease in ‘width’ on axial extension, thus exhibiting a positive in-plane Poisson's ratio in agreement with previous reports [127, 142–146]. We found these effective in-plane Poisson's ratios to range (for the most part) from +0.2 to +0.6 for NW1 specimens, treated and untreated (Equation 4). These in-plane Poisson's ratios were calculated at the same strain values as those described above – by optically measuring the distance between an orthogonal set of small ink dots (two along the width and two along the length) marked on the face of the specimen. A digital camera was used to capture images at each strain level. ImageJ, an image processing software provided by National Institutes of Health (Maryland, USA), was used to measure the strains digitally. Figure 68 shows instantaneous and effective in-plane Poisson's ratio values calculated for compressed and heat-compressed NW1 specimens. Instantaneous values of in-plane Poisson's ratio showed no regular trend but remained positive all along.

Large error bars are mostly due to the smearing of ink marks during the non-uniform deformation of the web structure. The nonwoven web structure is quite heterogeneous which can cause non-uniformity in stresses especially at high strains. Since the out-of-plane Poisson’s ratio is negative and the in-plane Poisson’s ratio is positive, these fabrics should be considered as partially auxetic as defined by Wojciechowski et al. [3].

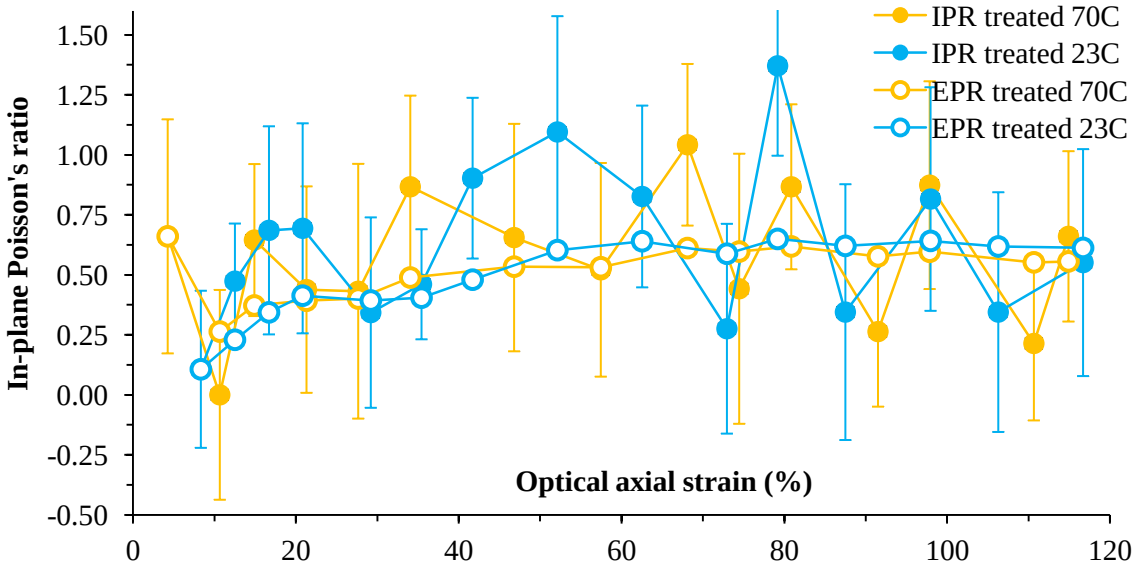

Figure 68: Instantaneous (IPR) and effective (EPR) in-plane Poisson's ratio values for compressed and heat-compressed NW1 specimens calculated from images captured by a digital camera and using ImageJ to calculate strains. Error bars represent the standard deviation in Poisson's ratio at each data point as calculated over five specimens of each type

4.4.4 Reversibility of thickness change

Mean thickness of the specimen (for three points) at 0% strain level and at final strain level (n %) expressed as a percentage change from original specimen thickness is shown in Figure 69. This experiment was only performed on heat-compressed NW1 samples (please refer back to Section 4.3.4 and Figure 55 for experimental details). Results indicated that the specimens returned close to their original thickness (i.e. % thickness change close to zero) when the strain applied was low. This was an indication of the reversibility of thickness change. Specimens strained at 1 % or 2 % strain showed remarkable reversibility of thickness change. For higher strains, the reversibility decreased regularly and was found to be lowest for 10 % strains. Specimens stretched at 1

% or 2 % axial strain increased in thickness by up to 3-10 % at peak strain value and returned to within 1 % of their original thickness upon strain removal. However, specimens stretched to 10 % axial strain attained thickness increase of up to 90 % but could recover only about 40-50 % thickness increase on strain removal.

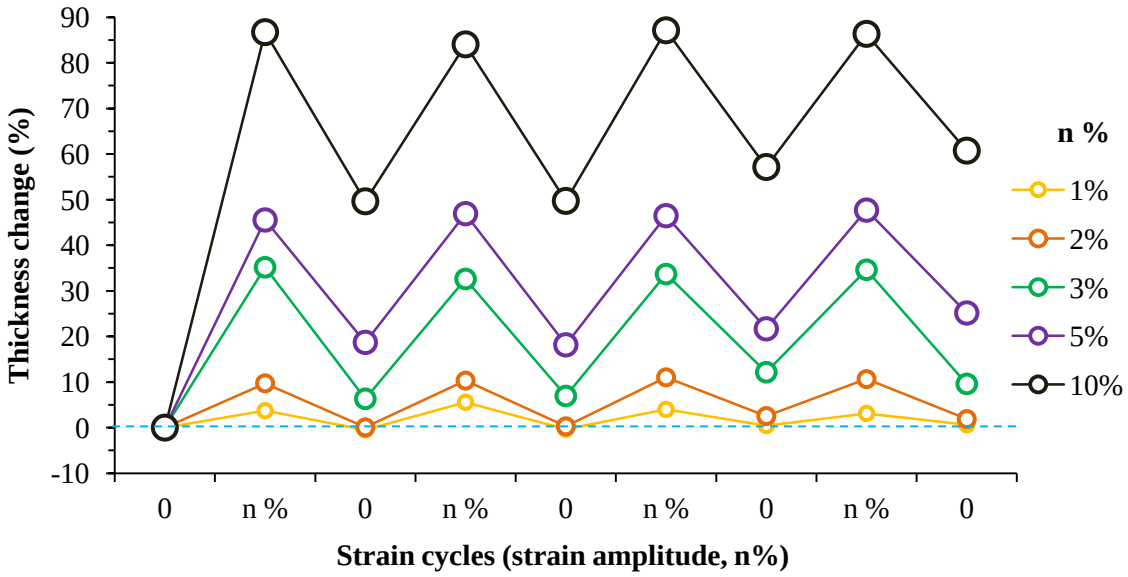

Figure 69: Percentage of thickness change with strain applied (n %, n = 1, 2, 3, 5 and 10) and strain removal over four cycles for a heat-compressed NW1 specimen. Each data point was calculated from the mean of thickness measurement taken at three points on a specimen.

Cyclic loading in this experiment also exposed a remarkable property of auxetic response in these materials. At low strains, the thickness increase (upon stretching) and reversibility (on load removal) was found to be consistent over four cycles. But at higher strains, thickness increase seemed consistent but the reversibility kept decreasing. This observation can be explained by understanding the reversible and irreversible parts of the mechanism of thickness increase in these nonwovens (Section 4.5).

4.4.5 Effect of fiber length on entanglements and thickness recovery

Thickness of each of the marked region on a strip of as-received and heat-compressed NW1 has been shown in Figure 70 and Figure 71 respectively (please refer back to 4.3.7 and Figure 57 for experimental details). For each region, thickness was measured each time the strip was cut at the center.

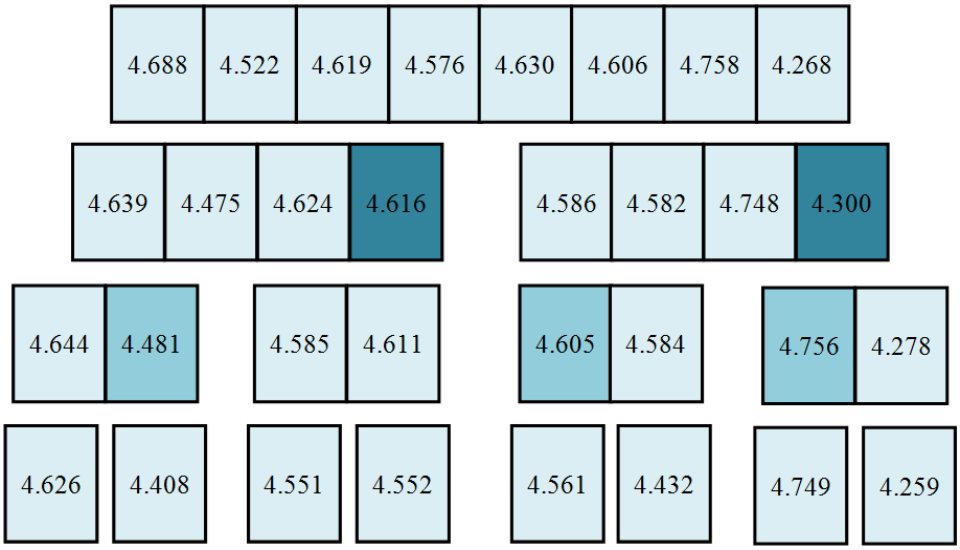

Figure 70: Thickness (in mm) at each of the eight marked region of an as-received NW1 strip (16 cm long, 2.5 cm wide) before cutting and after it was cut into half repeatedly at the center until individual eight pieces were obtained. Darker and darkest shades of blue indicate a thickness difference of 5-20 μm and more than 20 μm respectively.

Fibers in a needle-punched fabric can be a part of both the needle-column and the matrix. In NW1 and NW2 the fiber length (3 inch) is much greater than the column spacing (in the order of 1 mm) suggesting that a fiber can easily be a part of more than one column. When the fabric is cut, the entanglements between the column and the matrix and between two points within the matrix are released. Thickness was visually

observed to increase as the strip was cut into shorter segments. However, because the micrometer exerts a considerable pressure of 20 kPa, measured thickness was lower than visually observed and often found to be lower on a second measurement of the same region. An increase in thickness measured by the micrometer despite the pressure should however mean a certain increase as a result of cutting.

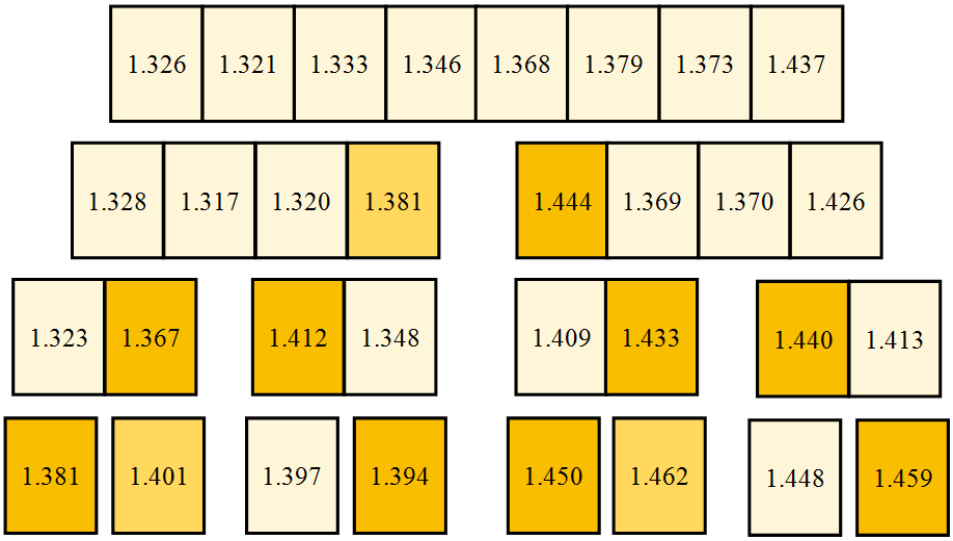

Figure 71: Thickness (in mm) at each of the eight marked region of a heat-compressed NW1 strip (16 cm long, 2.5 cm wide) before cutting and after it was cut into half repeatedly at the center until individual eight pieces were obtained. Darker and darkest shades of orange indicate a thickness difference of 5-40 μm and more than 40 μm respectively.

Figure 70 shows the thickness of different regions of an as-received strip of NW1. Dark shades of blue indicate the regions where a certain increase in thickness was observed (darker shade denotes a change in thickness between + 5-20 μm while darkest shade denotes a change in thickness of more than + 20 μm). Note that the thickness decreased for smaller pieces probably because of the pressure applied by the micrometer

(visually, these were observed to increase in thickness upon cutting). Figure 71 shows the same readings for a heat-compressed NW1 strip. Dark shades of orange indicate the regions where a certain increase in thickness was observed (darker shade denotes a change in thickness between + 5-40 μm while darkest shade denotes a change in thickness of more than + 40 μm). The increase in thickness upon cutting was much more apparent in treated samples. Same experiment was also performed on NW2 as-received and heat-compressed samples and very similar results (see Figure 72) were obtained.

It will be seen from μCT imaging that the needle columns are perpendicular to the plane of the fabric in as-received nonwovens (NW1 and NW2) and become buckled or highly inclined upon treatment. This will be explained in detail in the following section on mechanism. It is our hypothesis that there are fibers entangled between the columns and the matrix. When heat-compressed nonwoven was cut, these fiber entanglements were released causing the columns to rotate back to their vertical positions and causing the thickness to increase. In as-received nonwoven, because the columns are already vertical, any increase in thickness (that is smaller than that in a treated nonwoven) can probably be attributed to cutting of fibers that were tying the web down in thickness due to their entanglements within the matrix or with the columns.

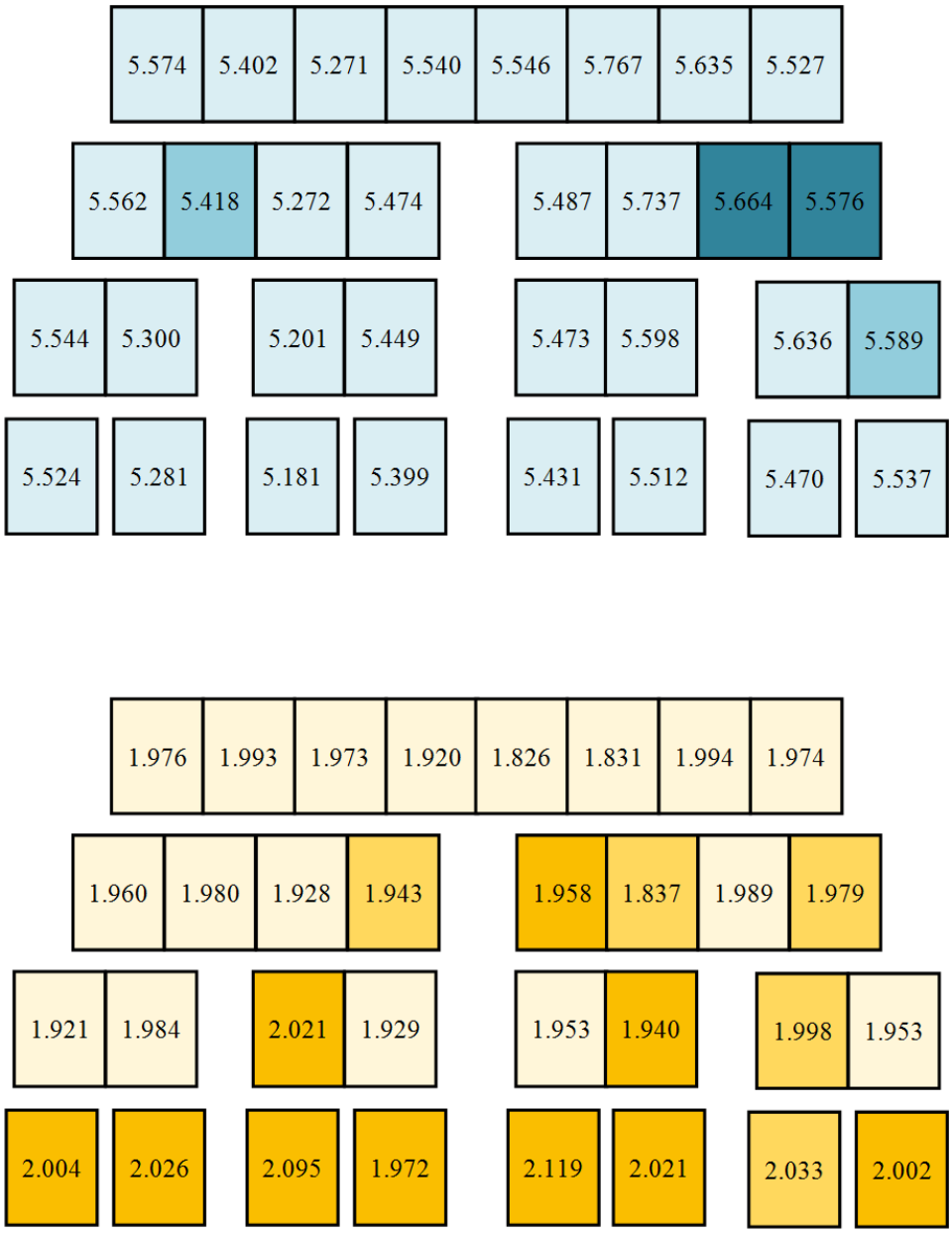

Figure 72: Thickness (in mm) at each of the eight marked region of a compressed (above, blue) and heat-compressed (below, blue) NW2 strip (16 cm long, 2.5 cm wide) before cutting and after it was cut into half repeatedly at the center until individual eight pieces were obtained. Darker and darkest shades of blue indicate a thickness difference of 5-20 μm and more than 20 μm respectively. Darker and darkest shades of orange indicate a thickness difference of 5-40 μm and more than 40 μm respectively.

4.4.6 Preliminary results for heat-compression at 100 °C

To test the auxetic response at a temperature higher than the T_g of PET, a temperature of 100 °C was also used for heat-compression treatment of our NW1 samples. The treatment protocol was the same – 10 tons of force for a period of 24 hours (20 hours of heating and 4 hours of cooling down) – but at an elevated temperature of 100 °C.

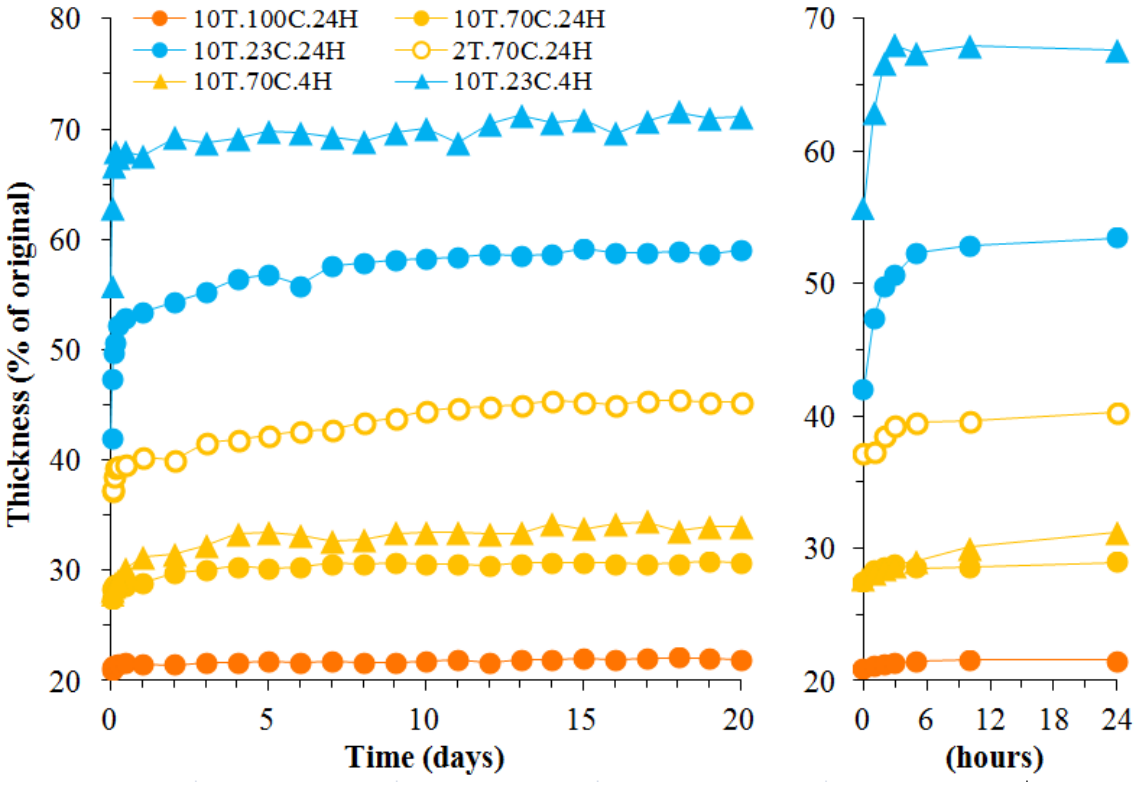

Figure 73: Thickness recovery with time after heat-compression at 100 °C for NW1 samples over a period of 20 days (left) and for the first day (right) (burnt orange lines). NW1 samples treated under other conditions have also been shown for comparison.

Thickness recovery with time was studied over a period of 20 days. The sample had a mean as-received thickness of 4.524 mm and a mean thickness of 0.951 mm as soon as it was taken out from the press. The sample attained near constant thickness in as quickly as a few hours (5 hours). Between taking out from the press and 5 hours, the sample recovered only 0.48 % of its original thickness. After 5 hours and up to 20 days the thickness remained constant, the final value at 20^{th} day being 0.993 mm. This showed that the compression set was achieved quickly and was very permanent when the NW1 was treated at 100 °C (above T_g of PET fibers). Thickness recovery plot for heat-compressed (100 °C) NW1 has been shown (Figure 73) along with other NW1 samples to aid in comparison.

Similarly, change in thickness with axial strain and out-of-plane Poisson's ratio was measured under the same experimental conditions as other nonwovens. The plots of thickness versus sample length and instantaneous Poisson's ratio versus axial strain are shown in Figure 74 and Figure 75 respectively, along with other NW1 samples for comparison. It was seen that the samples heat-compressed at 100 °C showed a thickness increase curve similar to those of heat-compressed (70 °C) samples, but the compression set was greater and the initial increase in thickness was more rapid. The Poisson's ratio value at 5 % strain was found to be -11.9 (see Figure 75). Thickness increase was initially rapid, reached a maximum value at 80 % axial strain and then decreased slightly until sample failure after 130 % strain.

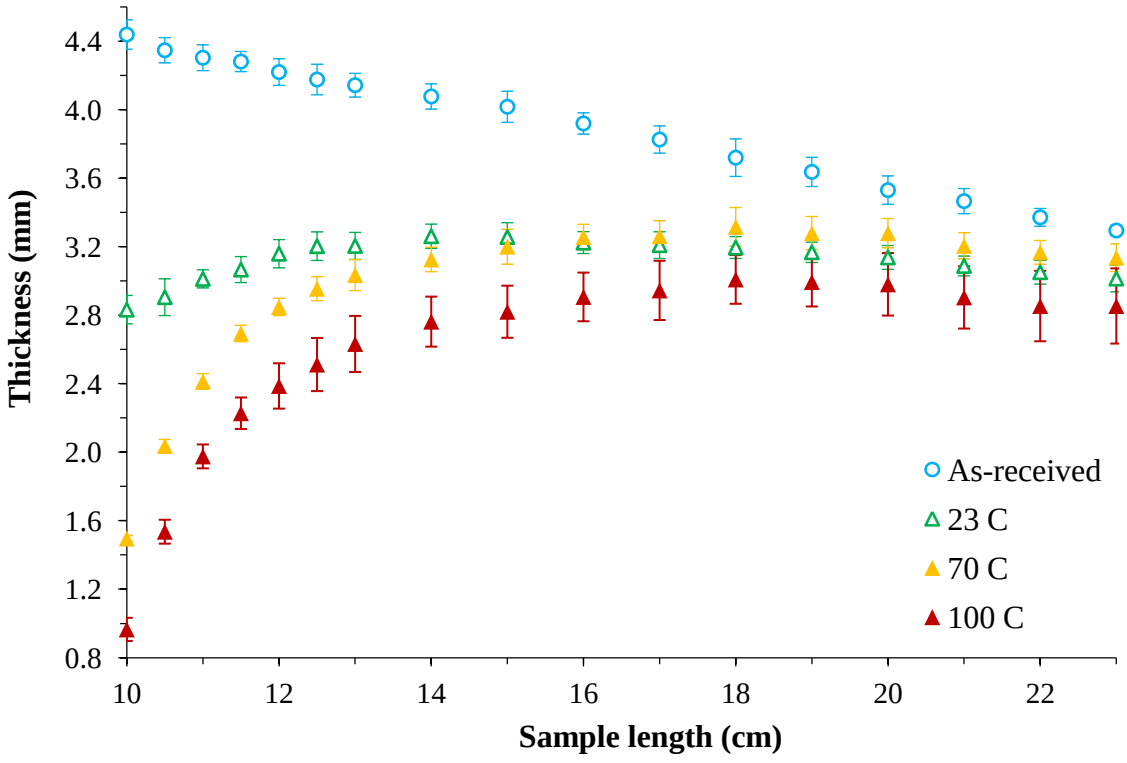

Figure 74: Plots of thickness (mm) versus specimen length (cm) for as-received, compressed and heat compressed (70 °C and 100 °C) NW1 needle-punched nonwoven samples tested along the machine direction. Error bars represent the standard deviation in thickness at each strain level calculated over five specimens of each type.

A temperature higher than T_g resulted in a more permanent compression set and likely provided a greater margin for thickness extension upon extension, thus resulting in a faster auxetic response in the initial strain region. A more permanent compression set was a favorable result for commercial applications.

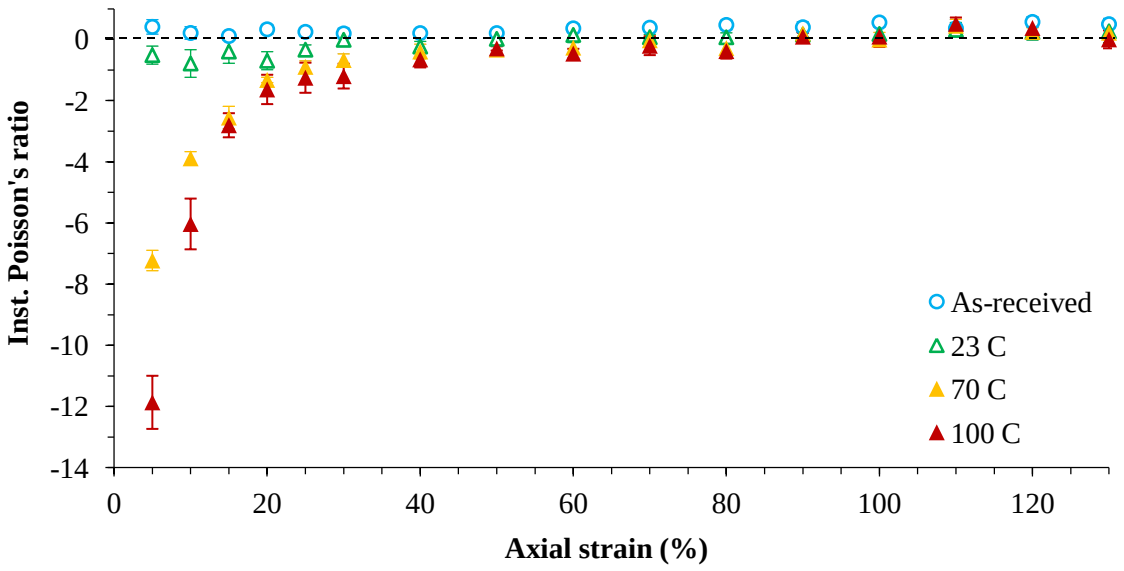

Figure 75: Variation of instantaneous Poisson's ratio with respect to axial strain for as-received, compressed and heat-compressed (70 °C and 100 °C) NW1 needle-punched nonwoven specimens tested along the machine direction. Error bars represent the standard deviation in Poisson's ratio at each data point as calculated over five specimens of each type.

4.5 Mechanism of auxetic response in nonwovens

To gain insight into the fiber arrangement and other structural details of these nonwovens, the imaging technique of µCT was employed. Figure 76 shows µCT images of as-received and heat-compressed (70 °C) nonwoven sample, NW1. Figure 77 shows µCT images of compressed (no heat used) nonwoven sample, NW1. Note that the thickness of NW1 after taking out from the press was about 2.8 mm for compressed samples and about 1.4 mm for heat compressed samples, while the as-received thickness was about 4.5 mm. Because these nonwovens are needle-punched, several vertically aligned (along the thickness direction) columns of fibers were observed in the as-received samples reflecting the fiber orienting effect of needling (Figure 76b). The barbs on the

entering needle catch fibers and transfer them from the top surface to the bottom of the fabric creating bundles of oriented fibers [137]. Figure 78 shows that in the as-received state, the aramid needle-punched nonwovens have inclined columns. This is due to the higher speed of movement of batt (when compared to PET nonwovens) during the needling process.

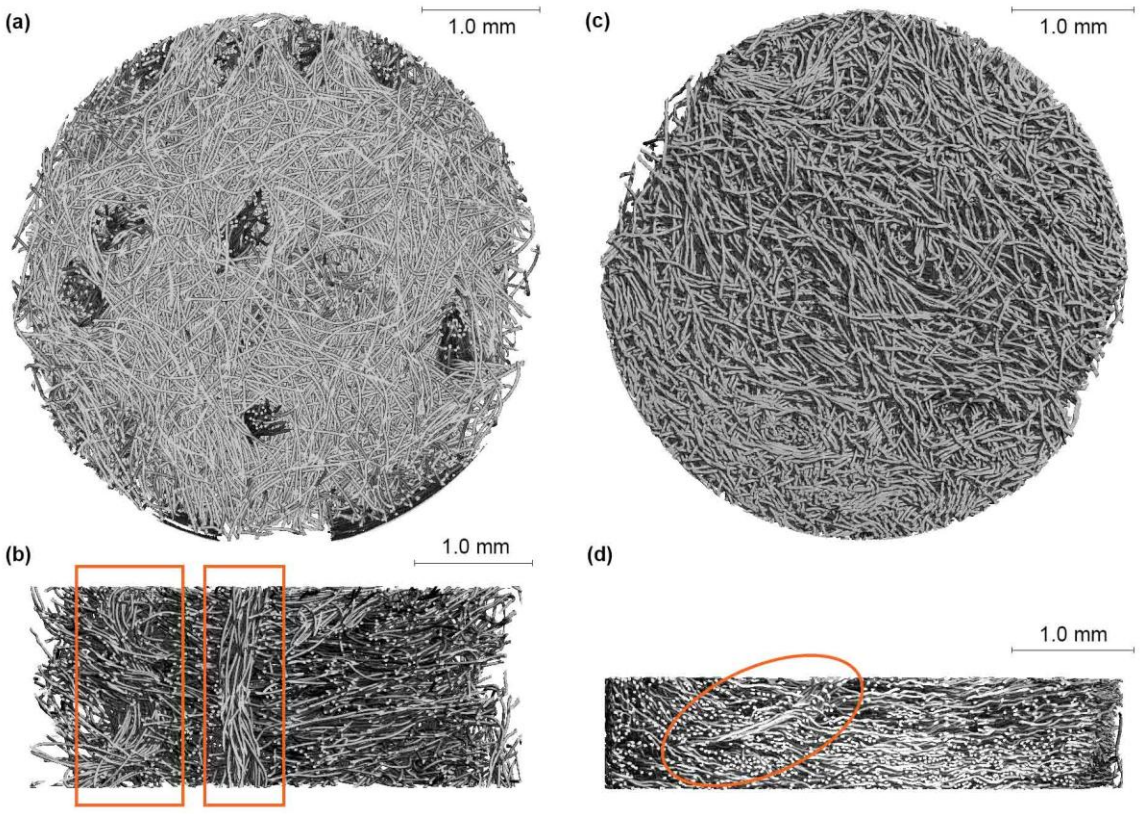

Figure 76: µCT images of as-received and heat-compressed (70 °C) NW1. (a) NW1 as-received sample top-view (b) NW1 as-received section view (c) NW1 heat-compressed sample top view and (d) NW1 heat-compressed sample section view. The section chosen is from a cut-plane normal to the nonwoven surface and near diameter that shows salient structural features (*adapted from [61]).* Enclosed areas in (b, d) show fiber columns/bundles.

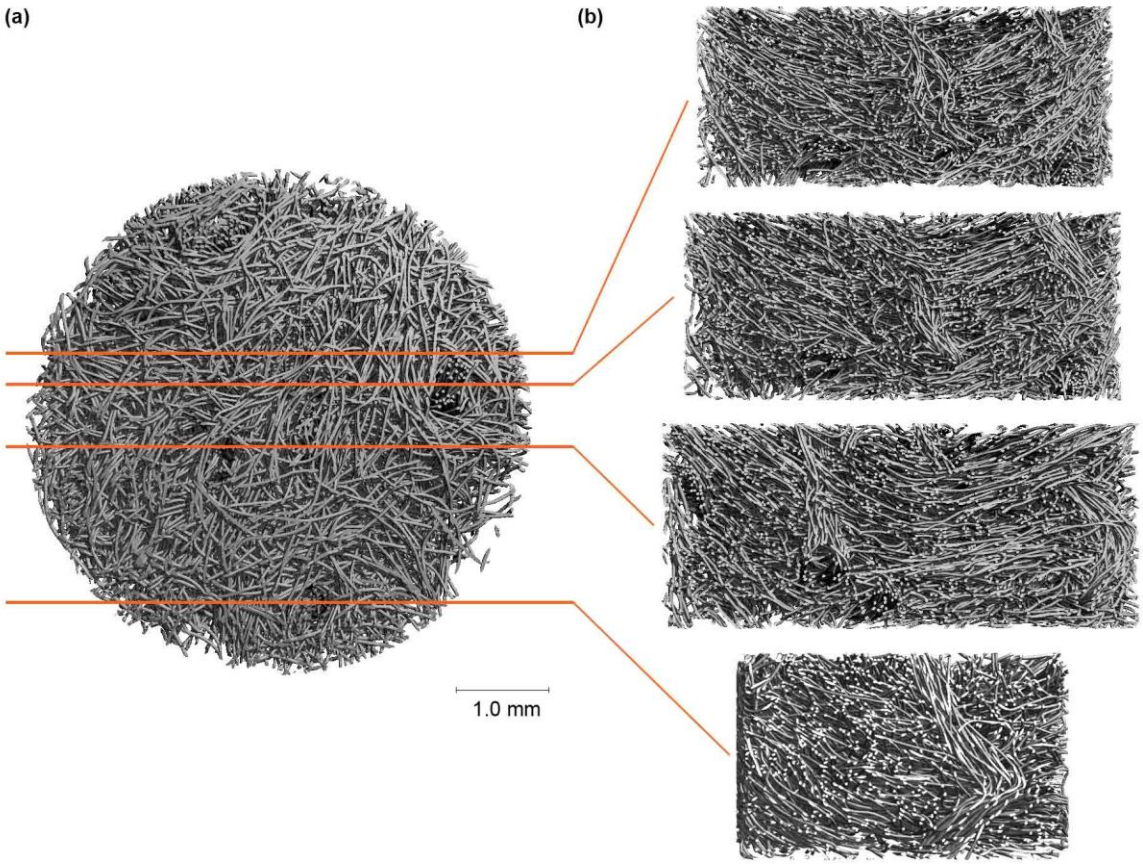

Figure 77: µCT images of compressed NW1 (a) top-view (b) different section views (not to scale) obtained from a cut-plane normal to the nonwoven surface passing through lines shown in (a) (*adapted from [61]*)

The vertical fiber columns apparent in the 'as received' fabric were not found in any of our treated nonwovens. An image of a compressed sample (Figure 77b) shows the presence of inclined columns and one buckled column. In the case of heat-compressed samples, inclined columns were less apparent in the µCT images but a few were seen, such as that in Figure 76d. These fiber columns appeared to be highly tilted or embedded in the matrix likely due to the combined effect of heat and large compressive forces. One can anticipate that there might also be columns that are splayed or bowed under these

conditions. Some of these features (inclined and buckled) were corroborated by optical images taken using a handheld Dino-Lite Pro microscope (see Figure 79). It is thought that when compressed or heat-compressed samples are subjected to uniaxial strain, the tilted/buckled fiber columns can rotate back toward the original vertical orientation or (for buckled columns) increase the angle at the buckling point, resulting in an increase in thickness. This compression-induced column tilting and buckling is a key structural transformation during the compression protocol in these needle-punched nonwovens which is likely contributing to the observed auxetic behavior.

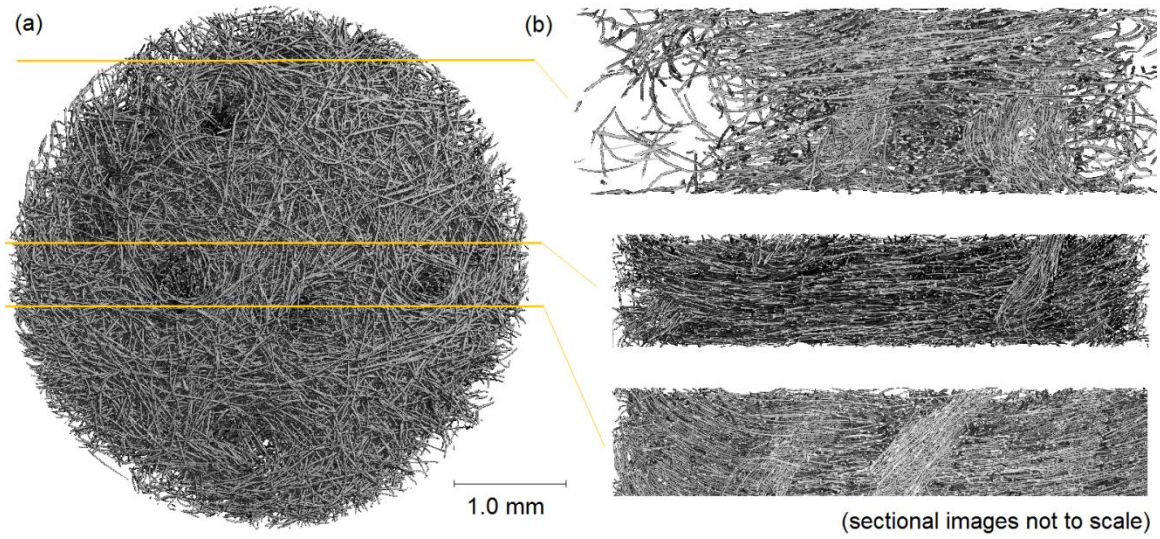

Figure 78: µCT images of as-received NW3 (a) top-view (b) different section views (not to scale) obtained from a cut-plane normal to the nonwoven surface passing through lines shown in (a). Notice inclined fiber columns in the as-received state.

An illustration for a possible mechanism for thickness increase on extension (based on µCT images) is shown in Figure 81. We believe that the interplay between columns and connecting fibers analogous to the microstructure of Evans's expanded

polytetrafluoroethylene (PTFE) [40] might offer mechanistic insight into the auxetic response exhibited by our nonwovens. In the case of expanded PTFE, rigid oblong nodes are connected to each other through several fibrils. After a preliminary compression and expansion conditioning, the long axes of the nodes are roughly parallel to the fibril orientation. When tension is applied, the fibrils become taut causing first, transverse displacement of nodes, and then, further rotation of nodes resulting in more transverse expansion.

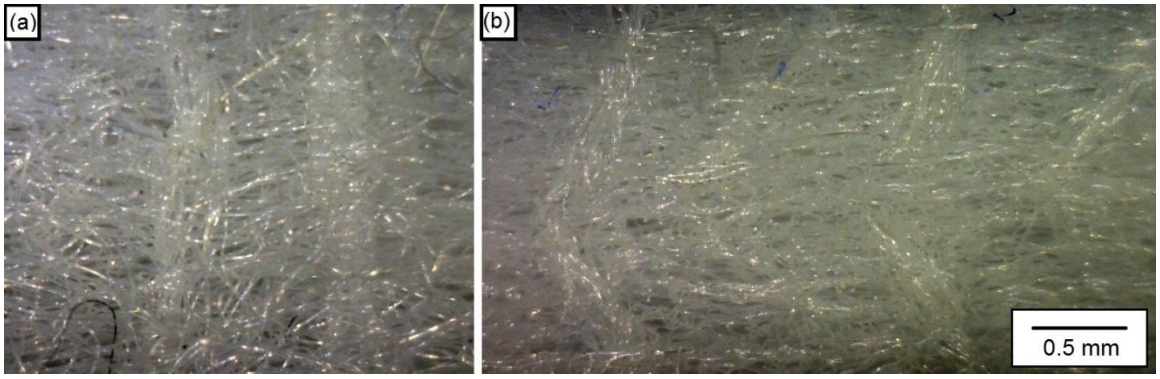

Figure 79: DinoLite microscope images of side-view (thickness view) of (a) as-received NW1 showing vertical fiber columns and (b) compressed NW1 showing chevron shaped buckled fiber columns. Image contrast has been computationally enhanced.

As described above, as-received needle-punched nonwoven samples contain through thickness fiber bundles oriented perpendicular to the surface. This structure is shown with the help of a cartoon in Figure 81. Some planar fibers are shown in blue and the needle columns are shown in black. The space between the columns is occupied by fibers oriented mostly in the plane of the batt (a few are shown in blue). Since our staple fiber length is three inches and the approximate average distance between columns is a

few millimeters as judged from µCT images, it can be assumed that there will be a number of fibers that are part of more than one column contributing to the inter-columnar connectivity of the fiber network. These inter-columnar fibers are flexible and not fully extended initially. Due to the nature of the needle punching operation, fiber entanglements are much more prominent in the top surface (the surface on which the needle first penetrates); which will have a higher density of inter-columnar fibers. The bottom surface is characterized by fiber loops and hanging-fibers that have been deposited there by the retreating needle (Figure 80).

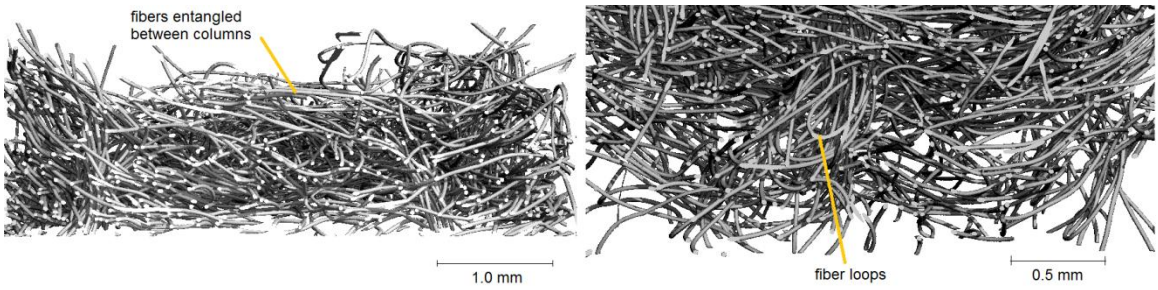

Figure 80: µCT images of the top and bottom surface of an as-received NW1 sample showing fiber entanglements between two columns on the top (left) and fiber loops at the bottom surface (right)

Besides the inter-columnar fibers, entanglements between other fibers can also act as connections between columns, especially since the fibers are crimped. There are entanglements among the fibers that lie in the plane of the batt and also entanglements between the in-plane fibers and the fibers that are part of a column. Due to the direction of travel of the batt during needling, there is a small uniform tilt in the initial column orientation (Figure 81, top). When compressed, these fiber columns assume a buckled or

an even greater inclination (Figure 81, middle). When these treated samples are subsequently strained, it is the inter-columnar fibers that pull the columns back towards their original near vertical orientation. Because the entanglements are mostly in the top part of the fabric, any applied strain engages to pull the top part of the buckled/tilted columns first. This moment of force acting on the top of the fiber columns results in the rotation of the column back towards its original vertical orientation. Figure 81 (bottom) shows top face fibers in blue that are instrumental in reorienting the columns. Since the columns are not highly rigid (and some are likely severely deformed by the processing conditions), they may never fully return to their original near vertical state.

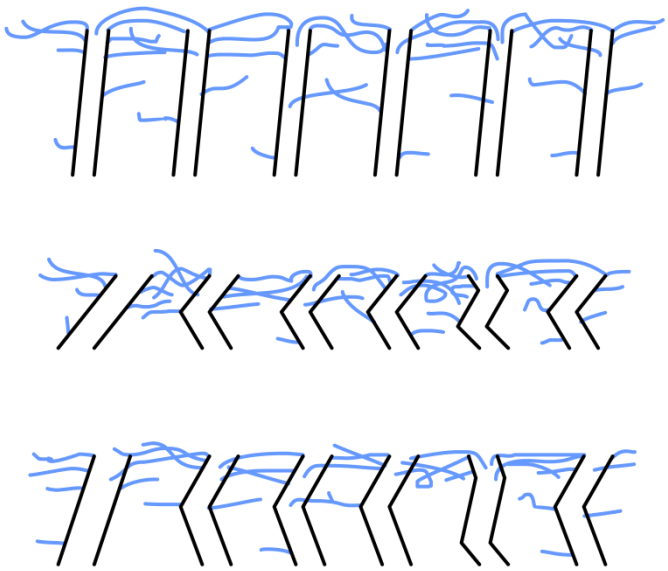

Figure 81: Mechanistic illustration for auxetic response in treated nonwovens. As-received sample showing through-thickness needle columns of fibers bounded by black lines (top); compression induced tilting/buckling of columns (middle); column reorientation due to tensional force experienced by inter-columnar fibers shown in blue (bottom).

The opening of chevron shaped buckled columns was supported by videos taken by DinoLite microscope during uniaxial deformation (stretch) of a compressed NW1 sample. Snapshots of the recorded video where particular buckled columns could be tracked were taken and the angle of the chevron shaped was measured digitally in ImageJ software. These snapshots along with angle measurements have been shown in Figure 82. The opening up of the buckled column angles was clearly observed. As the sample was strained from 0 % to 10 % strain, the angle of a particular buckled column increased from about 75° to 87° while the angle of another buckled column increased from 81° to 92° when it the strain increased from 10 % to 20 %.

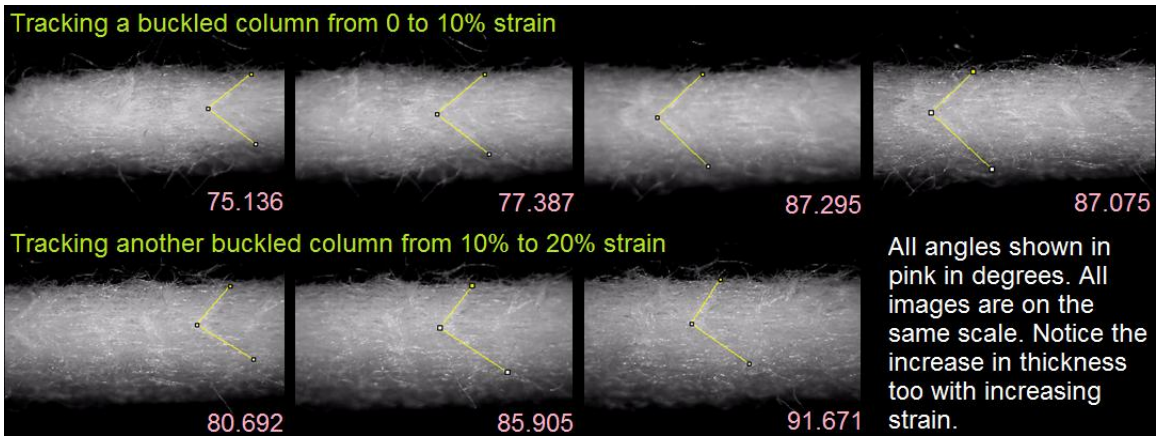

Figure 82: Snapshots of a video taken by a DinoLite Pro microscope of the side-view (thickness view) during straining of a compressed NW1 sample. Snapshots show opening up of buckled columns with increasing strain thought to be likely contributing to the thickness increase.

µCT scans were also performed for NW1 treated samples that were stretched to 20 % and 80 % axial strains. Note that these samples attained maximum thickness at 80 % strains. Figure 83b, at 20% strain, shows some bundles of fibers embedded in the

matrix or highly inclined to the vertical. A single continuous column tilted at large angle to the vertical could not be isolated. Figure 83a at 80 % strain however, shows some columns that could have rotated back (to make smaller angles to the vertical) on application of a large strain – supporting our hypothesis of rotating columns causing the thickness increase. One limitation with these images was that since the µCT instrumentation could not scan nonwoven samples *in situ* while in tension (due to small size of the sample tubes), specimens first had to be strained in the Instron, taken out and then cut before they could be scanned. This caused the specimen to recover some of the thickness upon strain release from the Instron and then gain some thickness when they were cut to put into the µCT sample tubes. The images shown in Figure 83 are therefore not completely representative of the network structure at given strain values. However, they do clearly show the re-appearance of tilted fiber bundles in highly strained samples.

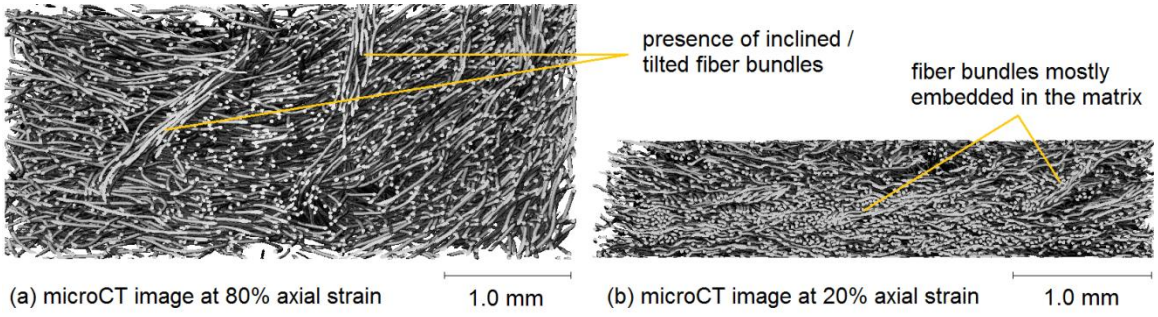

Figure 83: µCT images for NW1 treated (70 °C) sample stretched to (a) 80% strain showing slightly inclined / tilted fiber bundles and (b) 20 % strain showing highly tilted or embedded fiber bundles

An important structural feature that may contribute to the auxetic response in treated fabrics, are locally bent fibers that are positionally constrained to lie over a given

fiber and then below another proximal fiber. When this bent fiber is stretched, it acts to push the fibers above and below causing an increase in fabric thickness. This mechanism is possible in a dense structure where local forces can be transferred to neighboring bent-fiber configuration, and where fibers can offer some resistance to slippage (frictional contacts). This suggestion is analogous to that used to explain the out-of-plane auxetic response in paper (Section 3.5) [30, 55]. Since the heat-compressed samples are of a denser structure as compared to the compressed (only) samples and since the columns are inclined at larger angles in heat-compressed fabrics, a greater auxetic response is seen for them.

Auxetic response in these nonwovens was also found to be quite reversible for strains below 3% as shown in Figure 69. The increase in thickness could be thought of as a combination of reversible and irreversible processes. At small strains – straightening of bent/crimped fibers, fiber rotations and straightening of buckled/tilted columns – are likely reversible processes. At larger strains, the same processes may become irreversible. Additionally, any slippage of fibers from contact points, disentanglement of fibers, formation of new entanglements or fiber breakage are irreversible changes. At small strains (1%, 2% and 3%) when only the reversible processes are dominant, the thickness value goes back to the original after multiple strain cycles. However, as the strain value is increased, irreversible processes start to dominate and hence the original thickness cannot be fully recovered after strain removal. Multiple cycles can cause further disentanglements resulting in even lesser thickness recovery at higher cycles for higher strain values (5% and 10%).

In the case of aramid based nonwovens, it can be hypothesized that because of the shorter fibers (1 inch) the entanglements release rapidly upon the application of strain. This could explain why the aramid nonwovens continued to increase in thickness until failure – perhaps the web structure fails before the short fibers could fully rotate the columns back to their vertical orientation. Short fiber lengths can also explain the early failure (at ~60% strain or below), when compared to PET nonwovens. Apart from the short fiber length, the stiffness of fibers and other needling parameters might also play a role in determining the auxetic response of aramid nonwovens.

Other factors, such as the nature of fiber-fiber entanglements, fiber curl and crimp, fiber staple length, fiber modulus and column rigidity, needle-punching parameters etc. in these and similar systems would surely affect the nature of auxetic response and are a matter of further research. The simple process of treatment on needle-punched nonwovens described here and the proposed mechanism should be a useful design guide for generating novel auxetic materials and structures not only in such nonwovens but other network and fiber based structures too.

4.6 Conclusions

Thickness and width of commercially produced polyester and aramid based as-received needle-punched nonwovens was found to decrease with axial strain. The out-of-plane and in-plane Poisson's ratios for these nonwovens was therefore found to be positive (like many other common materials).

An out-of-plane auxetic response was induced in these needle-punched fabrics using a heat-compression protocol. Although the fabrics regained some of their thickness after the compression treatment over a few days, the treatment protocol was found to cause varying degrees of permanent compression set in the fabrics – dependent upon the fiber type and process parameters. Heat-compression and compression (alone) treatments were both found to be an effective way to generate out-of-plane auxetic response in these nonwovens. However, heat-compression was found to cause a more permanent compression set and higher values of auxetic response when compared to compression (at room temperature) alone.

The magnitude of auxetic response was found to be especially large for heat-compressed samples in the small strain regions for both polyester and aramid based nonwovens. Values as large as –7.2 (NW1), –6.6 (NW2) and –4.8 (NW3) were found for nonwovens heat-compressed at 70 °C and 2.5 MPa pressure for 24 hours. After the treatment, in-plane Poisson's ratio was still found to be positive and therefore, the processing was found to have produced ‘partially auxetic’ fabrics. The effect was seen to be reversible at strains lower than 2% and was found to be highly dependent on the fiber type, fiber length and processing parameters of temperature, pressure and time.

The technique of μCT was found to produce 3D images with well resolved fibers in polyester fiber needle-punched nonwoven fabrics. Using μCT scanning and optical microscopy it was found that the vertical fiber bundles/columns, produced in the needle punching step of fabric manufacture, are tilted and/or buckled as a result of the heat-compression treatment. It is suggested that it is likely the reorientation of these columns during subsequent uniaxial strain that drives thickness increase (auxetic response). In

addition to the reorientation of fiber-columns, a mechanism similar of straightening of bent fibers in paper is also likely to contribute to thickness increase in treated nonwovens.

4.7 Suggested future work

Our observations on auxetic behavior in these needle-punched nonwovens can be used as a guide in tailoring the processing conditions that can lead to out-of-plane auxetic response in needle-punched nonwovens made from other kinds of fibers like polypropylene, nylon etc. For instance, a nonwoven made of virgin (no recycled) aramid fibers would be an interesting candidate to examine. Nonwovens compressed at T > T_g should also be fully investigated, following our example of enhanced compression set and auxetic response of PET nonwovens treated at 100 °C. Micro-CT scanning of nonwovens while the samples are being strained is also suggested to future researchers. This will help directly examine the deformation of fiber bundles during stretching. The results from this work have the potential to be extended to other types of web consolidation techniques (nonwoven bonding techniques) which would let the researcher test the criticality of needle-punched consolidation technique in the observed auxetic phenomenon.

CHAPTER 5

COMPREHENSIVE SUMMARY

Auxetic behavior has rare occurrence in nature. A Poisson's ratio value in the range of -1.0 to +0.5 is theoretically allowed for isotropic materials under elastic strain limits, but most common materials tend to have a Poisson's ratio value greater than zero and around about +0.3. Very few examples of auxetic materials have been discovered in nature so far in the form of certain minerals and biological tissue. The fundamental origin of an auxetic response, almost always, was seen to be opening up of angles formed by ribs/struts in the internal structure of the material while under tension. This also meant expansion of a reentrant pore size. Synthetic auxetic materials have been recently synthesized by cleverly modifying the microstructure of common-use polymers (like polyurethane, polyethylene, PTFE etc.) using novel processing techniques or by constructing a material from scratch based upon a geometrical (usually regular) auxetic design.

The study of auxetic behavior in fiber network structures was found to be largely unexplored. Fiber networks occur naturally in animal tissues (membranes, muscles, skin, collagen), as well as in plants (cellulosic fibers, membranes), some of which have been shown to be auxetic. Fiber networks in the form of textiles, nonwovens, construction materials, paper, etc. are also manufactured and used in huge quantities across the globe. Because many known auxetic structures have a regular and repeating geometrical pattern, the examination of random (but anisotropic) fiber networks, like paper and nonwovens, presented a new kind of challenge.

We found several kinds of commercial paper to be out-of-plane auxetics except for some specialty papers like glassine paper and filter paper. A simple geometrical and finite element model depicting the arrangement of hydrogen-bonded cellulose fibers was presented to explain the likely origin and mechanism of this thickness increase in paper. In our experiments, both mechanical and modeling, structural parameters like fiber diameter, fiber type and shape, bulk density and contact spacing were found to affect the nature and extent of network deformation under strain. We produced paper handsheets to examine the effect of these parameters in detail. By choosing the appropriate conditions during the production of a paper handsheet, a Poisson's ratio as negative as -4.0 and as positive as about +0.5 could be achieved. This provides future researchers with a design space to engineer auxetic paper or another similar auxetic material (based on the presented model) with known out-of-plane auxetic response. The processing protocols responsible for imparting auxetic character to the paper network are inherent to the commercial paper production and not an additional pre- or post-production processing requirement. If one desired to produce a cellulosic or another fiber-based auxetic paper having a certain Poisson's ratio, it would only require changing the values of these processing parameters (like compression pressures, drying temperatures, refining extents) and not building an entirely new set of machinery dedicated to auxetics. This means that for instance, handsheets with Poisson's ratio of say -1.0 could in principle be produced inexpensively in the laboratory using the understanding of auxetic response in paper that we have achieved through this study.

Going forward, researchers are advised to think of ways to more closely mimic, in their models, the random orientation of fibers in real paper and introduce the viscoelastic

and dynamic mechanical properties of fibers in their simulations. It will be interesting to see which fibers, other than cellulose, can be used to synthesize an auxetic paper as well as what kind of composite materials may benefit from such networks.

Nonwoven fabrics, on the contrary, did not have any report or history of showing an auxetic behavior. There are numerous kinds of nonwovens and there exists a possibility of producing an auxetic response in some of them, analogous in design to the auxetic response in paper. For e.g. thermally bonded nonwovens (not auxetic as-produced) might have the potential of being converted into an auxetic material through heat-compressive treatments.

Needle-punched nonwovens are structurally very different from other types of nonwovens because they contain through-thickness bundles of fibers created during the needling process. Needle-punched nonwovens were studied extensively in this work because of their unique structural features and due to a possible mechanism of auxetic response distinct from that observed for paper. It was shown that, although, as-received (or as-produced) needle-punched nonwovens are mechanically conventional; a heat-compressive treatment protocol induced an out-of-plane auxetic response in them. This treatment caused a permanent compression (decrease in thickness) of varying extents dependent upon the pressure, temperature and time of compression. The fiber network structure was found to be set into a denser, more entangled network containing buckled, tilted and bowed-out columns. It was primarily, in-fact, this buckling of columns that would cause the fabric to increase in thickness when stretched. There are a few things noteworthy about inducing auxetic behavior in needle-punched nonwovens – 1) the observed magnitude of auxetic response is large when compared to other common

auxetic materials, 2) the prescribed treatment condition is simple, effective and easy to optimize and 3) the behavior is reversible up to at least 3% uniaxial strain.

Enough pressure and duration of compression, along with a temperature within or above the glass transition temperature of the fibers, ensures a permanent set in the nonwoven. Fibers other than polyester and fibers of more than one kind constituting the batt should also show similar behavior, although likely under a different set of conditions. Knowing the deformation effect caused by the fiber bundles and their orientation, it should be possible to create other materials and structures where such a design could be used to produce auxetic behavior.

The experimental methods used here for the measurement of Poisson's ratio (use of an Instron and a pressure-sensitive micrometer) have merit over say, optical measurement of thickness because pressure negates the edge/surface effects in fibrous materials. The technique of micro-CT was also found to be very useful in examining the internal structure of nonwovens. Going forward, again, different kinds of needle-punched nonwovens varying in fiber types, fiber lengths, network density and processing parameters etc. could be examined experimentally. Additionally, simple geometrical designs or even the micro-CT 3D image itself may be used as a model to feed into a simulation program developed to predict the out-of-plane Poisson's ratio in nonwovens.

Both paper and nonwovens are very common in their production and use. They themselves are fairly inexpensive, but the rarity of auxetic materials means that the processes and mechanisms developed and explained here have potential to add significant value to this class of materials (paper, nonwovens and fiber networks in general). For example, auxetic nonwovens may find use in breathable bandages, surgical implants,

biodegradable tissue scaffolds and conformable support structures. Auxetic properties like rarefaction, double curvature coupled with low density of nonwovens make them likely suitable for biomedical applications. Auxetic design inspirations, which by nature are material and scale independent, from paper and nonwovens could be used to advantage in such diverse applications as – protective clothing (impact resistance), water filters (rarefaction), stronger composites and noise dampeners.

APPENDIX A: µCT OF PAPER

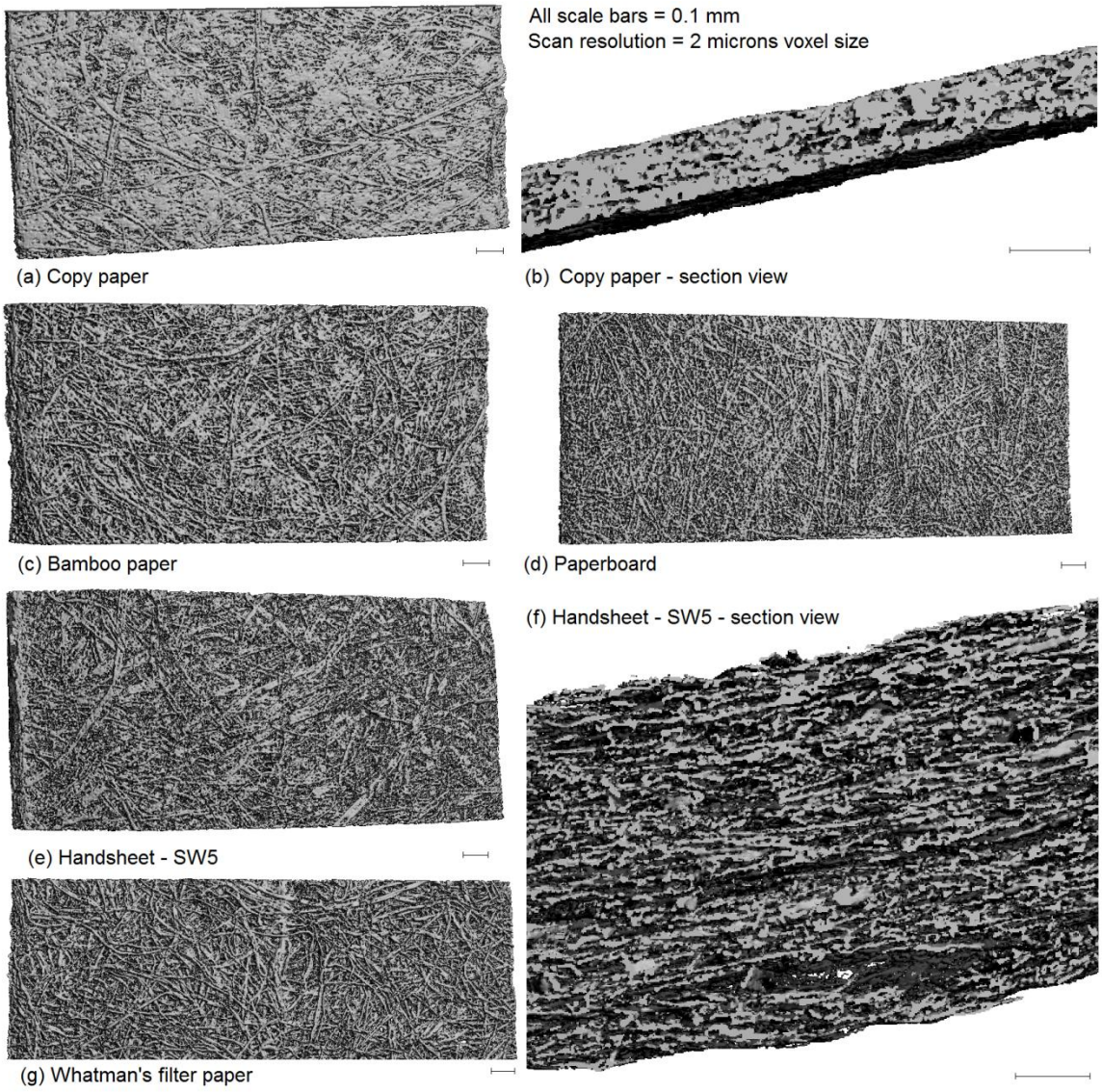

Figure 84: Scans of paper using µCT technique. Images show that fibers could not be resolved very well likely because the scan resolution (the best available) of 2 µm was too close to the fiber dimension of 5-10 µm.

APPENDIX B: μCT PROCEDURE

The micro-CT facility used is located in Dr. Robert Guldberg's lab (0405) at IBB in Georgia Tech. Scanco Medical – μCT50 was specifically used for our purposes. Angela Lin is the research engineer responsible for the supervision of the facility and training new users. There are several other micro-CT instruments that differ with respect to sample size/type and maximum attainable resolution etc.

The following procedure corresponds specifically to the μCT50 instrument and have been compiled with the help of 'instrument manual' and an 'instruction handout' available in the lab and the training provided by Angela.

Sample preparation

1) The sample is placed in a tube that ultimately goes into the scanner.
2) The tube diameter (and hence the sample size) and the resolution of the scan are related.
3) Choose a tube diameter depending upon your sample dimensions and the required resolution of scan. Lower diameters generally correspond to higher resolutions.
4) Cut the sample in a way that it fits in the tube. For our nonwoven fabrics, we chose a tube of outer diameter 7 mm. The thickness of our sample was about 2-5 mm. The tubes are about 1 inch deep.
5) Place the sample in the tube.

Computer interface

1) The computer comes with its own operating system (OpenVMS).

2) There is a terminal window to issue commands. You will see a $ prompt in this window.

3) You can use the 'Session Manager' it to browse files on disk.

4) The Scanco micro-CT software window is used to start running a scan, a 3D evaluation or to manage data between computer and backup drives.

Placing the sample in the scanner

1) Start the "Scan" application from the Scanco software window.

2) Place the sample tube in the scanning carousel of the instrument. Open the glass door on the top-front of the instrument. You can place more than one sample tube at a time. The carousel has numbers to indicate the sample holders.

3) The instrument prepares itself for a scan. The x-ray lamp starts to warm-up which takes about 15 minutes before it is ready for a scan.

4) The software detects any sample tubes on the carousel and matches them with the number on the carousel.

5) Next step is to define the parameters for the scan – these are described in the 'control file'.

Defining the control file

1) The parameters in control file instruct the instrument on how to scan – including the resolution, the X-ray power etc.

2) These parameters depend upon the sample – the density of material w.r.t. X-rays, the resolution you are looking for depending on the features of your structure etc.

3) Some of the important parameters set for our samples were – X-ray: 45 kVp, 200 uA, 9 W, voxel size: 2 um, number of slices: 500, integration time: 1000 ms etc.

4) Select a carousel position for the corresponding sample and then pick up the control file you wish to be applied to this sample.

5) Next click on scout-view for a quick view of your sample inside the scanner where you will be able to choose the actual volume that will be scanned.

Scout-view

1) When scout-view is clicked, the sample is taken inside the scanner and a view is presented on screen. You can change the contrast (shift + middle mouse button), pan (right-button) and zoom (middle-button) into the view to see the sample clearly.

2) If all looks good, left click once (you'll see a green reference line) and drag the mouse to select the number of slices. Click again to confirm. The scan time and number of slices will be displayed. In our case the number of slices varies between 500 to 1500 slices and scan time from 2 to 9 hours.

3) Click on "Add scan" to queue this as a task. If you need to add more samples, start from choosing the carousel position, then the control file and then finalize the volume in scout-view.

4) Open "Task-list" and click "Submit batch scans". Wait for all windows to close by themselves, while the actual scan starts.

Terminal commands

At any time, you can issue the following commands in the terminal window

```
$ show que  // shows a list of task to check if your tasks are running
$ disks     // shows the disk usage and free space on all drives
```

Evaluation

After the scan is complete (can take from a few minutes to several hours), you must run an evaluation to convert the raw scan data into readable image slices. This converts .RSQ files to .ISQs.

1) In the software window on the 'desktop', click on the "Evaluation" button.
2) Select the sample (identified by its number) and the appropriate measurement (measurement is the sub-sample within a sample set). The scan will be loaded as slice images and you will see all of the slices, numbered.
3) You can select an area within the slice for actual evaluation and 3D construction. This can be rectangular (to generate a cuboid), circular (to generate a cylinder) or a random shape which can also vary from slice to slice. All this is set in the "Contour (C…)" window. You can save contours as .GOBJ files.
4) Next step is to define the threshold which tells the sample apart from background. Open the "Threshold (T…)" window and select a predefined 'evaluation script' file. This file also has protocols to carry out the evaluation.
5) For our samples, we chose a custom file based upon '3D segmentation of VOI' file. You can modify an evaluation script and save it as your own for future use.
6) You must make sure that gauss sigma, gauss support, lower threshold and upper threshold values are set to your need. You can change these parameters and preview your slices in black (background) and white (sample). Choose a setting that you think best represents actual physical sample.
7) Click "Start Evaluation". This can take a few hours as well.

3D-View / Image saving

1) Once the evaluation is complete, you can click on the '3D' button on the software window on the 'desktop'. Choose your sample and a greyscale 3D view will be constructed from the slices on-screen.
2) You can change the position, elevation (viewing angle), lighting and sectioning of 3D images in this view.
3) Views can be either saved as TIFs or printed from the 3D-view. Slice images (2D) can be exported as TIFs (greyscale) or DICOMMs (binary or black and white) from the terminal window.

Don'ts

1) Don't start a scan on low disk space.
2) Don't use the full tube diameter to be your contour line. Make the contour dimensions a little smaller than the tube. Otherwise walls can appear in your 3D reconstruction.
3) Do not attempt to open the door on the instrument when a batch is running or when the lamp is warming up. Instruments operating on X-rays must be handled very carefully.

REFERENCES

[1] K. Evans, M. Nkansah, I. Hutchinson, S. Rogers, Molecular Network Design, *Nature*. **353** (1991) page 124.

[2] K.E. Evans, A. Alderson, Auxetic Materials: Functional Materials and Structures from Lateral Thinking!, *Advanced Materials*. **12** (*9*) (2000) pages 617–628.

[3] A. C. Brańka, D.M. Heyes, K.W. Wojciechowski, Auxeticity of Cubic Materials, *Physica Status Solidi (B)*. **246** (*9*) (2009) pages 2063–2071.

[4] C.W. Smith, R.J. Wootton, K.E. Evans, Interpretation of Experimental Data for Poisson's Ratio of Highly Nonlinear Materials, *Experimental Mechanics*. **39** (*4*) (1999) pages 356–362.

[5] A.E.H. Love, A Treatise on the Mathematical Theory of Elasticity, (Edition: Second), *Cambridge University Press*, London, (1906).

[6] M. de Podesta, Understanding the Properties of Matter, (Edition: Second), *Taylor & Francis*, London, (2002).

[7] J.M. Gere, B.J. Goodno, Mechanics of Materials, (Edition: Eighth), *Cengage Learning*, Stamford, USA, (2012).

[8] E.G. Wolff, Introduction to the Dimensional Stability of Composite Materials, *DEStech Publicaitons Inc.*, Lancaster PA, USA, (2004).

[9] K.E. Evans, (Book chapter) Manipulation of Poisson's Ratio, *in book*: G.M. Swallowe (Editor), Mechanical Properties and Testing of Polymers: An A-Z Reference, *Kluwer Academic*, Dordrecht, Netherlands, (1999): page 134.

[10] G.N. Greaves, A. L. Greer, R.S. Lakes, T. Rouxel, Poisson's Ratio and Modern Materials., *Nature Materials*. **10** (*11*) (2011) pages 823–37.

[11] R. Lakes, Foam Structures with a Negative Poisson's Ratio, *Science*. **235** (*4792*) (1987) pages 1038–1040.

[12] V.H. Carneiro, J. Meireles, H. Puga, Auxetic Materials — A Review, *Materials Science-Poland*. **31** (*4*) (2013) pages 561–571.

[13] S.P. Silva, M. a. Sabino, E.M. Fernandes, V.M. Correlo, L.F. Boesel, R.L. Reis, Cork: Properties, Capabilities and Applications, *International Materials Reviews*. **50** (*6*) (2005) pages 345–365.

[14] K. E. Evans, Tensile Network Microstructures Exhibiting Negative Poisson's Ratios, *Journal of Applied Physics.* **22** (1989) pages 1870-1876.

[15] D.J. Gunton, G. A. Saunders, The Young's Modulus and Poisson's Ratio of Arsenic, Antimony and Bismuth, *Journal of Materials Science*. **7** (*9*) (1972) pages 1061–1068.

[16] Y. Li, The Anisotropic Behavior of Poisson's Ratio, Young's Modulus, and Shear Modulus in Hexagonal Materials, *Physica Status Solidi (a)*. **38** (1976) pages 171–175.

[17] R.H. Baughman, J.M. Shacklette, A.A. Zakhidov, S. Stafstro, Negative Poisson's Ratios as a Common Feature of Cubic Metals, *Nature*. **392** (1998) pages 362–365.

[18] F. Milstein, K. Huang, Existence of a Negative Poisson Ration in Fcc Crystals, *Physical Review B*. **19** (*4*) (1979) pages 2030–2033.

[19] A. Yeganeh-Haeri, D. Weidner, J. Parise, Elasticity of α-Cristobalite: A Silicon Dioxide with a Negative Poisson's Ratio, *Science (New York)*. **257** (*5070*) (1992) pages 650–652.

[20] D.R. Veronda, R. A. Westmann, Mechanical Characterization of Skin-Finite Deformations., *Journal of Biomechanics*. **3** (*1*) (1970) pages 111–122.

[21] C. Lees, J.F. V Vincent, J.E. Hillerton, Poisson's Ratio in Skin, *Bio-Medical Materials and Engineering*. **1** (*1*) (1991) pages 19–23.

[22] J.L. Lewis, J.L. Williams, J.L. Lewis, Properties and an Anisotropic Model of Cancellous Bone From the Proximal Tibial Epiphysis, *Journal of Biomechanical Engineering*. **104** (*February*) (1982) pages 50–56.

[23] W. Voigt, Allgemeine Formeln Für Die Bestimmung Der Elasticitätsconstanten von Krystallen Durch Die Beobachtung Der Biegung Und Drillung von Prismen, *Annals of Physics*. **16** (1882) pages 273–310, 398–415.

[24] R. Chelikowsky, Structural Properties of Nine Silica Polymorphs, *Physical Review B*. **46** (*1*) (1992) pages 1–14.

[25] N.R. Keskar, J.R. Chelikowsky, Negative Poisson Ratios in Crystalline SiO_2 from First-Principles Calculations, *Nature*. **358** (1992) pages 222–224.

[26] H. Kimizuka, H. Kaburaki, Y. Kogure, Mechanism for Negative Poisson Ratios over the α - β Transition of Cristobalite, SiO_2: A Molecular-Dynamics Study, *Physical Review Letters*. **84** (2000) pages 5548–5551.

[27] J.N. Grima, R. Gatt, A. Alderson, K.E. Evans, On the Origin of Auxetic Behaviour in the Silicate α-Cristobalite, *Journal of Materials Chemistry*. **15** (*37*) (2005) page 4003.

[28] A. Lorato, P. Innocenti, F. Scarpa, A. Alderson, K.L. Alderson, K.M. Zied, et al., The Transverse Elastic Properties of Chiral Honeycombs, *Composites Science and Technology*. **70** (*7*) (2010) pages 1057–1063.

[29] B.D. Caddock, K.E. Evans, Negative Poisson Ratios and Strain-Dependent Mechanical Properties in Arterial Prostheses., *Biomaterials*. **16** (*14*) (1995) pages 1109–15.

[30] P. Verma, M.L. Shofner, A.C. Griffin, Deconstructing the Auxetic Behavior of Paper, *Physica Status Solidi (B)*. **251** (*2*) (2014) pages 289–296.

[31] A. Alderson, A Triumph of Lateral Thought, *Chemistry and Industry*. **10** (*May*) (1999) pages 384–391.

[32] Web-pages, Grima JN, T. Cecil, Auxetic Materials, (2000) Accessed: 05 May 2015.
http://groups.exeter.ac.uk/auxetic/auxetic_f2.html
http://www.timesofmalta.com/articles/view/20090802/education/maltese-researchers-develop-foam-that-can-save-lives.267756
http://www.despoke.com/wp-content/uploads/2013/03/Tom-Cecil_Auxetic-Table.jpg

[33] J.N. Grima, K.E. Evans, Auxetic Behavior from Rotating Squares, *Journal of Materials Science Letters*. **19** (2000) pages 1563–1565.

[34] J.N. Grima, K.E. Evans, Auxetic Behavior from Rotating Triangles, *Journal of Materials Science*. **41** (2006) pages 3193–3196.

[35] K.W. Wojciechowski, A. C. Brańka, Negative Poisson Ratio in a Two-Dimensional "Isotropic" Solid, *Physical Review A*. **40** (*1*) (1989) pages 7222–7225.

[36] K.W. Wojciechowski, Non-Chiral, Molecular Model of Negative Poisson Ratio in Two Dimensions, *Journal of Physics A: Mathematical and General*. **36** (2003) pages 11765–11778.

[37] J.W. Narojczyk, K.W. Wojciechowski, Elastic Properties of Two-Dimensional Soft Polydisperse Trimers at Zero Temperature, *Physica Status Solidi (B)*. **244** (*3*) (2007) pages 943–954.

[38] K.W. Wojciechowski, K. V Tretiakov, M. Kowalik, Elastic Properties of Dense Solid Phases of Hard Cyclic Pentamers and Heptamers in Two Dimensions., *Physical Review. E, Statistical, Nonlinear, and Soft Matter Physics*. **67** (2003) page 036121-1 to -14.

[39] R.M. Neville, A. Monti, K. Hazra, F. Scarpa, C. Remillat, I.R. Farrow, Transverse Stiffness and Strength of Kirigami Zero-N PEEK Honeycombs, *Composite Structures*. **114** (2014) pages 30–40.

[40] B.D. Caddock, K.E. Evans, Microporous Materials with Negative Poisson's Ratios. I. Microstructure and Mechanical Properties, *Journal of Physics D: Applied Physics*. **22** (*12*) (1989) pages 1877–1882.

[41] K.L. Alderson, K.E. Evans, The Fabrication of microporous Polyethylene Having a Negative Poisson's Ratio, *Polymer*. **33** (*20*) (1992) pages 4435–4438.

[42] J.N. Grima, K.E. Evans, Self Expanding Molecular Networks, *Chemical Communications*. (*16*) (2000) pages 1531–1532.

[43] J.N. Grima, J.J. Williams, R. Gatt, K.E. Evans, Modelling of Auxetic Networked Polymers Built from calix[4]arene Building Blocks, *Molecular Simulation*. **31** (*13*) (2005) pages 907–913.

[44] J.N. Grima, D. Attard, R.N. Cassar, L. Farrugia, L. Trapani, R. Gatt, On the Mechanical Properties and Auxetic Potential of Various Organic Networked Polymers, *Molecular Simulation*. **34** (*10-15*) (2008) pages 1149–1158.

[45] J.N. Grima, C. Zerafa, J.-P. Brincat, Development of Novel Poly(phenylacetylene) Network Polymers and Their Mechanical Behaviour, *Physica Status Solidi (B)*. **251** (*2*) (2014) pages 375–382.

[46] R.H. Baughman, D.S. Galvão, Crystalline Networks with Unusual Predicted Mechanical and Thermal Properties, *Nature*. **365** (1993) pages 735–737.

[47] C. He, P. Liu, A.C. Griffin, Toward Negative Poisson Ratio Polymers through Molecular Design, *Macromolecules*. **31** (*9*) (1998) pages 3145–3147.

[48] C. He, P. Liu, P.J. McMullan, A.C. Griffin, Toward Molecular Auxetics: Main Chain Liquid Crystalline Polymers Consisting of Laterally Attached Para-Quaterphenyls, *Physica Status Solidi (B)*. **242** (*3*) (2005) pages 576–584.

[49] X. Lu, C. He, P. Liu, A.C. Griffin, Structures and Properties of Liquid-Crystalline Polymers Based on Laterally Attached Oligop-Phenylenes, *Journal of Polymer Science Part A: Polymer Chemistry*. **43** (*15*) (2005) pages 3394–3402.

[50] C. He, P. Liu, A.C. Griffin, C.W. Smith, K.E. Evans, Morphology and Deformation Behaviour of a Liquid Crystalline Polymer Containing Laterally Attached Pentaphenyl Rods, *Macromolecular Chemistry and Physics*. **206** (*2*) (2005) pages 233–239.

[51] J.N. Grima, R. Jackson, A. Alderson, K.E. Evans, Do Zeolites Have Negative Poisson's Ratios?, *Advanced Materials*. **12** (*24*) (2000) pages 1912–1918.

[52] L.J. Hall, V.R. Coluci, D.S. Galvão, M.E. Kozlov, M. Zhang, S.O. Dantas, et al., Sign Change of Poisson's Ratio for Carbon Nanotube Sheets., *Science (New York)*. **320** (*5875*) (2008) pages 504–7.

[53] V. Coluci, L. Hall, M. Kozlov, M. Zhang, S. Dantas, D. Galvão, et al., Modeling the Auxetic Transition for Carbon Nanotube Sheets, *Physical Review B*. **78** (*11*) (2008) page 115408.

[54] S. Tanpichai, F. Quero, M. Nogi, H. Yano, R.J. Young, T. Lindstro, et al., Effective Young's Modulus of Bacterial and Microfibrillated Cellulose Fibrils in Fibrous Networks, (2012).

[55] O.E. Öhrn, Thickness Variations of Paper on Stretching, *Svensk Papperstidning*. **68** (*5*) (1965) pages 141–149.

[56] N. Stenberg, C. Fellers, Out-of-Plane Poisson's Ratios of Paper and Paperboard, *Nordic Pulp and Paper Research Journal*. **17** (*4*) (2002) pages 387–394.

[57] H.L.L. Baumgarten, L. Gottsching, H.L.L. Baumgarten, (Book chapter) Triaxial Deformation of Paper under Tensile Load, *in book*: F. Bolaim (Editor), Fundamental Properties of Paper Related to Its Uses, First Edit, *British Paper and Board Ind. Federation*, London, (1976): pages 227–252.

[58] G. Baum, K. Pers, D.R. Shepard, T.R. Ave'Lallemant, Wet Straining of Paper, *Tappi*. **67** (*5*) (1984) pages 100–104.

[59] Z. Ge, H. Hu, Innovative Three-Dimensional Fabric Structure with Negative Poisson's Ratio for Composite Reinforcement, *Textile Research Journal*. **83** (*5*) (2012) pages 543–550.

[60] M. Glazzard, P. Breedon, Weft-Knitted Auxetic Textile Design, *Physica Status Solidi (B)*. **251** (*2*) (2014) pages 267–272.

[61] P. Verma, M.L. Shofner, A. Lin, K.B. Wagner, A.C. Griffin, Inducing out-of-Plane Auxetic Behavior in Needle-Punched Nonwovens, *Physica Status Solidi (B)*. 252 (7) (2015) pages 1455–1464.

[62] K. Alderson, A. Alderson, S. Anand, V. Simkins, S. Nazare, N. Ravirala, Auxetic Warp Knit Textile Structures, *Physica Status Solidi (B)*. **249** (*7*) (2012) pages 1322–1329.

[63] Z. Wang, H. Hu, Auxetic Materials and Their Potential Applications in Textiles, *Textile Research Journal*. **84** (*15*) (2014) pages 1600–1611.

[64] M. Tatlier, L. Berhan, Modelling the Negative Poisson's Ratio of Compressed Fused Fibre Networks, *Physica Status Solidi (B)*. **246** (*9*) (2009) pages 2018–2024.

[65] S. Jayanty, J. Crowe, L. Berhan, Auxetic Fibre Networks and Their Composites, *Physica Status Solidi (B)*. **248** (*1*) (2011) pages 73–81.

[66] L. Berhan, A. M. Sastry, On Modeling Bonds in Fused, Porous Networks: 3D Simulations of Fibrous-Particulate Joints, *Journal of Composite Materials*. **37** (*8*) (2003) pages 715–740.

[67] K.L. Alderson, V.R. Simkins, V.L. Coenen, P.J. Davies, A. Alderson, K.E. Evans, How to Make Auxetic Fibre Reinforced Composites, *Physica Status Solidi (B)*. **242** (*3*) (2005) pages 509–518.

[68] J.F. Clarke, R. A. Duckett, P.J. Hine, I.J. Hutchinson, I.M. Ward, Negative Poisson's Ratios in Angle-Ply Laminates: Theory and Experiment, *Composites*. **25** (*9*) (1994) pages 863–868.

[69] E. Hadi Harkati, A. Bezazi, F. Scarpa, K. Alderson, A. Alderson, Modelling the Influence of the Orientation and Fibre Reinforcement on the Negative Poisson's Ratio in Composite Laminates, *Physica Status Solidi (B)*. **244** (*3*) (2007) pages 883–892.

[70] A. Bezazi, W. Boukharouba, F. Scarpa, Mechanical Properties of Auxetic Carbon/epoxy Composites: Static and Cyclic Fatigue Behaviour, *Physica Status Solidi (B)*. **246** (*9*) (2009) pages 2102–2110.

[71] J.N. Grima, D. Attard, R. Gatt, R.N. Cassar, A Novel Process for the Manufacture of Auxetic Foams and for Their Re-Conversion to Conventional Form, *Advanced Engineering Materials*. **11** (*7*) (2009) pages 533–535.

[72] J.N. Grima, R. Caruana-Gauci, M.R. Dudek, K.W. Wojciechowski, R. Gatt, Smart Metamaterials with Tunable Auxetic and Other Properties, *Smart Materials and Structures*. **22** (*8*) (2013) page 084016.

[73] S.C. Ugbolue, Y.K. Kim, S.B. Warner, Q. Fan, C.L. Yang, O. Kyzymchuk, et al., The Formation and Performance of Auxetic Textiles. Part I: Theoretical and Technical Considerations, *Journal of the Textile Institute*. **101** (*7*) (2010) pages 660–667.

[74] A Alderson, K.L. Alderson, Auxetic Materials, *Proceedings of the Institution of Mechanical Engineers, Part G: Journal of Aerospace Engineering*. **221** (*4*) (2007) pages 565–575.

[75] W. Miller, P.B. Hook, C.W. Smith, X. Wang, K.E. Evans, The Manufacture and Characterisation of a Novel, Low Modulus, Negative Poisson's Ratio Composite, *Composites Science and Technology*. **69** (*5*) (2009) pages 651–655.

[76] M. Uzun, Mechanical Properties of Auxetic and Conventional Polypropylene Random Short Fibre Reinforced Composites, *Fibres & Textiles in Eastern Europe.* **5** (*94*) (2012) pages 70–74.

[77] D. Skertchly, Composite Auxetic Armour, Patent no. US 20110214560A1, (2011).

[78] M. Burke, A Stretch of the Imagination, *New Scientist*. **2085** (1997) pages 36–39.

[79] A. Alderson, J. Rasburn, S. Ameer-Beg, P.G. Mullarkey, W. Perrie, K.E. Evans, An Auxetic Filter: A Tuneable Filter Displaying Enhanced Size Selectivity or Defouling Properties, *Industrial & Engineering Chemistry Research*. **39** (*3*) (2000) pages 654–665.

[80] M. Ek, G. Gellerstedt, G. Henriksson, Pulp and Paper Chemistry and Technology I: Wood Chemistry and Wood Biotechnology, (Edition: First), *Walter de Gruyter*, Berlin, (2009).

[81] R. Shmulsky, P.D. Jones, Forest Products and Wood Science: An Introduction, (Edition: Sixth), *Wiley-Blackwell*, (2011).

[82] M. Alava, K. Niskanen, The Physics of Paper, *Reports on Progress in Physics*. **69** (*3*) (2006) pages 669–723.

[83] M. Ek, G. Gellerstedt, G. Henriksson, Pulp and Paper Chemistry and Technology II: Pulping Chemistry and Technology, *Walter de Gruyter*, Berlin, Germany, (2009).

[84] C. Ververis, K. Georghiou, N. Christodoulakis, P. Santas, R. Santas, Fiber Dimensions, Lignin and Cellulose Content of Various Plant Materials and Their Suitability for Paper Production, *Industrial Crops and Products*. **19** (2004) pages 245–254.

[85] A. Ebringerova, Z. Hromadkova, T. Heinze, Hemicellulose, *Advances in Polymer Science*. **186** (*August*) (2005) pages 1–67.

[86] A. Rafsanjani, M. Stiefel, K. Jefimovs, R. Mokso, D. Derome, J. Carmeliet, Hygroscopic Swelling and Shrinkage of Latewood Cell Wall Micropillars Reveal

Ultrastructural Anisotropy, *Journal of the Royal Society: Interface*. **11** (*95*) (2014) pages 1–10.

[87] J. Gierer, Chemical Aspects of Kraft Pulping, *Wood Science and Technology*. **14** (1980) pages 241–266.

[88] A.H. Nissan, G.L. Batten, On the Primacy of the Hydrogen Bond in Paper Mechanics, *Tappi*. **73** (*2*) (1990) pages 159–164.

[89] W.E. Scott, J.C. Abbott, S. Trosset, Properties of Paper: An Introduction, *TAPPI Press*, (1989).

[90] J. Roberts, The Chemistry of Paper, *The Royal Society of Chemistry*, Cambridge, (1996).

[91] M. Ek, G. Gellerstedt, G. Henriksson, Pulp and Paper Chemistry and Technology III: Paper Chemistry and Technology, *Walter de Gruyter*, Berlin, (2009).

[92] M. Ek, G. Gellerstedt, G. Henriksson, Pulp and Paper Chemistry and Technology IV: Paper Products Physics and Technology, (Edition: First), *Walter de Gruyter*, (2009).

[93] J. Gratzl, The Chemical Principles of Pulp Bleaching with Oxygen, Hydrogen Peroxide and Ozone-a Short Review, *Papier*. **46** (*10A*) (1992) pages V1–V8.

[94] P. Fardim, N. Durán, Modification of Fibre Surfaces during Pulping and Refining as Analysed by SEM, XPS and ToF-SIMS, *Colloids and Surfaces A: Physicochemical and Engineering Aspects*. **223** (2003) pages 263–276.

[95] M.A. Hubbe, R.A. Venditti, O.J. Rojas, What Happens to Cellulosic Fibers During Papermaking and Recycling? A Review, *Bioresources*. **2** (*4*) (2007) pages 739–788.

[96] J.D. Llf, M. Wikstrom, C. Fellers, M. Rigdahl, Deformation of Paper Structure During Calendering as Measured by Electronic Speckle Photography, **23** (*10*) (1997) pages 481–486.

[97] R. Peterson, C.L. Whliams, Determining Paper-Coating Thickness with Electron Microscopy and Image Analysis, *Tappi Journal.* (*October*) (1992) pages 122-126.

[98] N. Xiao, J.W. Pu, Paper and Board Pigment Coating Raw Materials – A Review of Some Recent Innovative Novelties, *Advanced Materials Research*. **602** (2013) pages 1617–1623.

[99] Tappi, Forming handsheets for physical tests of pulp: Tappi Test Method T-205, (2002).

[100] A. Kelly, Concise Encyclopedia of Composite Materials, (Edition: First), *Elsevier Science*, (1994).

[101] R.W. Mann, G.A. Baum, C.C. Habeger, Determination of All Nine Orthotropic Elastic Constants for Machine-Made Paper, *IPC Technical Paper Series*. **84** (*84*) (1979) pages 1–18.

[102] K. Schulgasser, The in-Plane Poisson Ratio of Paper, *Fiber Science and Technology*. **19** (1983) pages 297-309.

[103] T. Yokoyama, K. Nakai, (Book chapter) Evaluation of in-Plane Orthotropic Elastic Constants of Paper and Paperboard, *in*: SEM Annual Conference & Exposition on Experimental and Applied Mechanics, (2007).

[104] G. Zhao, R. Lai, B. He, T. Greschik, X. Li, Replacement of Softwood Kraft Pulp with ECF-Bleached Bamboo Kraft Pulp in Fine Paper, *BioResources*. **5** (2010) pages 1733–1744.

[105] D. Sekyere, Potential of Bamboo (Bambusa Vulgaris) as a Source of Raw Material for Pulp and Paper in Ghana, *Ghana Journal of Forestry*. **1** (1994) pages 49–56.

[106] T. Paterson-Brown, B. Painter, S. Zuanic, T. White, Cotton Linter Tissue Products and Method for Preparing Same, Patent no. EP1058751B1, (2003).

[107] B. Shi, T.G. Shannon, E. Pelky, Novel Use of Waste Keratin and Cotton Linter Fibers for Prototype Tissue Papers and Their Evaluation, *BioResources*. **5** (2010) pages 1425–1435.

[108] Web page: Whatman Filter Papers, (2013) Date accessed: 06 Jan 14 http://www.whatman.com/CelluloseFilters.aspx.

[109] G. Borden, Method of Producing Supercalendered Plasticized Glassine Paper, Patent no. US 2636833, (1953).

[110] V. der Reyden, Dianne, C. Hofmann, M. Baker, Effects of aging and solvent treatments on some properties of contemporary tracing papers, *Journal of the American Institute for Conservation*. **32** (*2*) (1993) pages 177–206.

[111] C.S. Lee, E. Jones, R. Kingsland, Poisson's Ratio of Engineering Plastics, *Advances in Polymer Technology*. **6** (*1*) (1986) pages 85–90.

[112] S. Sim, K.J. Kim, A Method to Determine the Complex Modulus and Poisson's Ratio of Viscoelastic Materials for FEM Applications, *Journal of Sound and Vibration*. **141** (*1*) (1990) pages 71–82.

[113] TAPPI, Freeness of pulp (Canadian standard method): Tappi test method T-227, (1999).

[114] Tappi, Thickness (caliper) of Paper, Paperboard, and Combined Board: Tappi Standard T-411, *Tappi*. (2010).

[115] Tappi, Tensile Properties of Paper and Paperboard (using Constant Rate of Elongation Apparatus): Tappi Test Method T-494, *Tappi*. (2006).

[116] A. Ranger, L. Hopkins, (Book chapter) The Formation and Structure of Paper, *in*: F. Bolam (Editor), Technical Section of the British Paper and Board Makers' Association, London, (1962): pages 277–310.

[117] EDANA: Nonwoven Products and Applications, *EDANA*. (2015). http://www.edana.org/discover-nonwovens/products-applications

[118] R. Chapman, Applications of Nonwovens in Technical Textiles, *Elsevier Science*, (2010).

[119] EDANA: Nonwoven Facts and Figures, *EDANA*. (2015). http://www.edana.org/discover-nonwovens/facts-and-figures

[120] S. Batra, M. Thompson, E. Vaughn, L. Wadsworth, Nonwoven Glossary - Association of the nonwoven fabrics industry, *INDA*, Cary, North Carolina, (2002).

[121] A. Wilson, A. Brydon, A. Pourmohammadi, C. White, G. Bhat, S. Malkan, et al., Handbook of nonwovens, *Woodhead Publishing Limited*, Cambridge, (2007).

[122] N. Sherwood, Binders for Nonwoven Fabrics, *Industrial & Engineering Chemistry*. **51** (1959) page 907.

[123] K. Choi, J.E. Spruiell, J.F. Fellers, Strength Properties of Melt Blown Nonwoven Webs, *Polymer Engineering and Science*. (*2*) (1988) pages 81–89.

[124] M. Madhusoothanan, Thermal Insulation , Compression and Air Permeability of Polyester Needle-Punched Nonwoven, **35** (*March*) (2010) pages 38–44.

[125] M. Salajkova, L. Valentini, Q. Zhou, L. a Berglund, Tough Nanopaper Structures Based on Cellulose Nanofibers and Carbon Nanotubes, *Composites Science and Technology*. **87** (2013) pages 103–110.

[126] Y.J. Ryu, H.Y. Kim, K.H. Lee, H.C. Park, D.R. Lee, Transport Properties of Electrospun Nylon 6 Nonwoven Mats, *European Polymer Journal*. **39** (2003) pages 1883–1889.

[127] Mitra, A., M. Cybulska, and B. C. Goswami. Deformation Behavior and Structural Mechanics of Needle Punched Nonwovens. *Tappi Nonwovens Conference*, pp. 283-294. Tappi Press, 1999.

[128] ISO:11224, Textiles - Web formation and bonding in nonwovens - Vocabulary, *ISO:11224*, (1999).

[129] EDANA - International Association for the Nonwovens and Related Industries, (2013).
http://www.edana.org/

[130] J.H. Lin, Z.H. Xu, C.H. Lei, C.W. Lou, Effect of Fiber Arrangement on the Mechanical Properties of Thermally Bonded Nonwoven Fabrics, *Textile Research Journal*. **73** (*10*) (2003) pages 917–920.

[131] S. Michielsen, B. Pourdeyhimi, P. Desai, Review of Thermally Point-Bonded Nonwovens: Materials, Processes, and Properties, *Journal of Applied Polymer Science*. **99** (*5*) (2006) pages 2489–2496.

[132] X. Hou, M. Acar, V. V Silberschmidt, Tensile Behavior of Low Density Thermally Bonded Nonwoven Material, **4** (*1*) (2009) pages 26–33.

[133] J. Hearle, M. Sultan, A Study of Needled Fabrics. 1. Experimental Methods and Properties, *Journal of the Textile Institute*. **58** (*6*) (1967) pages 251–265.

[134] J. Hearle, M. Sultan, A Study of Needled Fabrics. 3. Influence of Fibre Type and Dimensions, *Journal of the Textile Institute*. **59** (*3*) (1968) pages 137–147.

[135] S.K. Batra, B. Pourdeyhimi, Introduction to Nonwovens Technology, *DEStech Publications*, Lancaster PA, USA, (2012).

[136] A. Bateman, Apparatus for Producing Needled Batts, Patent no. US Patent No. 2902746, (1959).

[137] N. Sun, (PhD Thesis), Structures of Needlepunched Fabrics and Needling Mechanism, North Carolina State University, (2014).

[138] J. Hearle, M. Sultan, T. Choudhary, A Study of Needled Fabrics. 2. Effects of Needling Process, *Journal of the Textile Institute*. **59** (*2*) (1968) pages 103–116.

[139] J. Hearle, A. Purdy, Influence of Depth of Needle Penetration on Needled-Fabric Structure and Tensile Properties, *Journal of the Textile Institute*. **65** (*1*) (1974) pages 6–12.

[140] H.S. Kim, B. Pourdeyhimi, P. Desai, A. S. Abhiraman, Anisotropy in the Mechanical Properties of Thermally Spot-Bonded Nonwovens: Experimental Observations, *Textile Research Journal*. **71** (*11*) (2001) pages 965–976.

[141] S. Maity, K. Singha, Structure-Property Relationships of Needle-Punched Nonwoven Fabric, *Frontiers in Science*. **2** (*6*) (2013) pages 226–234.

[142] H.S. Kim, B. Pourdeyhimi, A. S. Abhiraman, P. Desai, Effect of Bonding Temperature on Load-Deformation Structural Changes in Point-Bonded Nonwoven Fabrics, *Textile Research Journal*. **72** (*7*) (2002) pages 645–653.

[143] S. Adanur, T. Liao, Fiber Arrangement Characteristics and Their Effects on Nonwoven Tensile Behavior, *Textile Research Journal*. **69** (*11*) (1999) pages 816–824.

[144] A. Rawal, A. Priyadarshi, N. Kumar, S. V. Lomov, I. Verpoest, Tensile Behaviour of Nonwoven Structures: Comparison with Experimental Results, *Journal of Materials Science*. **45** (*24*) (2010) pages 6643–6652.

[145] S. Bais-Singh, B.C. Goswami, Theoretical Determination of the Mechanical Response of Spun-Bonded Nonwovens, *Journal of the Textile Institute*. **86** (*2*) (1995) pages 271–288.

[146] J.P. Giroud, Poisson's Ratio of Unreinforced Geomembranes and Nonwoven Geotextiles Subjected to Large Strains, *Geotextiles and Geomembranes*. **22** (*4*) (2004) pages 297–305.

[147] A. Rawal, S. Lomov, T. Ngo, I. Verpoest, J. Vankerrebrouck, Mechanical Behavior of Thru-Air Bonded Nonwoven Structures, *Textile Research Journal*. **77** (*6*) (2007) pages 417–431.

[148] H. Kim, B. Pourdeyhimi, The Role of Structure on Mechanical Properties of Nonwoven Fabrics, *International Nonwovens Journal*. (2001).

[149] V.K. Kothari, A. Das, Compressional Behaviour of Nonwoven Geotextiles, *Geotextiles and Geomembranes*. **11** (*3*) (1992) pages 235–253.

[150] S. Jaganathan, H. Vahedi Tafreshi, E. Shim, B. Pourdeyhimi, A Study on Compression-Induced Morphological Changes of Nonwoven Fibrous Materials, *Colloids and Surfaces A: Physicochemical and Engineering Aspects*. **337** (*1-3*) (2009) pages 173–179.

[151] D. Das, B. Pourdeyhimi, Compressional and Recovery Behaviour of Highloft Nonwovens, **35** (*December*) (2010) pages 303–309.

[152] M. Afshari, P. Chen, R. Kotek, N. Carolina, Relationship Between Tensile Properties and Ballistic Performance of Poly (Ethylene Naphthalate) Woven and Nonwoven Fabrics, **125** (2012) pages 2271–2280.

[153] S.C. Ugbolue, Y.K. Kim, S.B. Warner, Q. Fan, C. Yang, O. Kyzymchuk, et al., The Formation and Performance of Auxetic Textiles. Part II: Geometry and Structural Properties, *Journal of the Textile Institute*. **102** (5) (2011) pages 424–433.

[154] K. Singha, M. Singha, Fiber Crimp Distribution in Nonwoven Structure, *Frontiers in Science.* **3** (*1*) (2013) pages 14–21.

[155] Personal Communication from TenCate, Georgia (2014)

[156] D. Van Krevelen, K. Te Nijenhuis, Properties of Polymers, *Elsevier*, Amsterdam, (2009).